Doctoral Dissertation

Donor-Acceptor based Conjugated Polymeric Materials for Improving the Storage and Rate Performance of Lithium/Sodium-Ion Batteries

Saibrata Punyasloka

Supervisor: Noriyoshi Matsumi

Graduate School of Advanced Science and Technology
Japan Advanced Institute of Science and Technology

Materials Science
September 2024

Abstract

Designing sustainable active materials for energy storage systems has become a critically important research area. Given the increasing demand for metal-ion batteries, researchers are focusing on developing alternative materials to address issues with graphite and currently available commercial anode materials.

This thesis explores the potential applications of conjugated polymers in energy storage devices. It highlights how introducing heteroatoms can increase theoretical capacity. Moreover, by creating ion channels through microstructure regulation, researchers can reduce diffusion path lengths, facilitating fast-charging applications.

Chapter 1 provides an introductory review. Chapter 2 discusses the synthesis and application of a novel donor-acceptor type conjugated network polymer, POL 202, as an active material in Li-ion secondary batteries. It emphasizes POL 202's remarkable capability to support extremely fast charge-discharge cycles, directly attributed to its structural advantages.

In Chapter 3, a triazine-bithiophene-based porous organic polymer is designed and used as a precursor material for carbons. A hierarchical N, S co-doped micro/mesoporous carbon is synthesized from a POP, POL 102, at two different temperatures, 600°C and 800°C. Physical and chemical characterizations provide insights into variations in surface area, pore volume, and defects with increasing carbonization temperatures, and their impact on electrochemical and charge storage properties.

Chapter 4 summarizes the findings and discusses the prospects for this research.

Keywords: organic polymers, nanoporous carbon, fast charging batteries, lithium-ion batteries, sodium-ion batteries

Acknowledgements

The reported research was conducted under the supervision of Prof. Noriyoshi Matsumi at the Graduate School of Advanced Science and Technology, Japan Advanced Institute of Science and Technology, spanning the period from 2021 to 2024. The author extends heartfelt appreciation and gratitude to Prof. Noriyoshi Matsumi for his support.

The author also expresses sincere thanks to the esteemed members of the review committee, Prof. Takuya Tsujiguchi, Prof. Eijiro Miyako, Prof. Toshiaki Taniike, Prof. Kazuma Gotoh and Prof. Kosuke Okeyoshi for their valuable time and insightful suggestions, during the thesis evaluation process.

Additionally, the author is profoundly grateful to all past and present members of the Matsumi laboratory for their support and help.

The author feels indebted to his parents, family, friends, and mentors for their unwavering emotional and intellectual support throughout this academic pursuit.

Saibrata Punyasloka
Graduate School of Advanced Science and Technology
Japan Advanced Institute of Science and Technology
September 2024.

Preface

This thesis is a part of the doctoral research work conducted at Japan Advanced Institute of Science and Technology, Nomi, Japan between FY 2021 and FY 2024. It outlines the design and development of donor acceptor based conjugated polymeric active materials for improving the rate and storage performances in Li/Na-ion batteries and thereby addressing the issues of high-density anodes.

With the increase in the demand for energy, it is imminent to dive deeper into this area to understand and design materials with augmented performance to meet the needs. Donor acceptor polymers are known to have a low redox potential which can in turn help in achieving faster charge transfer and higher rate performance and also high-power density. Besides, presence of such atoms can also undergo reversible coordination with Li-ions resulting in provision of active sites and thereby increasing the specific capacity.

Moreover, such donor acceptor based porous polymers can also be used as robust precursors to derive hierarchical micro/mesoporous carbon materials without the use of hazardous chemicals like KOH and H_3PO4 as activating agents. This thesis summarizes the synthesis, characterization, and application of such materials and tries to provide a fundamental understanding on potential applications of such materials and aims to add to the development of basic science.

Saibrata Punyasloka
Graduate School of Advanced Science and Technology
Japan Advanced Institute of Science and Technology
September 2024.

Contents

CHAPTER 1 INTRODUCTION

Charting the Course: From Fossil Fuels to Electrochemical Energy Solutions

In the contemporary era, energy serves as the cornerstone of economic progress. The rapid industrialization of the late 18th century heavily relied on easily accessible fossil fuels such as oil, natural gas, and coal as primary energy sources. Fossil fuels, formed over time through the degradation of organic matter within the Earth's crust across various geological periods, played a pivotal role in this process.

Over the past three centuries of globalization, humanity's perspective on life has undergone a substantial shift. Meeting the evolving demands for a better lifestyle has made energy an indispensable requirement. Human innovation has led to significant technological progress in harnessing various forms of fossil fuels such as natural gas and petroleum, serving a multitude of purposes. Petroleum, commonly referred to as crude oil, undergoes refining to produce various derivative fuels like gasoline, kerosene, diesel, and petroleum jelly, extensively used in transportation, synthetic materials, and asphalt production. Similarly, non-renewable natural gas plays a vital role in everyday activities such as cooking, plastic production, and energy generation. The abundant availability of fossil fuels ignited a technological revolution spanning centuries.

However, the unchecked consumption of these non-renewable energy sources has raised several pressing issues including environmental pollution, greenhouse gas emissions, acid rain, deforestation, and disruption of habitats and seasonal cycles, alongside concerns regarding their finite reserves leading to eventual depletion. According to the IEEJ's Asia/World Energy Outlook 2016 analysis, global primary energy consumption is projected to rise by 1.2% annually, reaching 18.9 billion TOE (tons of oil equivalent) by 2040 from 13.7 billion TOE in 2014. Fossil fuels are expected to remain the predominant energy sources, constituting 78% of the total by 2040. According to Precedence Research, the global energy storage systems market size is projected to surpass around US$ 435.32 billion by 2030 and growing at a CAGR of 8.4% from 2022 to 2030 (Fig 1.1)[1,2]

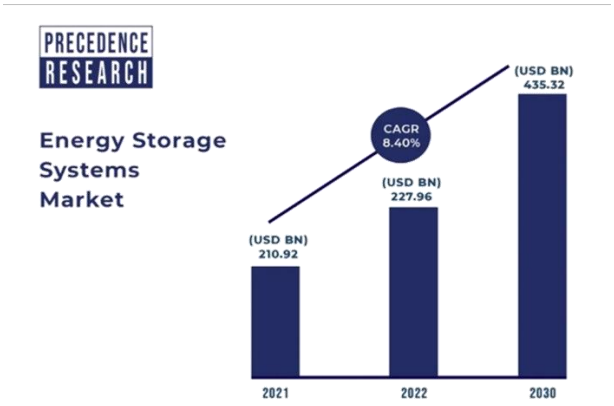

Figure 1.1: Predictions about the global energy storage market size.

Consequently, the necessity for sustainable energy sources at affordable rates, environmentally friendly, and capable of meeting the energy needs of future generations is paramount today. Electrochemical Energy Storage (EES) solutions function by converting and storing electrical energy in materials and devices that can later be converted back to electricity when necessary.

This chapter provides a brief overview of different energy storage devices that have recently drawn a lot of attention in terms of research. A brief account of ways to increase the energy density and power density has also been provided.

Supercapacitors

Supercapacitors, sometimes referred to as electric double-layer capacitors (EDLCs) or ultracapacitors, are advanced energy storage devices with quick energy delivery and storage. Supercapacitors store energy electrostatically, facilitating rapid cycles of charge and discharge, in contrast to conventional rechargeable batteries, which store energy through chemical reactions.[3,4] They are perfect for applications needing quick energy transfer, such energy harvesting systems, portable electronics, and regenerative braking in cars, because of their high-power density, which enables them to deliver energy bursts efficiently. Supercapacitors have the potential to completely transform energy storage technology with continued research and development, providing high-performance and sustainable power solutions to a wide range of sectors.[5,6]

Compared to traditional batteries, supercapacitors have several notable advantages. One such advantage is their extraordinary cycle life, which can reach hundreds of thousands or even millions of charge-discharge cycles. Because of their endurance, they are especially appealing for uses like electric and hybrid cars that need to charge and discharge at high speeds on a regular basis. Additionally, supercapacitors have a high power density, enabling them to rapidly charge and discharge currents. Fig 1.2 represents

a schematic diagram of a supercapacitor.

Supercapacitors may also function well across a broad variety of temperatures and show great temperature performance. Their adaptability increases their potential applicability in a variety of settings, including industrial, aeronautical, and automotive ones.

To close the gap between supercapacitors' and conventional batteries' energy storage capacities, research efforts are still being made to increase the energy density of these devices. The performance of supercapacitors could be further enhanced by developments in materials science and nanotechnology, opening the door for their wider use in cutting-edge technologies like wearable electronics, smart grids, and energy-efficient transportation systems.

.[7,8]

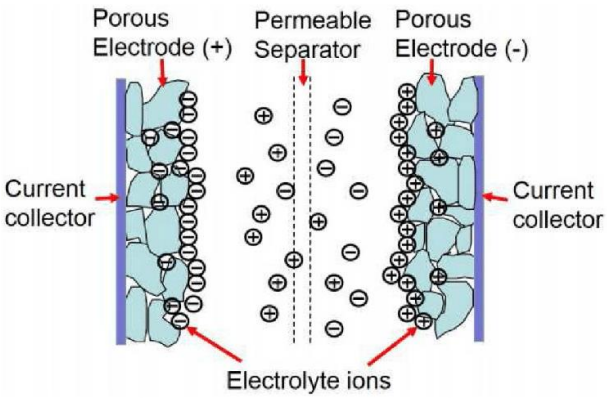

Figure 1.2: A schematic diagram of a supercapacitor at a charged state.

Fuel cells.

Because of their high efficiency, affordability, and green credentials, fuel cells have gained great interest. In essence, they offer a wide range of uses for both stationary and portable power generation. Within fuel cells, energy is directly converted from chemical energy to electrical energy, producing heat and water as byproducts. The anode of these cells receives hydrogen fuel, while the cathode receives oxygen from the surrounding air. The two electrodes of these cells are divided by an electrolyte. At the anode, hydrogen fuel is constantly broken down into protons. At the cathode of a fuel cell, oxygen from the air combines with electrons and protons (hydrogen ions) that have migrated through the electrolyte from the anode. [9]

Fig 1.3 shows a schematic diagram of a hydrogen fuel cell and its components. The electrolyte-membrane, which is an electron insulator, works as a bridge permitting only positive ions to travel toward the cathode. To recombine and preserve the charge equilibrium of the system, electrons move from the negative electrode to the positive

electrode via an external circuit.

Fuel cells can be classified into nine types based on the electrolyte and fuel used[10]:

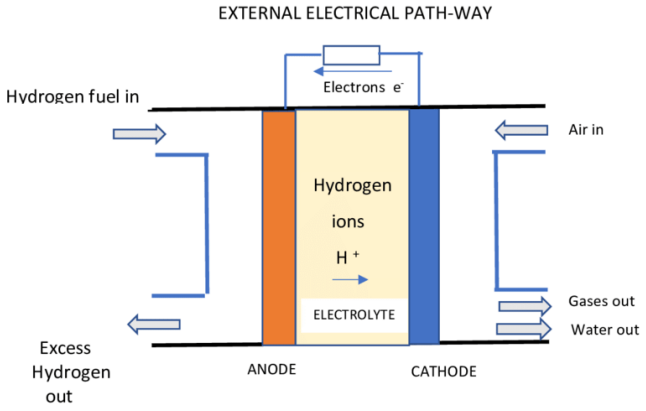

Figure 1.3 Schematic diagram of hydrogen fuel cell

i. Proton exchange membrane fuel cell (PEMFC)
ii. Direct formic acid fuel cell (DFAFC)
iii. Direct ethanol fuel cell (DEFC)
iv. Alkaline fuel cell (AFC)
v. Proton ceramic fuel cell (PCFC)
vi. Direct borohydride fuel cell (DBFC)
vii. Phosphoric acid fuel cell (PAFC)
viii. Molten carbonate fuel cell (MCFC)
ix. Solid oxide fuel cell (SOFC)

Batteries

An externally assembled battery is a chemical energy storage device made up of one or more electrochemical cells. It allows electrons to flow from the anode to the cathode via an external circuit. It is composed of two electrode terminals: the cathode (positive) and the anode (negative). The tendency of the reactants to go through chemical changes that result in the production of lower energy products triggers a redox reaction when they are connected to a load. The load receives this electrical energy conversion from the chemical energy source through an external connection.

In addition to the anode and cathode, the electrolyte plays a crucial role within the battery structure. It serves as an ion-conducting medium, and moreover is electronically insulating, meaning it only conducts ions and not electrons. However, while facilitating ionic conduction, the electrolyte enables electron transport through the external circuit, thus completing the electrochemical circuit.[11–13]

Batteries are broadly categorized into two types: *primary batteries and secondary batteries,* primarily distinguished by their rechargeability. Primary batteries, often termed non-rechargeable batteries, cannot undergo recharging due to the irreversible chemical reactions that occur upon discharge. Some of the prominent examples of primary batteries are lead acid batteries and nickel cadmium batteries. Consequently, they are commonly referred to as single-use or disposable batteries. As a result of their finite lifespan and inability to replenish energy, primary batteries fall short in meeting the escalating demand for energy.[11,14]

Rechargeable batteries, commonly referred to as secondary batteries, were developed in response to this constraint. A secondary battery's anode experiences reduction during charging while the cathode undergoes oxidation, giving off electrons. On the other hand, during discharge, the opposite procedure occurs. The electrolyte does not undergo oxidation or reduction throughout these cycles of charging and draining. As a result, rechargeable batteries have a long operating life before their basic parts—such as electrodes and electrolytes—wear out from repeated cycles of charging and discharging. As such, they offer a more ecologically responsible, economically feasible, and sustainable substitute for traditional power sources.

Lithium-ion secondary batteries

Lithium-ion batteries (LIBs) have emerged as the primary choice among secondary batteries for electrochemical energy storage, surpassing alternatives such as nickel-cadmium, lead-acid, nickel-zinc, and nickel-iron batteries. This superiority stems from several factors, including their low reduction potential, rapid diffusion, facile compatibility of lithium ions within various solid matrices, and high volumetric power density. As depicted in the Figure 1.4, a standard LIB comprises an anode capable of lithium intercalation or alloying or undergoing a redox reaction (e.g., graphite or silicon, redox organic polymers) and a cathode constructed from lithium-rich materials based on transition metal oxides like lithium cobalt oxide. Additionally, it features a porous polymer separator and an organic electrolyte containing lithium salt. Unlike other secondary batteries that generate energy through reversible redox reactions of electrode materials, the fundamental mechanism of a typical LIB hinges on "intercalation" chemistry.[11,14,15]

Working principle: Figure 1.4 provides a schematic outlining of the working principle of a lithium-ion battery. The electrode at which reaction occurs at lower potential or the electrode where oxidation occurs is termed as a cathode and similarly the electrode at

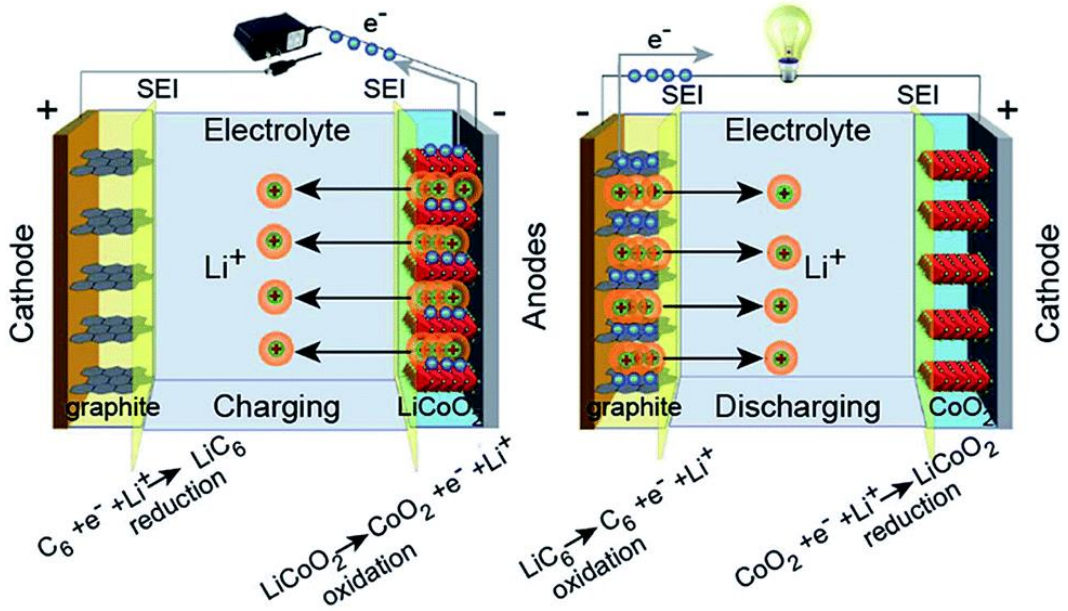

Fig 1.4 Schematic representation of working principle of a lithium-ion battery

which reaction occurs at higher potential or the electrode at which reduction takes places is anode. Lithium atoms on the positive electrode of a lithium-ion battery (LIB) are oxidized during the charge phase, producing lithium ions in the process. After migrating through the electrolyte to the negatively charged anode, these ions absorb an electron that is moved from the cathode to the anode via an external circuit. Conversely, during the discharge phase, the intercalated lithium within the anode's structure migrates back to the cathode through the electrolyte. This reversible process facilitates the exchange and shuttling of lithium ions between the electrodes, balanced by the electron flow in the external circuit. Electrolyte is sandwiched between both the electrodes. The general redox reaction in case of $LiCoO_2$ and graphite electrode materials are as follows[16,17]:

Cathode: $LiCoO_2 = CoO_2 + Li^+ + e^-$

Anode: $Li^+ + e^- + C_6 = LiC_6$

Full reaction: $LiCoO_2 + C_6 = LiC_6 + CoO_2$

A pictorial representation has been presented in Fig 1.5 outlining the growth of the lithium-ion batteries in the recent past.

A brief overview of basic components of a lithium-ion battery has been presented below.

Electrolyte

The development of lithium-ion batteries with high energy density, power density, and extended cycle life is largely dependent on the chemistry of the electrolytes. In order to create innovative electrolytes for enhanced lithium batteries, sophisticated research on

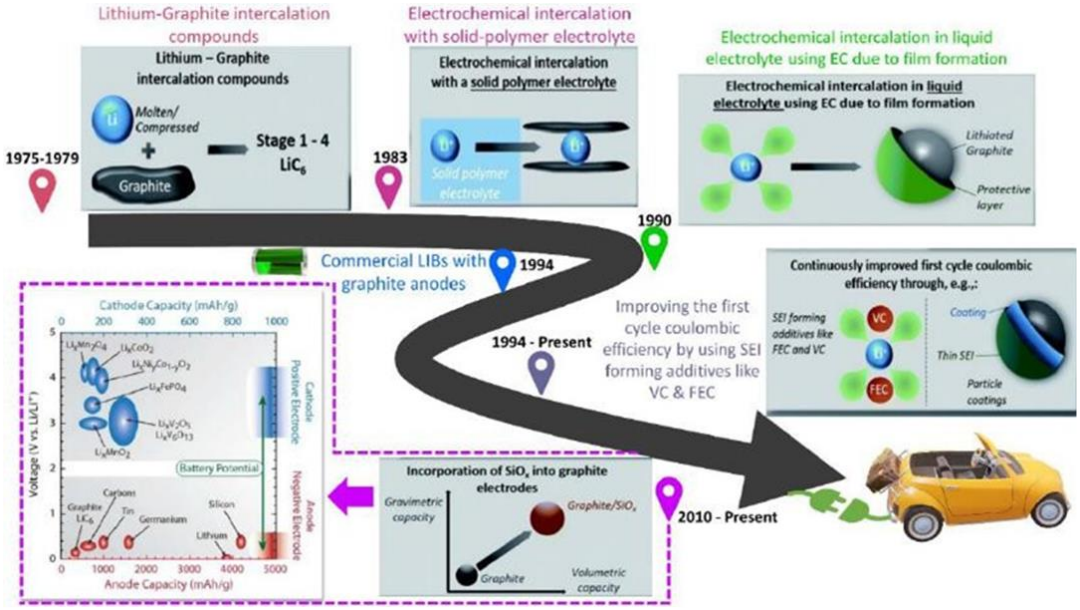

Fig 1.5 Growth of Lithium-ion battery in the recent past

new electrolytes has been conducted in conjunction with electrodes, binders, and salts. The following are the distinctive qualities of electrolytes:

i. High ionic conductivity $>10^{-4}$ S/cm and low electronic conductivity (10^{-10} S/cm).
ii. Inert towards cell components to prevent explosion or short circuit.
iii. Low glass transition temperature for faster ion kinetics.
iv. Lower crystallinity leads to better ionic conductivity.
v. Wide potential stability window for high energy density batteries.
vi. High trade-off temperature of electrolyte degradation.
vii. High cation transference number.

Binders

Binders play a crucial role in lithium-ion batteries by connecting the active material, conductive additive, and current collector at both the anode and cathode sides. Research on binders is generally less discussed. However, there is an increasing need for long cyclability, particularly for electric vehicles and portable electronics, which means that improved binders need to be thoroughly researched.

They majorly play two crucial roles:

(i)providing mechanical strength to active material during continuous cycling.

(ii)maintaining adhesion with current collector.

(iii) plays a significant role in the composition and morphology of the Solid Electrolyte Interphase (SEI).

Traditional binders, often based on polyvinylidene fluoride (PVDF) or its copolymers,

have been widely employed due to their excellent adhesion properties and chemical stability. However, when used in high-loading electrodes or in combination with silicon-based anode materials, which experience large volume changes during cycling, PVDF-based binders may have certain drawbacks, such as reduced flexibility and increased brittleness.

To get over these problems and enhance the functionality of LIB anodes, researchers have investigated employing various polymeric binders. Using polymeric binders has several advantages, including higher robustness against mechanical stress caused by volume variations, improved flexibility, and greater compatibility with high-capacity active materials. Some well-known examples of polymeric binders are sodium alginate, poly (acrylic acid) (PAA), styrene-butadiene rubber (SBR), and carboxymethyl cellulose (CMC). Polymeric ionic liquids are among the numerous classes of polymers that have garnered interest lately (PILs). PILs contain ionic liquid moieties attached to the polymer backbones thus exhibiting synergistic effects of both components. Recently, Matsumi et.al have reported the synthesis and application of an allylimidazolium-based poly(ionic liquids) as anodic binder for graphite.[18] Owing to the increased wettability and lowered LUMO leading to a thin SEI, a higher lithium-ion diffusion coefficient was obtained. Further, a discharge capacity of 210 mAh/g was observed at 1C with 95 % capacity retention even up to 500 cycles in contrast to 140 mAh/g for PVDF based anodic half cells.[19]

Also, the synthesis and application of a robust polymerized BIAN (p-BIAN) based binders for stabilization of graphite and silicon anodes have been studied. The excellent performance of these type of binders was attributed to the low-lying LUMO that enabled n-doping during lithiation and facilitated the formation of a thin SEI leading to lowered impedance and enhanced lithium-ion diffusion. The p-BIAN moiety of the composite provided n-type characteristics and dynamic self-healing electrostatic hydrogen bonding leading to robust mechanical support in case of Si based anodes.[18,19] Besides, the design of the lithiated composite BIAN/LiPAA not only helped in providing structural integrity at faster current rates of 10C in graphite but also helped in lowering the activation energy and increasing the diffusion coefficient across the interface.[20]

Overall, the choice of binder for LIB anodes depends on factors such as electrode composition, desired performance characteristics, and manufacturing considerations. Polymeric binders offer a promising avenue for optimizing the performance and durability of LIB electrodes, paving the way for advancements in lithium-ion battery technology.

Cathodes

The other important component of any secondary battery is the cathode which plays a critical role in lithium-ion batteries (LIBs), serving as the site of lithium-ion insertion and extraction during charge and discharge cycles. The most common cathode materials used in commercial LIBs include transition metal oxides, such as lithium cobalt oxide ($LiCoO_2$), lithium nickel manganese cobalt oxide ($LiNiMnCoO_2$ or NMC), lithium iron phosphate ($LiFePO_4$), and lithium manganese oxide ($LiMn_2O_4$). Each material offers unique advantages and limitations, making them suitable for different applications and performance requirements.

The high energy density and steady cycling behavior of lithium cobalt oxide ($LiCoO_2$) made it one of the first cathode materials for lithium-ion batteries to be commercialized. Notwithstanding, apprehensions regarding the expense, scarcity, and safety risks associated with cobalt, especially at elevated voltages, have spurred investigations into substituting cobalt with alternative transition metals such as manganese, aluminum, and nickel in varying ratios, with the aim of attaining elevated capacity, durability and potential energy density.

Lithium nickel manganese cobalt oxide (NMC) cathodes, with varying ratios of nickel, manganese, and cobalt, offer improved energy density, cycling stability, and safety compared to $LiCoO_2$. NMC cathodes are widely used in electric vehicles (EVs) and portable electronics, where high energy density and long cycle life are critical.
Lithium iron phosphate ($LiFePO_4$) cathodes are known for their excellent thermal stability, safety, and long cycle life, making them suitable for applications requiring high power output and durability, such as power tools and energy storage systems. To further enhance the energy density, sustainability, and safety of LIBs, ongoing research efforts are concentrated on creating novel cathode chemistries, such as solid-state cathodes, sulfur-based cathodes, and lithium-rich layered oxides, in addition to these conventional cathode materials.[14,21,22]

Anodes

The electrode at which reaction occurs at higher potential or the electrode at which reduction takes place is known as anode. Based on the mechanism by which Li-ions are stored, anodes can be classified into three different types such as intercalation-type, conversion-type, and alloy-type

Intercalation type anodes

The intercalation-type anodes mainly include carbonaceous anodes (e.g., graphite) however transition metal oxides (TMO) can also be intercalation type TMOs or conversion type TMOs. Apart from modified graphite and other carbon-based anodes, intercalated TMOs are also gaining attention. The insertion of ions into intercalated TMOs does not cause any crystal structure distortion. Further, it also causes insignificant volume changes. Intercalated TMOs such as TiO_2, $Li_4Ti_5O_{12}$ (LTO), and $Na_2Ti_3O_7$ store Li-ions using titanium as redox active site wherein it is reduced to Ti^{3+} when lithiated and oxidizes to Ti^{4+} when de-lithiated. The specific advantage of anodes like LTO lies in their high lithiation potential of 1.5 V Li/Li+ which eliminates chances of Li-plating and SEI film formation thus facilitating Li-ion diffusion. Carbon based anodes are especially attractive for commercial LIBs due to their features such as low toxicity, low cost of production, widespread availability, and high electronic conductivity.[15,17,23,24]

Conversion type anodes

The primary characteristics of conversion type anodes are their high specific capacity and stable cycling. LiO_2 is formed via the lithiation of conversion type TMOs, whereas TMOs themselves are converted back to TMOs during de-lithiation. Low ionic conductivity and volume expansion are two common issues with TMOs. A few example of conversion-based TMOs include Fe_2O_3, Co_3O_4, MnO, CuO, and NiO. Dichalcogenides of transition metals (TMDs) can also be classified as conversion or conversion-alloying types. MoS_2 has been extensively studied as a TMD, mostly because of its layered structure's resemblance to graphite.[25–27]

Alloy type anodes

Semi-metallic materials like Si and Ge are combined with metallic elements like Sn, Sb, and Bi to create alloy type anodes. Because these anodes alloy with numerous Li-ions to create $Li_{4.4}Si$, $Li_{2.5}Sn$, and other compounds, they are well recognized for having large specific capacities. Theoretical capacities of elements like Si, Sn, Ge, and Sb are as high as 4200, 994, 1625, and 665 mAh/g, respectively. The alloy anodes have a high specific capacity and can operate at a safe working voltage of 0.3-0.6 V versus Li/Li+, which is significantly higher than the 0.0 V Li-plating potential. Based on the research conducted by various groups, alloy type anodes mainly face three drawbacks:[28,29]

i) Material pulverization: During lithiation, alloy-type anodes, including silicon (Si) and tin (Sn), have a large volume expansion (>300%). The sharp expansion causes mechanical stress inside the electrode, which in turn causes the active material particles to shatter and pulverize.

ii) Loss of electrical contact with neighboring particles: Particles separate from the current collector because of mechanical stress that material pulverization places on the electrode structure. The separation between the active material and the current collector is made worse by the active material's volume expansion and contraction during charge-discharge cycles.

iii) Unstable Solid Electrolyte Interface: Due to mechanical fatigue during cycling, an unstable SEI may result in electrolyte loss and thicker SEI which impedes the fast charging and increases the resistance at the interface.

Organic anodes

Because of their low carbon footprint, sustainable production, and structure tunability, organic electrodes have also garnered a lot of interest and have emerged as a compelling substitute. Unfortunately, their broad and practical applications have been limited due to the low electronic conductivity and solubility of the organic molecules in the electrolyte, which causes a subsequent loss in capacity. Based on polyacetylene, polyaniline, polypyrene, and polythiophenes, these are the most researched conductive organic polymers. It is commonly known that Li-ions are stored by conductive polymers via redox processes. The imine response is one of the most studied tactics. Furthermore, since the organic electrodes' kinetics depend on the electron transfer of the redox reactions and the migration ratio of electrolyte ions, we can anticipate enhanced kinetics there as well.[30–34] Also, the limitations of these small organic molecules are overcome by covalent organic polymers and porous organic polymers. Especially the high crystallinity, ordered frameworks, and uniformly distributed pores favor excellent conductivity and can support fast charging. Furthermore, a highly networked structure guarantees low solubility, enhancing the materials' cyclability. Lithium coordination occurs on active sites, as demonstrated by DFT simulations and ex-situ techniques. Therefore, a higher number of active sites may contribute to a higher number of lithiation sites, possibly increasing the specific capacity. Recently, Matsumi et.al., reported the application of a BIAN-melamine based n-type porous organic polymer (PBM) as anode in lithium-ion battery.[35] The presence of nitrogen rich triazine moiety in the framework of the anode led to a higher reversible capacity and faster kinetics. At a current density of 750 mA/g, a reversible capacity of 740 mAh/g was observed for 2000 cycles with a coulombic efficiency of more than 99%.

2D materials

The range of two-dimensional (2D) materials is expected to broaden in the decades to come beyond graphene and its derivatives made of weakly bound van der Waals solids.

Two-dimensional (2D) materials have piqued the curiosity of researchers due to their large specific surface area. In addition to offering open 2D channels for quick ion transport and electrochemically active sites for ion storage, these materials effectively manage the mechanical strain brought on by volume change during cycling. Moreover, the reduced dimensions may shorten the routes for electron and ion transport..[26] The horizons with 2D materials as anodes are further expanded with black phosphorus (BP) which renders a higher theoretical capacity of 2596 mAh/g. However, its wide range of commercial uses has been constrained by its significant volume increase during the electrochemical process. According to recent findings, layered transition metal sulfides, such MoS_2, have been used because of their weak van der Waals contacts and ability to support Li insertion/extraction without significantly altering volume changes, which leads to increased cycling stability. The intrinsic structural design of many 2D materials can be well exploited for their application in fast charging batteries. The presence of boron honeycomb surfaces and multivalent transition metal atoms can provide much more interesting platforms for exploring the applications of the 2D materials based on the transition metal borides. Recently, Matsumi et. al., reported the application of a transition metal diboride based nanostructure–titanium diboride (TiB_2) hierarchical nanosheets (THNS) as anode material in LIBs which demonstrated a capacity of 385 mAh/g, at 0.025 A/g and at high current densities of 15 and 20 A/g, the capacity was observed to be 60 mAh/g with a charge-discharge time between 9 and 15 seconds.[36] This vouchsafes for the fact that indeed 2D transition materials can support ultrafast charge-discharge applications.

Strategies to obtain high power density and fast charging capability.

Heteroatom doping

One of the best methods for enhancing anode material electronic conductivity (σ), lithium-ion diffusivity, electrode wettability, and quick charging capability is heteroatom doping. N, S, P and B heteroatom doping in carbon materials is a broadly explored topic particularly with respect to active materials in battery anodes.[30,37,38] Generally, boron doping introduces p-type characteristics to the carbon framework by introducing holes with charge carriers and tuning the band gap thereby promoting excellent electron conductive properties. N-doping raises σ by p-π conjugation between lone pair electrons of nitrogen and π electrons of the carbon framework. P and S, being n-type dopants, also considerably contribute to σ. Apart from these, N, S and P doping introduce redox active sites which can store Li-ions through surface interactions called pseudo capacitance.[39,40] By virtue of the larger atomic size of N (75 pm), S (102 pm), and P(195 pm) than C(77

pm), they also enlarge the distance between planes which is further helpful for faster diffusion of Li-ions thus increasing the mass transport in electrode bulk. Recently, Matsumi et.al for the first time reported the synthesis of a heavily nitrogen doped carbon PYPBI800, from the pyrolysis of a bio-derivable poly(2,5-benzimidazole) (PBI) at 800°C, which had ~17 wt% nitrogen content and exhibited extremely fast charging (XFC) capability at 18.6 A/g and ultralong cyclability (3000 cycles) with 90% capacity retention. Further, the full cells fabricated using PY-PBI-800 based anodes and $LiCoO_2$ based cathodes an excellent cycling performance with a high initial capacity of 1.69 mA h and average coulombic efficiency of 99.9% with capacity retention of ~80% even after 350 cycles delivered at 0.2C current density (1.5 mAh/cm^2 = 1C). The XFC capability of this carbon material has been attributed to the conglomerative effects of heavy nitrogen doping, increased defect sites as well as enlarged d-spacing.[41]

Moreover, porous organic polymer based precursors can be used as a single source for obtaining uniformly distributed heteroatoms. Mitra et al studied the structural and morphological characteristics of a N-doped carbon derived from BIAN based porous organic polymer (PBM) at carbonization temperatures of 600 and 800°C (PyPBM 600 and PyPBM 800) and assessed their Li-ion storage properties. PyPBM600 and PyPBM800 based anodic half-cells demonstrated exceptional rate capability and capacity up to 4 A/g for more than 1000 cycles. Additionally, the full cell with PyPBM800 15-minute charging time, a 1.2 mAh reversible capacity, and 99.8% columbic efficiency.[42]

Microstructure regulation

Another effective strategy for promoting Li-ion kinetics at the material level is through modification of the microstructure of the anode, for example, introduction of pores and disorderliness in the carbon planes. Porous structure helps in reducing the ion diffusion length for Li-ions. It also improves the wettability of the anode material through increased electrode-electrolyte interaction thereby reducing the impedance at the anode surface. Ordered porous carbons are well known for their fast Li-ion kinetics owing to the presence of ordered pathways for ion diffusion. A detailed overview has been provided in chapter 3 where applications of hierarchical micro and mesoporous carbon as active materials in lithium and sodium ion batteries have been explored.

Hard carbons are another class of carbon materials which have been excellent contenders for high power density applications owing to their short-range graphitized domains and enlarged d-spacing than graphite. The disordered arrangement of graphitic domains introduces defect sites and pores which act as ion storage sites as well as transport channels for ions. However, the boon itself turns into a bane when a full cell is fabricated.

The large number of defects and nanovoids irreversibly trap ions leading to a significant lithium inventory loss.[6,40,43]

Sodium ion batteries

As we have understood so far, energy production and storage technologies have gained significant attention for various everyday applications. We realize that LIBs have become ubiquitous in most portable electronic devices and zero-emission electric vehicles, contributing to their widespread adoption. However, concerns have emerged regarding the integration of renewable energy sources into the grid, load leveling, and the sustainability of lithium sources due to their limited availability and potential price escalation. Furthermore, the uneven distribution of lithium in earth's crust is another major concern. Consequently, the ability of LIBs alone to meet the escalating demand for energy storage across small to large scales remains uncertain.

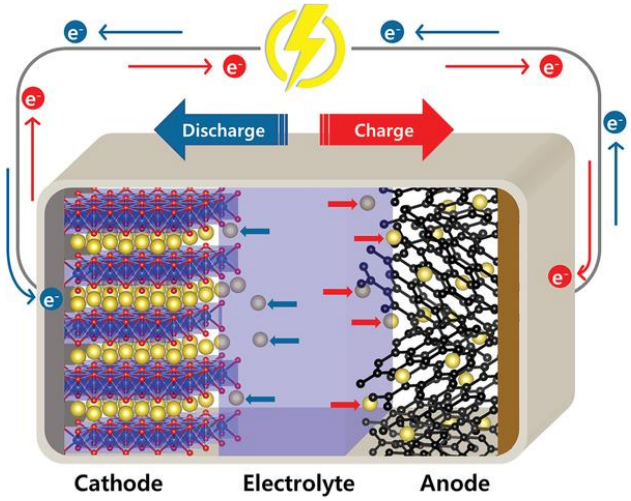

Figure 1.6 Schematic of the working principle of a sodium-ion battery.

In response to the challenges faced by current energy storage technologies, recent research has increasingly focused on the development of alternative systems, with sodium-ion batteries (SIBs) emerging as promising candidates. Due to the natural abundance of sodium and its chemical properties that closely resemble lithium, SIBs offer significant potential as next-generation alternatives to lithium-ion batteries (LIBs). Notable advancements have been made in the development of sodiated layer transition metal oxides, phosphates, and organic compounds as cathode materials for SIBs. Similarly, significant progress has been achieved in utilizing various carbonaceous materials, transition metal oxides (or sulfides), intermetallic compounds, and organic compounds as anode materials. Beyond electrode materials, the realization of practical

SIBs also depends critically on the development of suitable electrolytes, additives, and binders.[27,44–46]

Despite strides in electrode materials and ancillary components, challenges persist, including cell design optimization and electrode balancing, hindering the widespread application of sodium-ion cells. Fig 1.6 shows the basic components of a sodium ion battery.

Hard carbons have been the subject of much research for use as anode materials in sodium-ion batteries. A general mechanism explaining the observed electrochemical processes is, however, still lacking, despite the interesting explanations that have been offered. Also, research has grown towards optimizing the Initial Columbic Efficiency (ICE) by electrolyte optimization, defect and surface engineering, and presodiation process. Moreover, microstructure regulation can be an effective method to develop anodes suitable for fast charging applications. Developing porous structures is an effective strategy. Furthermore, heteroatoms like sulfur can be introduced to increase the d-spacing of carbon and hence accommodate the larger Na^+ ions.

The selection of electrolytes for sodium-ion batteries (SIBs) is crucial and is primarily guided by considerations of conductivity and electrochemical stability. Given that SIBs operate within a voltage range of 2.5 to 4.3 V, aqueous electrolytes are unsuitable as they decompose at a potential lower than 1.23 V versus H^+/H_2. Electrolytes for SIBs can take include aqueous, organic, solid-state, hybrid, or ionic liquids. Aqueous-based sodium-ion batteries, for instance, exhibit lower specific energies and rate capabilities compared to lithium-ion batteries. Also, solid-state electrolytes are emerging as a promising avenue for enhancing battery safety, reducing flammability risks, and improving electrochemical stability. A well-known sulfide-based inorganic solid electrolyte (Cubic Na_3PS_4) electrolyte is reported to have a high conductivity (10^4 S/cm) at room temperature. Ionic liquid-based electrolytes like NaTFSI-Pyr_{14}TFSI in Na-ion battery reported by Hasa et al shows an overall ionic conductivity of 10^{-3} S/ cm and 10^{-2} S /cm.[44,47] Cathodes for SIBs are another major area of research. Cathodes in sodium-ion batteries require materials with high sodium ion insertion/extraction capabilities and good structural stability. Sodium transition metal oxides, such as $NaCoO_2$, $NaFePO_4$, and $Na_3V_2(PO_4)_3$, are widely studied cathode materials for SIBs.

Outline of this thesis

The underlying objective of this research work is to explore and understand the applications of conjugated organic polymers embedding donor acceptor moieties and

exploiting their structural and chemical characteristics to increase the power density of energy devices. The aim of carrying out such a research work is to add to the understandings and knowledge of the scientific community about the potential advantages of designing a donor-acceptor based conjugated polymers which can act as active materials in LIBs. The research also motivates the development of fundamental science and accelerates the generation of new and potentially commercial and industrial products in the field of LIBs and SIBs.

Outline of Chapter 1:

The first chapter outlines a general introduction to energy storage systems and in particular, lithium-ion batteries, a field in which the research has frog leaped during the last couple of decades.

Outline of Chapter 2:

In the second chapter, the synthesis and application of a novel donor acceptor type conjugated network polymer as an active material in Li-ion secondary battery has been elucidated and its remarkable capability to support extremely fast charge-discharge has been discussed which is in direct relation to its structural advantages.

Uniqueness: In the recent past, most of the research that has been carried out in the field of COFs has been about employing n-type polymers for energy storage. In comparison, very few research work has been dedicated towards designing donor-acceptor type conjugated polymers with an innate porosity. Furthermore, the donor acceptor based microporous polymers do not outline simple synthetic procedures. Even though D-A type conjugated porous polymers have been explored for their optical properties, such polymers have not been well explored in Li-ion batteries. Moreover, D-A polymer with a rhombus type pore structure has not been explored for their lithium storage properties and mass transport properties which can benefit significantly the fast-charging applications. Rhombic-shape pores render the advantages of both acute and obtuse angles in each pore, and this can result in obtaining two different environments at the corner nanogrooves. The acute and obtuse angles create different diffusion pathways, allowing ions to move more efficiently through both narrow and wide channels. Besides, the sharp corners of the acute angles can enhance capillary action, drawing lithium ions into the pores more effectively. Hence, designing such porous materials can be advantageous for a faster and efficient mass and charge transport and the D-A pair can result in an increase in the power density, leading to development of more efficient battery systems.

Outline of Chapter 3:

Building upon the second chapter, in the third chapter, a triazine-bithiophene based porous organic polymer has been designed and is used as a precursor material for carbons.

Pore architecture manipulation plays an important role in the development of fast charging anode materials and in this regard, organic polymers with innate porosity provide an interesting avenue for pore structure engineering. Hence, herein the advantages of such carbon materials have been explored in the field of lithium-ion batteries.

Since current day techniques involve use of hazardous chemicals and expensive techniques to design porous materials, POP/COF based precursors can be a strategic imperative. The innate porosity and the high surface area of such polymers can be exploited to derive high surface area hierarchical nanoporous carbon. Furthermore, since the textural properties affect the electrochemical and charge storage properties, in this chapter, the change in the textural properties with change in the carbonization temperature was studied and its effect on the charge storage properties was evaluated.

Outline of Chapter 4:

Chapter 4 serves as a comprehensive summary, consolidating the outcomes and insights obtained from these explorations and scientific endeavors and a note on prospects of such materials.

CHAPTER 2 DONOR ACCEPTOR BASED CONJUGATED POLYMERIC ACTIVE MATERIAL WITH ENHANCED PSEUDOCAPACITIVE CONTRIBUTION FOR ULTRA-FAST CHARGING LITHIUM-ION BATTERIES.

Abstract

In the current LIBs, the capacity and the fast-charging applications are limited by the available active materials. In this regard, organic conjugated polymers, due to their tunability in the structure and high conductivity, have gained much focus in the current research community. Further, the introduction of a donor-acceptor structure into the framework helps in achieving a very narrow band gap between the HOMO and LUMO levels and enhances the electronic interaction, thereby increasing the power density. Hence, such organic polymers are expected to aid in fast-charging applications and help render a very high capacity making them an attractive choice as an anode material. Therefore, in this work, a donor-acceptor based imine linked conjugated network type porous polymer, POL 202 was designed via a simple polycondensation reaction of 2,2'-Bithiophene-5,5'-dicarboxaldehyde and 1,2,4,5-Benzene tetraamine tetrahydrochloride. The charge storage mechanism was found to be predominantly by a pseudocapacitive process which becomes a crucial factor when we consider fast charging applications in batteries. The polymer delivered a very high capacity of 850 mAh/g at a current density of 100 mA/g with a capacity retention of 100%. Further a reversible capacity of 205 mAh/g at the current rate of 5000 mA/g and a capacity of 270 mAh/g was observed at the current rate of 2000 mA/g. A striking feature of this polymer was the total time for charging which was 8 mins at a current rate of 2000 mAh/g and 2.5 min at a current rate of 5000 mA/g, making it avery attractive avenue as a next-generation electrode material

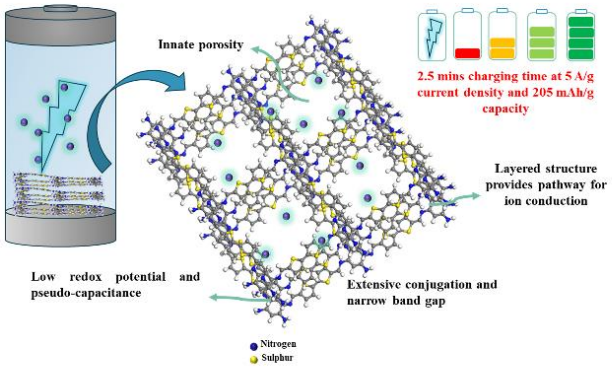

Introduction

With the growing energy needs of the ever-increasing population, the search for better alternatives of resources to meet the energy demands has always been on the fore. Traditional fossil fuels which are the common source of energy are in depletion and hence this makes the push for the search of renewable alternatives even more imminent. Further, the overuse of fossil fuels has resulted in serious climate issues like global warming and acid rain. Coupled with the recent rise in the consumer demands for electronic products and development in Electric Vehicles (EVs), the development of alternative renewable and clean energy resources is desirable, and the research has frog leaped during the last decade. In this regard, metal ion batteries, especially lithium-ion batteries (LIBs) have generated a huge interest in the scientific community.[13,15]

One of the key approaches recently made has been to develop and modify the electrode performance of anodes and develop batteries with faster charging rates and higher specific capacity. Graphite dominates the current day market, however the concerns about the cyclability and the specific capacity remain pertinent.[24,48,49] Further, its application in the fast charging is doubtful as the slow kinetics of lithium ions can result in plating and serious safety issues.[41] However, owing to its easy availability and low cost, it is widely used in commercial lithium-ion batteries. Recently, a lot of effort and focus have been directed using materials such as silicon and graphene as an anode material to increase the scope of lithium-ion batteries. Although graphene-based materials and silicon-based anodes offer better capacities, the expensive synthetic route to produce graphene and large volume expansion in the case of silicon in association with an unstable solid electrolyte interphase (SEI) has motivated scientists to look for alternatives which can support fast charging rates and at the same time can deliver a higher capacity.[35]

One of the approaches can be that of building molecules which can shorten the diffusion length. It is very desirable to design LIB electrodes with the lowest possible through-plane (i.e., along the electrode thickness) tortuosity factor. We can understand the following statement through the equation i[50]

$$D_n = D_{eff} / D_o = \varepsilon / \tau \text{ (equation i)}$$

wherein 'D_n' is the normalized effective diffusion coefficient, 'D_{eff}' is the effective diffusion coefficient, 'D_o' is the bulk diffusion coefficient of the ionic species which is to be considered in the absence of any obstacles or porous structure, 'ε' is the porosity of the material, and 'τ' is the tortuosity factor, the path that the ions follow during the diffusion process.

Furthermore, introducing polarity in the active materials through heteroatom doping can result in an augmented performance of the anode because of pseudo capacitance by involving fast and reversible surface redox reactions.[46] Pseudocapacitive reactions and materials can render more stable and have lower degradation rates than materials where intercalation mechanism is seen for charge storage, resulting in improved cyclability and longer battery lifetimes.[51]

Owing to shorter diffusion length and pseudocapacitive charge storage properties, researchers have recently shifted their focus towards organic electrode materials. Moreover, in view of their potentially sustainable production and low carbon footprint, besides structure tunability and low electrode volume change and ample number of precursor materials that are available, they are being considered as potential candidates when it comes to their application in lithium-ion or lithium organic batteries.[38,52–55] A special position in the research development of organic anodes is held by porous organic polymers.

Though the research in the field of organic anodes, especially porous organic materials is in its early stages from an industrial perspective, it motivates the development of fundamental science and accelerates the generation of new and potentially commercial and industrial products.

The structural robustness of the materials offers us the advantage of strategically tweaking the energy levels by the introduction of heteroatoms which can result in better conductivity and electrochemical performance. In this regard, introduction of a donor acceptor (D-A) pair not only helps in tuning the band gap; but also, a low redox potential arising due to the strong electronic interaction between the D-A can result in the increase of the power density.[56] Introducing polarity in the active material can improve the performance of the anode because of pseudo capacitance.[57] A non-diffusional redox process can lead to pseudo capacitance which is a very important characteristic when it comes to overcoming slow and sluggish ion diffusion kinetics through the anode material. Furthermore, the electrical conductivity of organic charge transfer complexes (OCTC) has been reported to have an electrical conductivity of 8×10^{-10} S/cm which is 105 and 20 times higher than that of phenazine and Tetracyanoquinodimethane respectively.[58]

Chen et al. have reported the 2,4,6-triaminopyrimidine based organic anodic active materials with 1,3,5-triformylbenzene and 1,4-pthaladehyde, wherein the anodic half cells delivered a reversible discharge capacity of 401.3 and 379.1 mAh/g respectively.[59] Besides, there have been reports by Haldar et al which focuses on the application of a triazole- triformyl phloroglucinol-based active material, which delivered 720 mAh/g.[60] Wang et al have demonstrated hexaazatrinaphthylene based porous organic polymers as

organic cathode materials which deliver a high specific capacity of 309 mA h/g, and long-term cycling stability with 92% capacity retention after 1200 cycles.[61] Most of the work so far in the field of porous organic polymers has been dedicated to the 2D and 3D covalent organic frameworks (COFs) and there are several reports of their applications as high energy density anode materials.

It has also been observed that polymerization not only enhances the capacity of the organic material, but also results in the augmentation of the cyclability. Moreover, Liang and co-workers have studied the donor–acceptor based copolymers such as poly{[N,N′-bis(2-octyldodecyl)-1,4,5,8-naphthalenedicarboximide-2,6-diyl]-alt-5,5′-(2,2′-bithiophene)} or (P(NDI2OD-T2)) and poly{[N,N′-bis(2-octyldodecyl)-1,4,5,8-naphthalenedicarboximide-2,6-diyl]-alt-5,5′-[2,2′-(1,2-ethanediyl)bithiophene]} or (P(NDI2OD-TET)) and have shown their potential applications as ultrafast lithium-ion battery cathodes.[57]

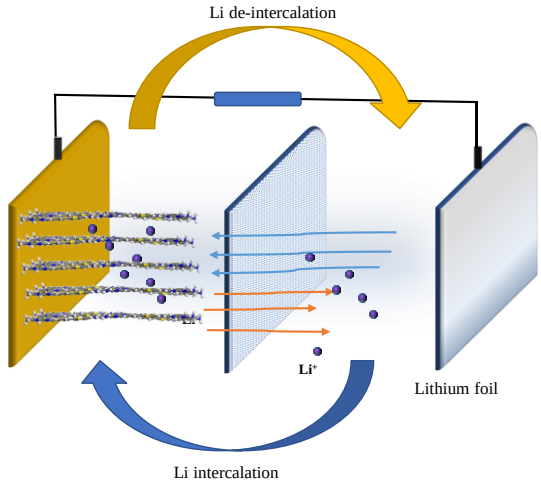

Fig 2.1: Schematic representation of POL 202 based Li-ion anodic half cell

Realizing the need to push the research in the field of organic polymers to exploit their potential as suitable anode materials, in this work a bithiophene based imine linked conjugated network type porous polymer, POL 202, which serves as an anodic active material for the LIBs will be presented. Thereby the issues of high energy density anode materials which can support fast charging applications through the design of this anode material is addressed. Even though it has been predicted that graphite is to dominate the market in upcoming years, this work adds to the understandings and knowledge of the scientific community about the potential advantages of designing a donor-acceptor based organic molecules which can act as charge host materials in LIBs. Hence, the research aims at exploring such materials and their prospective applications as anode materials.

Materials and Methods

Materials

2,2'-Bithiophene-5,5'-dicarboxaldehyde, glacial acetic acid and N-methyl pyrrolidone

(NMP) were purchased from Tokyo Chemical Industries, Ltd., and were used without further purification. 1,2,4,5-benzene tetraamine tetrahydro-chloride, 1.0 M $LiPF_6$(50/50) ethylene carbonate/diethyl carbonate (EC/DEC) electrolyte and poly(vinylidene difluoride) (PVDF) binder (molecular weight: 540,000) were purchased from Sigma-Aldrich. Battery-grade acetylene black was purchased from Denka Japan Private Co., Ltd. Copper foil of a thickness of 20μm was purchased from the Nilaco Corporation.

Synthesis

2,2'-Bithiophene-5,5'-dicarboxaldehyde (1 mmol, 222 mg) and 1,2,4,5-benzene tetraamine tetrahydrochloride (0.5 mmol, 142 mg) were taken in a Schlenk tube with 1:1 volume ratio of n-butanol (2 mL) and o-dichlorobenzene (2 mL). To the reaction mixture 0.2 mL of acetic acid (6 M) was added. The contents of the tube were degassed via three freeze-pump thaw cycles. The reaction was carried out at 120°C for 72 hours. A reddish-brown product was obtained which was filtered and was washed with 20 mL acetone and methanol. The product (yield amount=60%) was then dried at 80°C in vacuum following which it was used as the active material.

Synthetic Characterization

Following the synthesis of POL 202, the physical and chemical properties of the polymer were characterised using various techniques. The ATR-FTIR spectra were recorded with a PerkinElmer 100 FTIR spectrometer, averaging 50 scans at a resolution of 2 cm^{-1}. ^13C cross-polarized magic angle spinning (CP MAS) NMR measurements were performed using a Bruker Avance 500 MHz Solid State spectrometer equipped with a Bruker 4 mm double resonance probe-head, operating at a spinning rate of 10 kHz. X-ray photoelectron spectroscopy (XPS) measurements were conducted using a Fisons Instruments S-Probe TM 2803 instrument. Surface area and pore size distributions were determined using a BELSORP mini accelerated surface area and porosity analyser. Powder XRD studies were carried out on a SmartLab X-ray diffractometer (Rigaku) with Cu Kα radiation (λ = 0.154 nm, step size of 0.02°). Transmission Electron Microscopy (TEM) and Scanning TEM (STEM) observations were performed at an acceleration voltage of 200 kV using a JEM-ARM200F microscope from JEOL Ltd.

Electrode Fabrication

First, a slurry composing of POL 202 was used as the active material with PVDF as binder and acetylene black as the conductive additive in the weight ratio 80:10:10 in N-methylpyrrolidine (NMP) was prepared. The slurry was then cast onto a 20μm copper foil using a 0.1mm doctor blade and was dried under vacuum at 80°C for 24 hours. Then it

was roll pressed at 0.4 mm thickness at 80°C and electrodes were punched and weighed. The mass of the active material (80% of the weight of the electrode) was calculated to be between 1.0 mg and 1.1 mg (0.56 mg/cm^2) in the electrodes punched. Following this, CR2025 Li-ion anodic half cells were fabricated inside the glove box (H_2O and O_2 < 0.5ppm). Lithium metal was used as the counter and reference electrode and LiPF6 (1.0M in EC: DEC 50:50) was used as the electrolyte. Electrochemical studies were performed using lithium-ion anodic half cells (CR 2025) where lithium metal foil was used as the counter and reference electrode (Fig 2.1).

Electrochemical Test

Cyclic voltammetry (CV) studies were conducted using Bio-Logic Science Instruments, with a voltage range of 0.01-3.0 V and scan rates of 0.1, 0.3, 0.5, 0.8, and 1.0 mV/s to determine the lithium-ion diffusion coefficient in the anode. Electrochemical impedance spectroscopy (EIS) was performed before and after CV in the frequency range of 1.0 MHz to 0.1 Hz with an AC amplitude of 10 mV. Dynamic electrochemical impedance spectroscopy (DEIS) measurements were conducted at various voltage perturbations within the same frequency range and AC amplitude. Galvanostatic cycling measurements were carried out using an Electrofield ABE 1024 instrument, operating between 0.01-3.0 V in constant-current mode.

DFT Studies

The theoretical calculations were based on density functional theory in the DMol3 module of the Materials Studio. The Gibbs free energy was utilized to assess the energy levels of the lithiated states at various stages of lithiation. ΔG is evaluated using the following equation,

$$\Delta G = E_{Li+polymer} - E_{polymer}$$

where $E_{Li+polymer}$ is the energy of lithiated polymer and $E_{polymer}$ is the energy of POL 202 in the unlithiated state.

Results and Discussion

Material Characterization

POL 202 was synthesized by a polycondensation via a Schiff's base reaction between 2,2'-bithiophene-5,5'-dicarboxaldehyde and 1,2,4,5-benzene tetraamine tetrahydrochloride in a 1:1 volume ratio of n-butanol and o-dichlorobenzene as shown in Fig 2.2a. To characterize the obtained product, various physical and chemical techniques

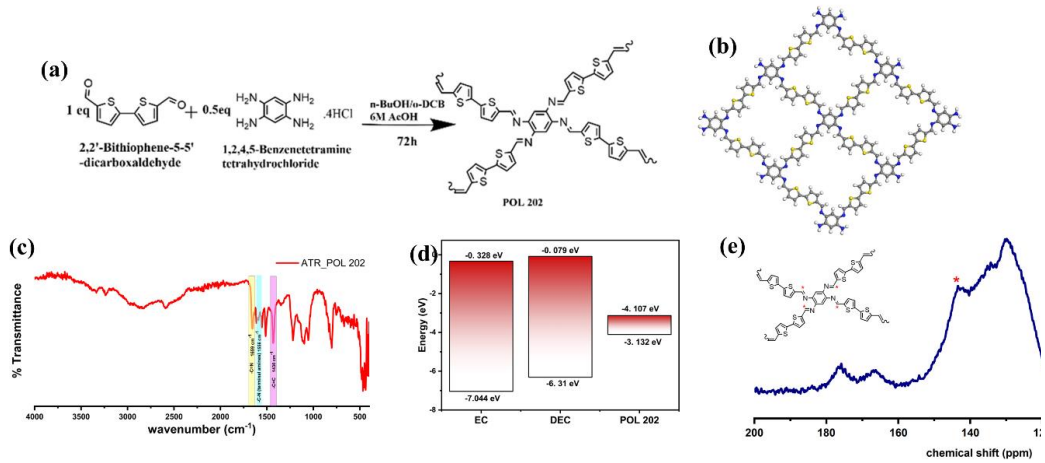

Fig 2.2 (a) Synthetic scheme for POL 202 (b) Computationally designed POL 202 (c)ATR spectrum of POL 202 (d) HOMO−LUMO energy level comparison of POL 202 with EC and DEC (e)ss-NMR spectrum of POL 202

were used. The HOMO and the LUMO energy levels were evaluated using DFT studies (DMol3 module of Material Studios software) (Figure 2.2d). The results show that the LUMO energy level of POL 202 is significantly lower than used EC: DEC-based electrolyte.

This ensures that the material undergoes reduction more easily than the electrolyte and

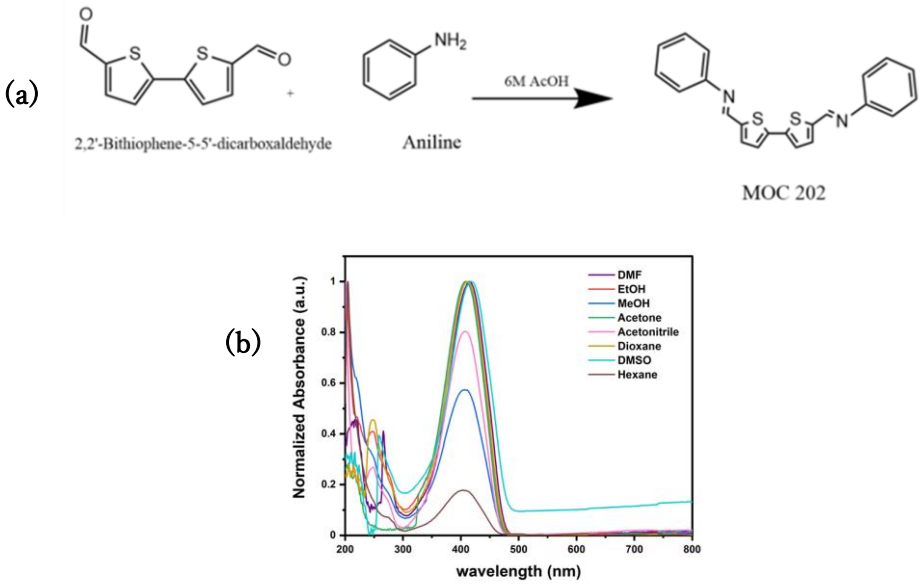

Fig 2.3 (a)Synthetic scheme for model compound MOC 202 (b)UV-Vis spectrophotometry absorbance plot of MOC 202

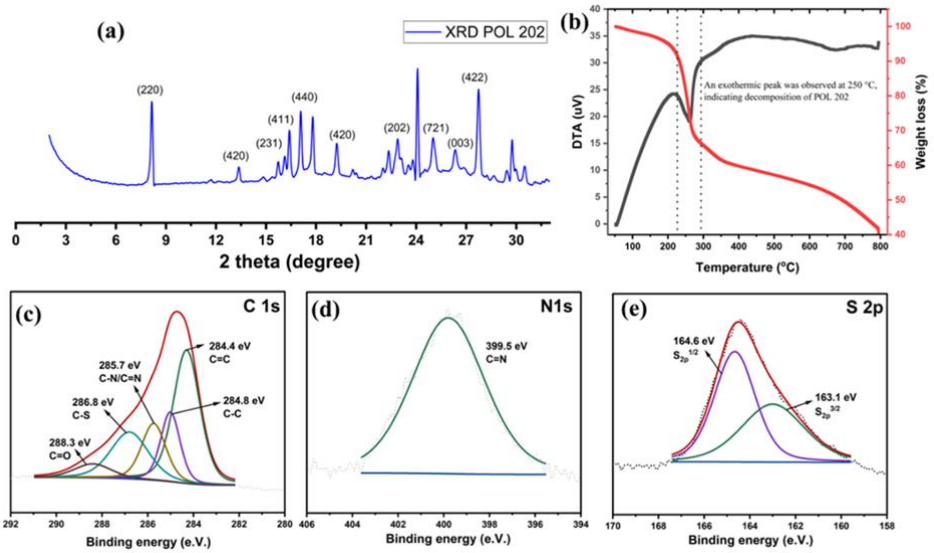

Fig 2.4 (a) (a) p-XRD diffractogram of POL 202 (b) TGA profile of POL 202 (c)Deconvoluted C 1s XPS spectra (d) Deconvoluted N 1s XPS spectra (e) Deconvoluted S 2p XPS spectra

there is no excessive reduction of the electrolyte during the initial charge discharge cycles.[62] In this kind of a molecule, we predicted that there is a charge transfer that can be occur between the N and the S moieties. To confirm this, a model compound MOC 202 was prepared using aniline and 2,2'-Bithiophene-5,5'-dicarboxaldehyde (Fig 2.3a). The intramolecular charge transfer was studied under different solvents spectrophotometrically and the results have been presented in Fig 2.3b and Table 2.1. An intramolecular charge transfer in these kinds of molecular systems ensures that there is a polarity that exists in the molecule, enhancing its electrochemical properties.

In the case of POL 202, an ATR-IR spectroscopy (Fig 2.2c) was conducted to understand the chemical nature of the bonds of the synthesized material. A peak at 1659 cm^{-1} was observed which corresponds to the imine -C=N bond in the polymer. Furthermore, the peaks at 1430 cm^{-1} correspond to the -C=C and this shift can be because of the extensive conjugation.[42] An XPS spectrum of the polymer showed the presence of carbon, nitrogen, and sulfur at their respective binding energies. On deconvolution, the carbon 1s (C 1s) spectrum (Fig 2.4c) showed the presence of -C=N bond at 298.5 eV and C-S bond at 284 eV. Further, on deconvolution of the nitrogen 1s spectra (N 1s) (Fig 2.4d), the 399.8 eV peak confirmed the presence of the -C=N (imine) linkage, and we can draw the conclusion of a successful synthesis of the polymer. Furthermore, the deconvoluted sulfur 2p spectra (S 2p) (Fig 2.4e) showed the presence of an S $2p^{3/2}$ and $2p^{1/2}$ doublet with an energy

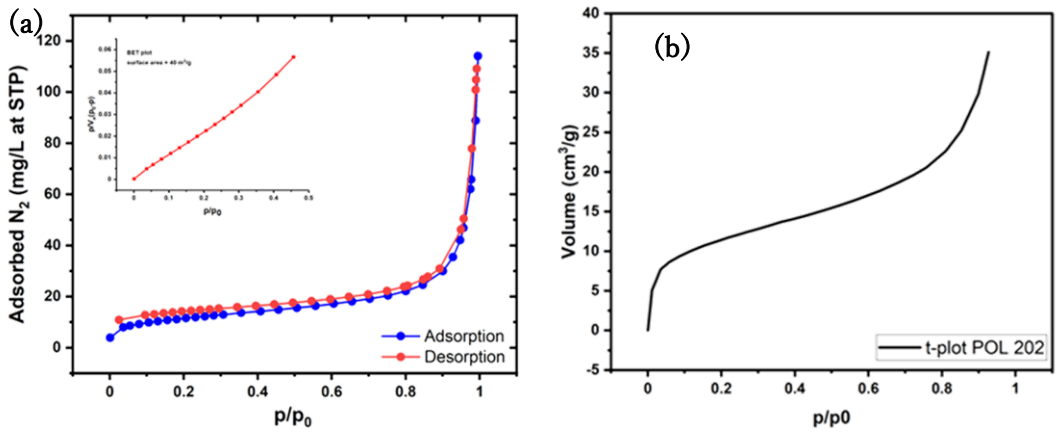

Fig 2.5 (a)Nitrogen adsorption isotherm of POL 202 (b)t-plot for micropore analysis of POL 202.

separation of 1.3 eV, which reconfirms the presence of C–S bonds.[35,63,64]

Table 2.1 Values of MOC 202 in different solvents with respective $E_T(30)$values and λmax(nm)

Solvent	$E_T(30)$	$\lambda_{max\ (nm)}$
Hexane	70.8	404
1,4-Dioxane	69.4	412
Acetone	70.1	408
DMF	69.2	413
DMSO	68.7	416
Acetonitrile	70.1	408
Ethanol	69.9	409
Methanol	70.4	406

In ^{13}C CP/MAS NMR spectrum (Fig 2.2e) for POL 202 a peak at ~144-145 ppm can be assigned to the carbon atoms of the C=N bonds, confirming the condensation reaction of aldehyde.[65] In addition, thermogravimetric analysis (TGA) studies were performed in the temperature range of 30–800 °C under flow of nitrogen (N_2) at 200 mL/min. Figure 2.4b illustrates the thermogravimetric analysis (TGA) profile of POL 202 under a nitrogen atmosphere, revealing a 5% weight loss between 50 and 200 °C attributed to desorption of adsorbed gas or moisture. A significant 60% weight loss occurs between 200 and 300 °C due to degradation of edge groups and the polymer backbone. Differential thermal analysis (DTA) indicated a molecular phase change around 260 °C, marked by an exothermic peak at 250 °C indicating POL 202 decomposition. Beyond 300 °C, a broad

plateau suggests a transition from a porous polymer to a carbonaceous material. X-ray diffraction (XRD) studies were conducted to examine crystallinity and morphology. Figure 2.4a displays a sharp peak at 8.0°, corresponding to the (2 2 0) plane, crucial for porous materials, suggesting an interlayer spacing of 0.98 nm conducive to Li-ion diffusion. Additional peaks at 13.35°, 15.73°, 16.42°, 17.1°, and 19.22° correspond to the (4 2 0), (2 3 1), (4 1 1), (4 4 1), and (4 2 0) planes, respectively, providing further insights into the material's crystalline structure.[66–68] The interlayer spacing of 0.98 nm supports enhanced lithium-ion diffusion through the anode material, reinforcing the potential of porous organic materials like POL 202 to facilitate fast charging. Nitrogen adsorption and desorption studies (Fig. 2.5a) were conducted to assess the surface area and porosity characteristics of POL 202. Utilizing the Brunauer-Emmett-Teller (BET) method, it was determined that the polymer exhibits a surface area of approximately 40 m^2/g. Besides, the pore diameter of the polymer was found out to be ~1.8 nm (Fig 2.5b) which is in very good agreement with the computational data. The pore volume was determined to be 0.1425 cm^3/g. The structure of the POL 202 was theoretically optimized using $DMOl^3$ module of Material Studios software and the pore diameter is well supported by BET and computationally determined value.

We expect the material to be layered taking into consideration the extensive π-π stacking and confirm such expectations of ours in the design of our experiment is correct since the TEM micrograph (Fig 2.6) show stacking structures with quasi-spherical shaped particles around 10 to 20 nm in size. Besides, the uniform distribution of the pores can be observed in the TEM images confirming the porous nature of the material.[69]

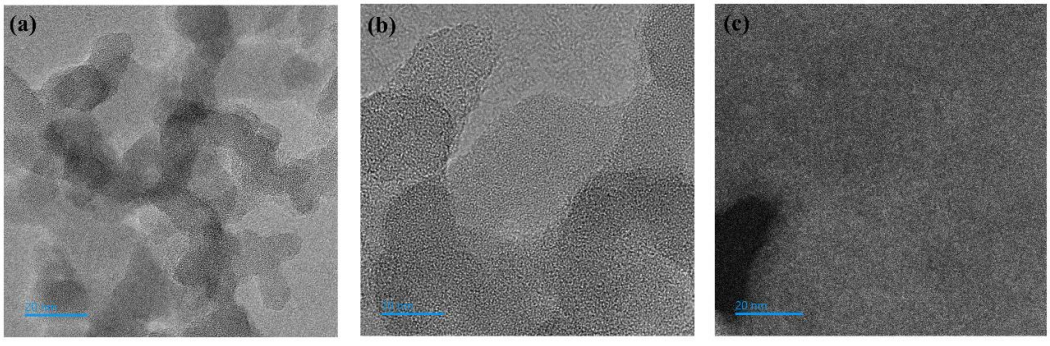

Fig 2.6 (a,b) TEM images of POL 202 at different magnifications showing the porous and stacked nature of the polymer (c)STEM image of POL 202 at 20nm.

Electrochemical Studies

Cyclic voltametric and impedance studies

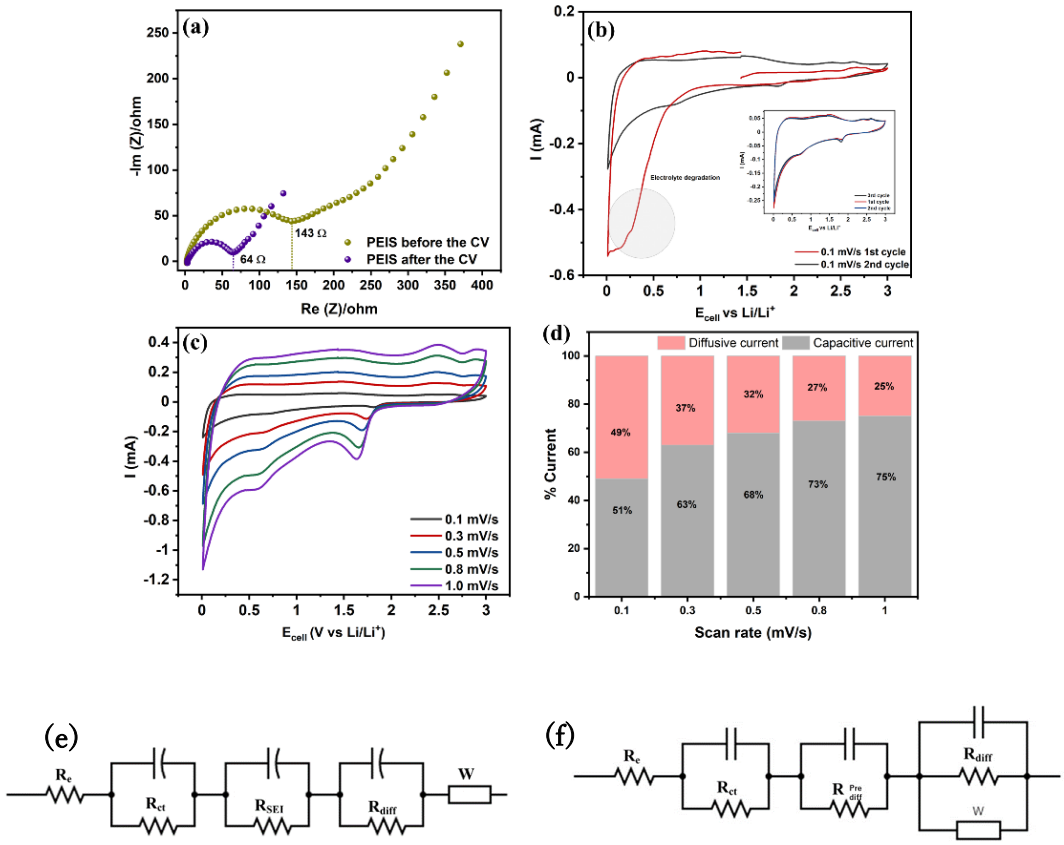

Fig 2.7 (a)PEIS Nyquist plot of Li-ion anodic half-cell before and after cyclic voltammetry (b) CV studies at 0.1 mV/s scan rate (c) CV studies at different scan rates (d) comparative data of the current contribution from capacitance and diffusion (e) Equivalent circuit used for fitting impedance data before conducting cyclic voltammetry (f)Equivalent circuit used for fitting impedance data after conducting cyclic voltammetry.

Cyclic voltametric (CV) studies were conducted for the CR 2025 cells in the potential window of 0.01V and 3V (vs Li/Li+) at a scan rate of 0.1 mV/s. During the initial cycle, asymmetric peaks were observed at 0.6/1.5 V and 2.5/1.6 V, in addition to an irreversible peak at 0.3 V during the lithiation half (Fig 2.7b). The irreversible peak at 0.3V can be assigned to the formation of the Solid Electrolyte Interface (SEI) layer due to electrolyte reduction. In the voltammogram half, the asymmetric peaks at 0.6/1.5 V can be assigned to the redox process taking place at the nitrogen moiety while the asymmetric peaks at 2.5/1.6V can be assigned to the redox process occurring at the thiophene unit.[70,71] At a

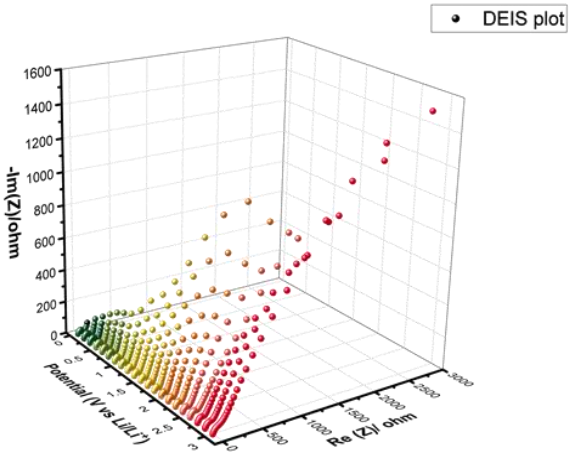

Fig 2.8 DEIS plot for the POL 202 based anodic half-cell recorded at different potentials between 0.01 and 3V (vs Li/Li$^+$)

scan rate of 0.1 mV/s, in the subsequent cycles, overlapping voltammograms were observed which shows the electrode stability. Potentiostatic Electrochemical Impedance Spectroscopy (PEIS) was conducted on OCV before and after CV studies. Figure 2.7a shows the Nyquist plots. As we observe, there is a significant decrease in the internal resistance of the cell after the CV studies were conducted. This can be attributed to the ease of lithium-ion diffusion through the interface facilitated by the conductive solid electrolyte interphase (SEI) layer.[35,72]Additionally, equivalent circuit fitting was performed, and the contributions of individual components were recorded (Figure 2.7e, f). Galvanostatic charge-discharge studies were conducted in the potential range of 0.01-3 V vs. Li/Li$^+$ at various current densities to evaluate the specific capacity of the active material POL 202 when used as an electrode. Dynamic Electrochemical Impedance Spectroscopy (DEIS) was also conducted to understand and analyze the types of interfaces and their contribution to the impedance.

Table 2.2 Circuit fitting details for PEIS data

	R_e	R_{ct}	R_s	R_{diff}	χ^2
Before CV (ohms)	2.198	36.4	111.6	269.5	9.35×10^{-4}
After CV (ohms)	0.2417	2.82	54.76	51.71	5.72×10^{-4}

Rate and long cycling studies.

Rate studies and long cycling studies were conducted to understand the capacity and cyclability of the cells at very high current densities of 1000, 2000 and 5000 mA/g. At a current density of 50 mAh/g the specific capacity of POL 202 was recorded to be 850

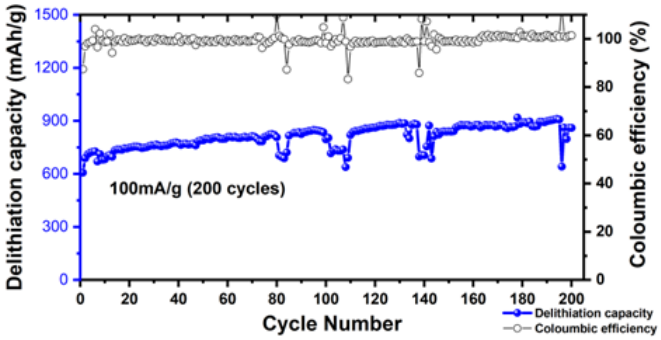

Fig 2.9 Long cycling studies with POL 202 as the active material at a current density of 100 mA/g

mAh/g and at a current density of 100 mA/g the specific capacity was recorded to be 810 mAh/g. At a high current density of 500 mA/g the capacity was observed to be 610 mAh/g The abundant redox active sites can interact with the Li^+ ions and hence foster a higher capacity with a cation insertion mechanism.[73] While carrying out the rate studies, after cycling at 5000 mA/g current, the cell was cycled at 50 mA/g current rate, and the capacity was observed to be 820 mAh/g, and this proves the electrode stability and the integrity of the electrode materials. At a current density of 100 mA/g, when the cell was cycled for 200 cycles, a reversible capacity of 850 mAh/g was observed with a retention of 100% (Fig 2.9). When the cells based on POL 202 as the active material was studied for understanding the material cyclability under very high currents of 1,2 and 5 A/g (1000,

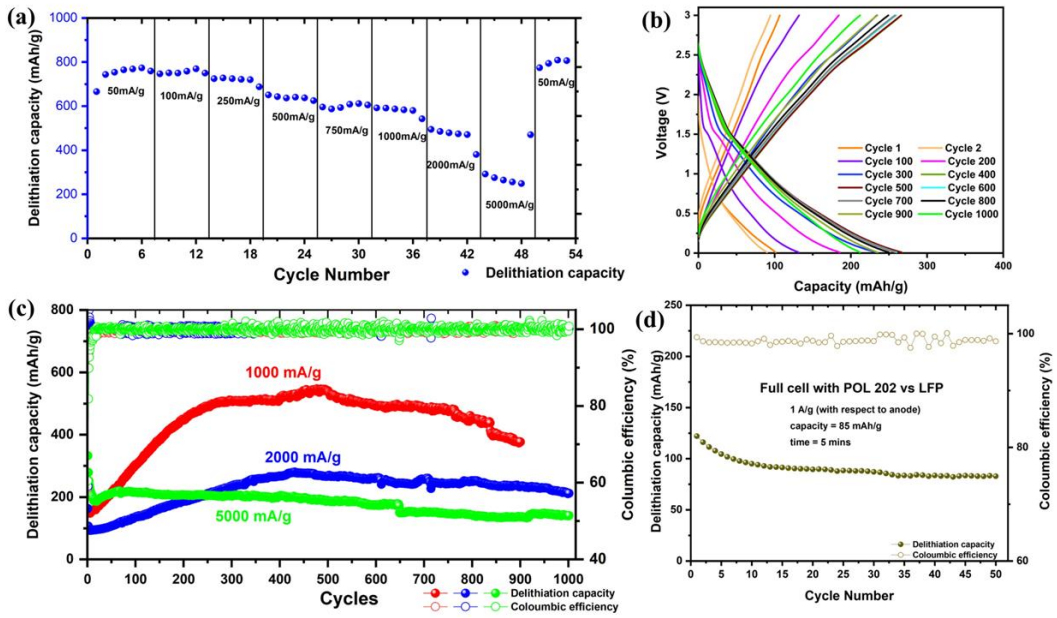

Fig 2.10 (a) Rate studies conducted with POL 202 based Li-ion anodic half cell (b) Charge-Discharge profile for anodic half-cell at a current rate of 2 A/g (c)Long cycling studies with POL 202 based Li-ion anodic half-cell (d)Full cell studies with POL 202 based anode vs $LiFePO_4$ cathode.

2000 and 5000 mA/g), the specific capacity was observed to be 515, 270 and 205 mAh/g for 1000 cycles with a capacity retention of around 80% in each of the cases (Fig 2.10c). Another striking feature was the charging time that was recorded. At a current rate of 2 A/g, the charging rate was observed to be 7.5 minutes while at a current rate of 5 A/g, the charging time was recorded to be only 3 minutes with a mass loading of 0.56 mg/cm^2. A full cell fabricated with $LiFePO_4$ as the cathode (specific capacity = 122 mAh/g) and POL 202 based anode (1.5 mg loading or 0.85 mg/cm^2) rendered a reasonable capacity of 85 mAh/g after 50 cycles at 1 A/g current density with respect to the anode (Fig 2.10 d). The

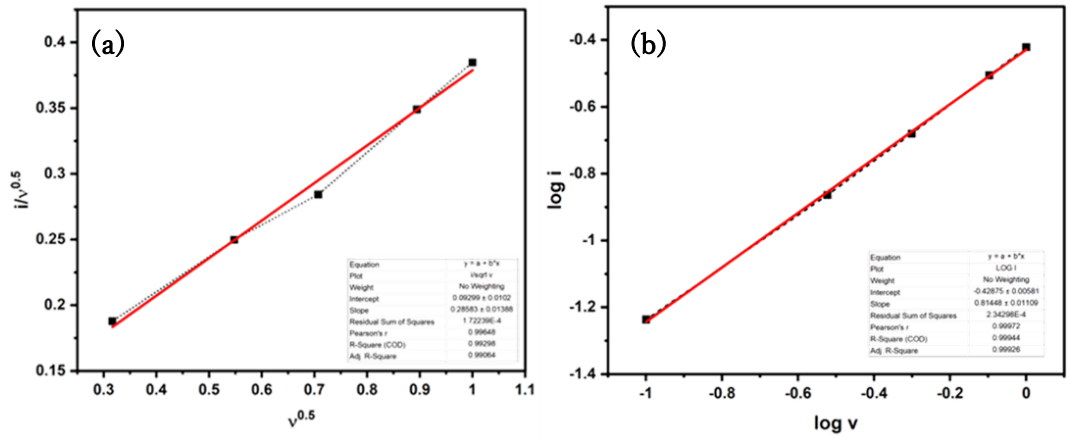

Fig 2.11 (a)log i vs log v plot. The value of b was determined to be 0.89 (b) i/(v)0.5 vs (v)0.5 (v=scan rate)

full cell was cycled between the potential 2.8 V and 3.8 V.

This following feature of fast charging can be attributed to the highly stacked and porous nature of the POL 202. The nanochannels aid the process of the lithium-ion diffusion through the anode material.[73,74] The stacking is a resultant of the π-π interaction between the adjacent monolayers. Owing to the well-defined and regular channels, as we expected, POL 202 shows excellent ion conducting abilities. The regular channels help in the process of the lithium-ion diffusion as these decrease the ionic diffusion energy barrier and the diffusion length. The nanochannel renders a host guest interaction which favors the ion conduction. It also provides a free volume for the fast conduction of the lithium ion and the structure is stable even when a very high current density is applied. The presence of a dense electron cloud generated in the slab region due to π-π interaction allows the establishment of a conduit or a pathway for charge transport between the layers. This contributes to an increase in electrical conductivity.[58] In the case of an electrochemical redox reaction, the ionic conduction can be achieved by 4 pathways and a crystallographic orientation of the molecule plays a very important role. As evident from

the XRD and computational simulation, POL 202 is believed to be an AA stacked molecule and it can be speculated that the ion conduction is along a perpendicular pathway.

To evaluate the charge storage mechanism in POL 202, CV studies were carried out at various scan rates and power law as mentioned in the equation ii was employed[20,35],

$i=av^b$ (equation ii)

In the above equation, 'i' the peak current, while ν is the scan rate, 'b' is the exponent of the scan rate, and 'a' is the proportionality constant. Figure 2.7c shows the cyclic voltammograms at 0.1, 0.3, 0.5, 0.8, and 1.0 mV/s. Figure 2.11a shows a plot of linear log i vs log ν and the value of b was evaluated from the slope and was determined to be 0.89.

The cathodic peak current observed in the cyclic voltammogram corresponds to the delithiation process of the anode in half-cells. In graphite, which follows a bulk-controlled charge storage mechanism, lithium-ion diffusion kinetics are typically sluggish due to limited surface area and interlayer spacing. This results in a current response dependent on the square root of the voltage scan rate (b = 0.5). However, materials exhibiting a surface-controlled charge storage mechanism show a current response directly proportional to the voltage scan rate (b = 1).

The determined b value of 0.89 suggests a mixed charge storage mechanism in the studied material, indicating a combination of diffusion-controlled and capacitive processes, which are predominantly surface phenomena. Furthermore, to quantitatively evaluate the charge storage contribution from the diffusion and pseudocapacitive processes, equation iii was employed. Additionally, to rigorously assess the contributions of charge storage mechanisms from diffusion and pseudocapacitive processes, equation iii was employed:

$i = k_c\nu + k_d\nu^{0.5}$ (equation iii)

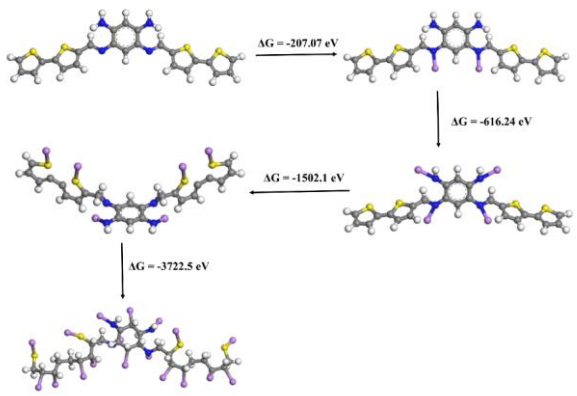

Fig 2.12: Lithiation scheme of POL 202

wherein i is the peak current, k_c and k_d are the proportionality constants for capacitance and diffusion, respectively, and ν is the scan rate. The values for k_d and kc were determined though a plot of $i/\nu^{0.5}$ vs $\nu^{0.5}$ (Figure 2.11b)

As we see in Figure 2.7d, the dominant mechanism that is followed for the charge storage is through a capacitive process and this is very

evident when the cell was studied at higher scan rates. The surface/interface involved pseudo-capacitance largely contributes to the fast Li-storage kinetics of the POL 202 based electrode. While the contribution due to diffusion mechanism was 49% at 0.1mV/s scan rate, it reduces to 27% at a scan rate of 0.8 mV/s and just 25% at a scan rate of 1.0 mV/s. Consequently, we see there is an increase in the capacitive current with the increase in the scan rate and 75% contribution of the same is seen at a scan rate of 1.0 mV/s as shown in Figure 2.7d.

DFT-based theoretical studies were undertaken to analyze and comprehend the lithium storage mechanism. Using CV studies as a reference, these investigations identified three distinct lithiation stages per monomer unit of POL 202, as illustrated in Figure 2.12. Herein, we consider that the first stage of lithiation is the lithium coordination at the imine nitrogen followed by the coordination of the sulfur with the Li^+ ion by an oxidation process occurring at the S moiety. Computational studies highlighted the charge transfer interactions between nitrogen and lithium ions, underscoring the effectiveness of C=N groups in coordinating and storing lithium ions. The theoretically determined ΔG value for the monomer unit after lithiating all imine moieties was calculated as -616.24 eV. Subsequently, each thiophene unit underwent lithiation with a ΔG of -1502.1 eV. Following this, the benzene and thiophene rings were lithiated, involving coordination of Li^+ ions through donation of π electrons. The overall ΔG for the fully lithiated POL 202 unit, encompassing all potential storage sites, was determined to be -3722.5 eV. This calculation indicates that the molecule achieves its lowest free energy state, representing its most stable configuration after full lithiation across all available lithium storage sites. On evaluation of the Mulliken atomic charges on N and S (Fig 2.14 a), a significant decrease in the atomic charges can be seen on N and S atoms (Table 2.2) which suggests

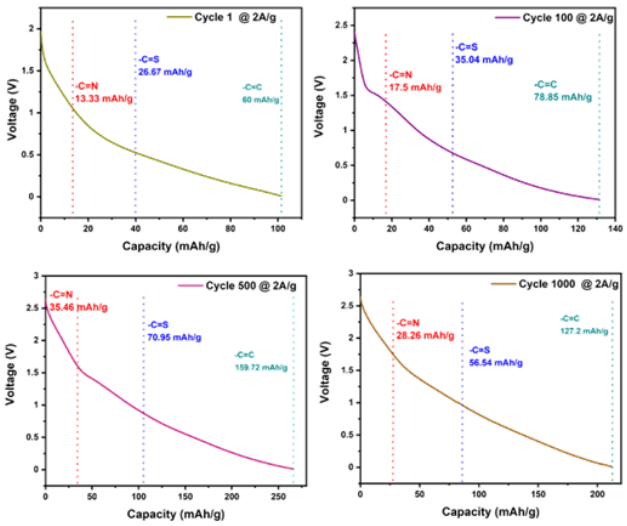

Fig 2.13 Lithiation scheme and capacity contribution of each of the storage sites in POL 202 anodic half-cell at cycles 1, 100, 500, and 1000 when cycled at 2 A/g.

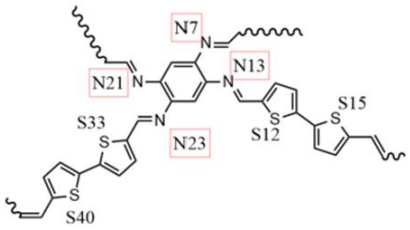

Fig 2.14 Different heteroatoms storage sites in POL 202

that the lithium ions are distributed over the N and S atoms mostly and undergo a possible coordination as shown in the Figure 2.13.[75] The theoretical capacity was calculated to be 953.76 mAh/g. Figure 2.13 illustrates the contribution of each of the storage sites when the cell was studied under a current density of 2000 mA/g (2 A/g).

Table 2.2 Decrease in the Mulliken atomic charges upon lithiation of POL 202

	0 Li	2 Li	4 Li	8 Li
N7	-0.21043	-0.347877	-0.402423	-0.4606678
N13	-0.22542	-0.347036	-0.362824	-0.485291
N21	-0.21994	-0.520834	-0.460979	-0.456669
N23	-0.218	-0.521246	-0.621553	-0.606235
S12	0.242895	0.193961	0.18085	0.113452
S15	0.241316	0.192246	0.17978	0.118664
S33	0.240426	0.213187	0.206953	0.164004
S40	0.244074	0.210613	0.206454	0.159764

Several inferences can be drawn from the dq/dV vs voltage plots (Figure 12.15a). We see electrolyte degradation occurring in the first cycle resulting in an SEI formation and an irreversible loss of Li-ions occurring between 0.5V and 0.1V (vs Li/Li+). On assessing the dq/dV plots of the 100th, 250th, 500th, 750th and 1000th cycle, it is evident that with the increase in potential from 1.0 to 3.0 V, there is a noticeable increase in peak height and broadening of the double layer region. This observation is accompanied by a decrease in the lithiation peak potential, indicating enhanced lithium diffusion during cycling. This phenomenon likely stems from the exposure of new active sites available for lithium storage, similar to findings reported for the PBM polymer synthesized by Matsumi and co-workers.[35]

Furthermore, it can also be inferred that an increase in the interlayer spacing of POL 202

layers facilitates the lithium ions insertion into its layers. Hence, we see a gradual increase in the capacity and an activation of the polymeric anode.

However, a decrease in peak height observed after the 1000th cycle indicates electrode decomposition and the consequent loss of active material, leading to capacity degradation. Following 1000 charge-discharge cycles at a current rate of 2000 mA/g current rate, the electrode was disassembled within an argon-filled glovebox (with O_2 and H_2O concentrations < 0.5 ppm). It was then washed with fresh EC/DEC solvent dropwise and subsequently dried overnight under vacuum for further analysis, including X-ray photoelectron spectroscopy (XPS) and field emission scanning electron microscopy (FE-SEM). FE-SEM studies were done to understand the change in the surface morphology and the volume expansion occurring in the electrode. Figure 12.15c shows the cross section of the cycled electrode and a clear contrast can be seen when we look at the cross section of the pristine electrode (Fig 12.15 e). The cross-section images reveal the electrode thickness to be 23 μm and 31 μm in the case of pristine and cycled electrodes respectively. Figure 12.15f and 12.15h show the lateral (aerial) FE-SEM images of the cycled and pristine electrode. In the case of the pristine electrode, the surface morphology reveals a distinct particle size and shape. However, in the case of the cycled electrode the electrode particles looked smaller and lacked clear boundaries as in the case of pristine electrode. This may be attributed to the SEI formation and the results of cycling an electrode at a very high current density. The volume expansion observed was 47.6% and

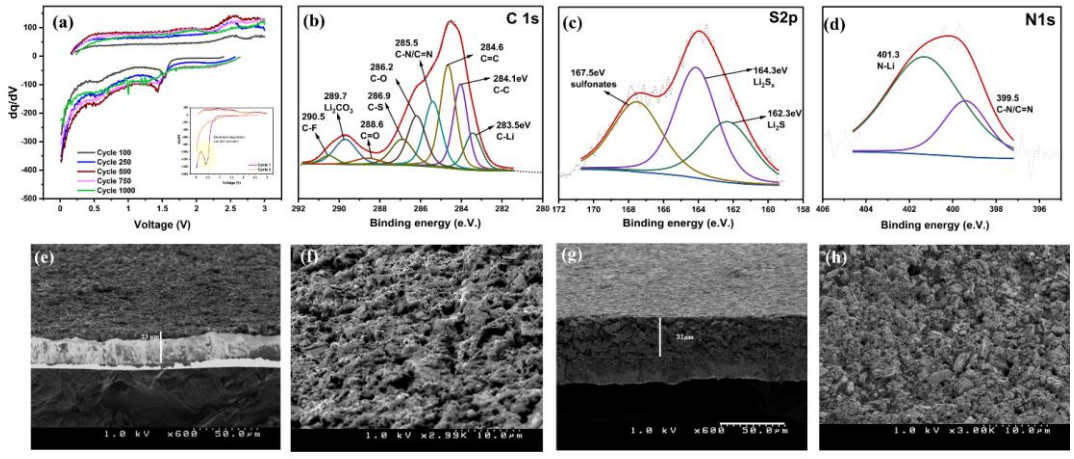

Fig 2.15 (a) dq/dV plot for different lithiation and delithiation cycles (b)Deconvoluted XPS spectra of C 1s in the POL 202 cycled electrode (c) Deconvoluted XPS spectra of S 2p of cycled electrode(d) Deconvoluted XPS spectra of N 1s cycled electrode. FE-SEM images of (e, f) Cross section and lateral view of pristine electrode (g, h) Cross section and lateral view of cycled electrode

the thickness can be attributed to the SEI formation and the change in the During the charge-discharge cycles, the morphology of the particles underwent significant changes. FE-SEM images revealed a noticeable volume increase in the electrode, indicating morphological evolution over 1000 cycles. This transformation exposed new active sites for lithium storage, contributing to a gradual rise in specific capacity. Remarkably, even with only 10% PVDF binder, the electrode surface showed minimal cracking after such extensive cycling at high rates. Additionally, XPS analysis of the disassembled cycled electrode in a lithiated state provided insights into its chemical composition post charge-discharge studies. Deconvolution of the C 1s spectra (Figure 12.15b) showed peaks at 283.5 eV corresponding to C-Li bonds, and at 284.1, 285.3, and 286.9 eV corresponding to functional groups like C-C, C=N, and C-S found in POL 202. Peaks at 286.2, 288.6, 289.7, and 290.5 eV in the deconvoluted spectra corresponded to C=O, C-O-C, Li2CO3, and C-F groups, components typically found in the solid electrolyte interface (SEI). The deconvoluted N 1s spectra (Figure 12.15d) exhibited peaks at 399.5 eV and 401.3 eV, corresponding to C=N and N-Li groups, respectively. The S 2p spectra (Figure 12.15c) showed peaks at 162.3 eV, 164.3 eV, and 167.5 eV, indicating the presence of Li2S, Li2Sx, and sulfonate species, highlighting the chemical transformations occurring during cycling.[35,70]

Given that the detection depth of XPS is typically around 5 nm, the identification of nitrogen and sulfur, elemental components of the active material POL 202, suggests that the solid electrolyte interface (SEI) layer is thinner than this depth.[35,42] The formation of a thinner SEI layer also indicates the resistance of the material toward reducing the

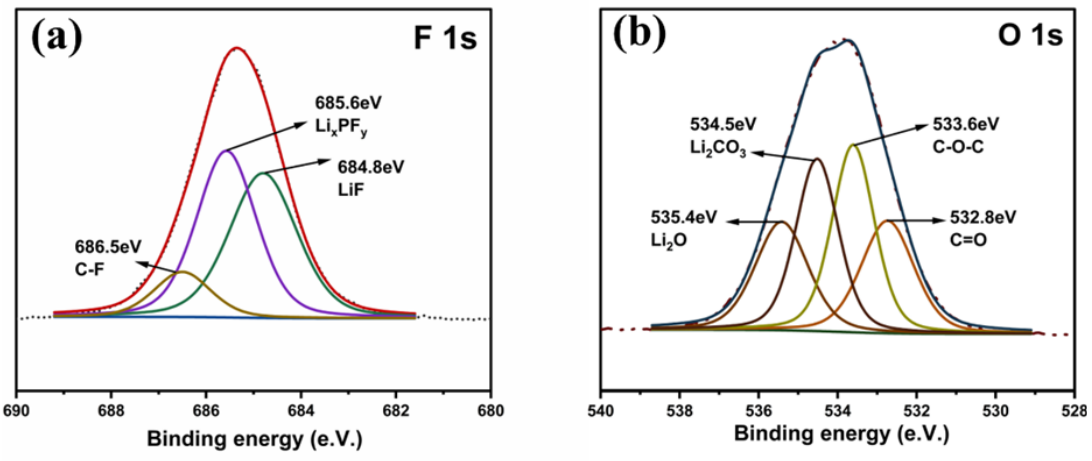

Fig 2.16(a) XPS spectra of F 1s in the POL 202 cycled electrode. (b) XPS spectra of O 1s in the POL 202 cycled electrode.

electrolyte and better kinetics. Besides F1s, and O1s signals of XPS were also deconvoluted and the peaks were assigned to the species that may result during the formation of the SEI layer (Figure 12.16 a, b).

As discussed in the above sections, this bithiophene based donor acceptor organic active material showcases diffusive and capacitive charge storage properties. An excellent charge storage property and cyclability were observed at very high current densities. In comparison to the BIAN based porous organic polymer reported by us[35] this shows augmented capacity and charging rates. It has a superior performance to the BIAN based POP which was only n doped. The presence of a donor acceptor pair, as in this case can result in increased power density due to an enhanced electronic interaction. Further, a narrow band gap and the change in the dipole moment due to an intramolecular charge transfer from donor to an acceptor aids the electronic and the electrochemical properties. Introduction of such species into porous frameworks can lead to very excellent electrochemical properties to the anode material. As we saw, in this case we were able to achieve a maximum specific capacity of 850 mAh/g at a current rate of 100 mA/g and 205 mAh/g at a current rate of 5000 mA/g within 5 minutes. This is comparable to the zinc blende variant of silicon carbide reported by us which provides a capacity of 1066 mAh/g at a current rate of 100 mA/g.[76] Jiang et al. have showcased the anodic applications of polythiophene and porous poly(3,3′-bithiophene) polymers in lithium-ion batteries.[70] Porous poly(3,3′-bithiophene) demonstrated a remarkable reversible capacity of 663 mAh/g at a current density of 500 mA/g over 1000 cycles. In comparison, polythiophene exhibited a lower reversible capacity of 100 mAh/g under identical cycling conditions. The research on donor-acceptor based porous organic materials has been relatively few. Liu et al have reported the electrochemical performance of conjugate donor–acceptor organic polymers as anode materials of lithium-ion battery and have also studied the storage mechanism. In their research, they developed donor–acceptor (D–A) type polymers that integrate phenanthraquinone (PQ) as the acceptor unit and thiophene as the donor unit, specifically designed for use as anode materials.[56] Three polymers were synthesized with varying content of the donor unit to explore its impact on electrochemical properties. Their investigations revealed that reducing the donor unit content in the polymer enhances specific capacities. However, this adjustment did not lead to an improvement in the rate capability of the electrode. Also, Wang et al have tried to introduce an aqueous electrolyte design using asymmetric donor-acceptor molecule in their studies. Chen et al have reported polymeric Schiff bases comprising of benzene and thiophene rings for sodium ion batteries.[75] Their studies concluded that the introduction

of the thiophene ring fostered enhanced properties of electron delocalization, structural stability, and intrinsic conductivity which led to an improved electrochemical performance. On incorporation of multi walled carbon nanotubes, there was a further improvement in the reversible capacity (from 174.7 mAh/g to 290 mAh/g at a current density of 50 mA/g). A porous framework and a low redox voltage achieved by the introduction of sulfur and nitrogen species is believed to aid the superior performance of POL 202 as an electrode material and opens a vast scope for the scientific community to research and analyze such type of donor-acceptor based organic active materials.

Conclusion

In conclusion, a polymeric Schiff's base type network porous polymeric material POL 202 was synthesized via a polycondensation reaction between 2,2'-bithiophene-5,5'-dicarboxaldehyde and 1,2,4,5-benzene tetraamine tetrahydrochloride. Due to the presence of a donor acceptor moieties i.e., sulfur and nitrogen, a very low redox potential was achieved. POL 202 based anodic half cells showed excellent electrochemical properties, rendering a reversible capacity of 850 mAh/g at 100 mA/g current density. At higher current densities of 1000, 2000 and 5000 mA/g, the reversible capacity observed was 510, 270 and 205 mAh/g respectively. The most striking feature of the polymer was that apart from having a very high capacity, the charging time was observed to be just 2.5 minutes. We believe that the low redox potential and the strong electronic interaction increases the power density of the material. The porous structure helps in the lithium-ion diffusion by shortening the diffusion length and aiding the fast-charging process. The lithium-ion storage mechanism was evaluated by DFT studies, and we found that pseudocapacitive behavior was responsible for the storage. POL 202 can be considered as a very prospective anode material as it shows high capacity, supports fast charging, and has stable electrochemical activity at the same time.

CHAPTER 3 ENHANCING THE PERFORMANCE OF LITHIUM- AND SODIUM-ION BATTERIES WITH POROUS POLYMER DERIVED N, S CO-DOPED HIERARCHICAL MICRO/MESOPOROUS CARBON

Abstract: The microstructure and morphology of carbonaceous materials are critical in regulating the diffusion of lithium and sodium ions within the anode. Yet, synthesis of carbon materials with optimal pore structures, textural properties, and surface areas poses challenges, often involving template methods or the use of hazardous chemicals for activation. However, Porous Organic Polymers (POPs) serve as considerable precursors due to their high rigidity and π-π stacking arrangement, facilitating the preservation of high surface area, porosity, and uniform incorporation of heteroatoms from a singular source. Herein, a hierarchical N, S co-doped micro/mesoporous carbon is reported using a POP, POL 102, as a carbon precursor at two temperatures of 600 and 800°C. Characterization via BET, Raman, XRD, XPS, and HR-TEM was done to understand variations in the surface area, pore volume, and defects with increasing carbonization temperatures, impacting electrochemical properties and charge storage. Particularly, the carbon synthesized at 800°C exhibited superior electrochemical properties in both Li/Na-ion anodic half cells, owing to its optimal pore volume and surface area for ion diffusion and interaction with active sites. It demonstrated a high reversible capacity of 208 mAh/g at 2 A/g for over 2000 cycles in LIBs, 80 mAh/g at 10 A/g for up to 8000 cycles, and 250 mAh/g at 1 A/g in the case of SIBs. Further the cycled electrodes were analyzed via XPS and FE-SEM to understand the nature of the solid electrolyte interphase (SEI). This research investigates the potential applications of designing heterodoped nanoporous materials from conjugated polymers with enhanced electrochemical properties.

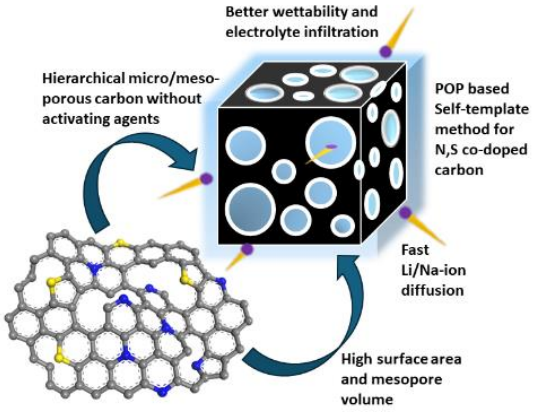

Introduction

An indispensable material in lithium-ion batteries (LIBs) that has underpinned the narrative of its success for over nearly three decades is graphite, fulfilling the critical role of providing a lithium-ion host structure within the negative electrode. However, even though graphite has so far remained the workhorse anode in lithium batteries, it is often considered unsuitable for fast-charging applications in lithium-ion batteries limiting their applications in certain extreme conditions. For example, there is a significant loss in capacity that is seen when graphite-based anodes are cycled at 2C or higher current densities.[12] Furthermore, the application of graphite as a charge host is only limited to LIBs is not suitable in sodium ion batteries (SIBs). The intercalation and deintercalation of sodium ions into graphite can lead to structural instability and irreversible changes in the graphite structure over multiple charge-discharge which results in drastic capacity loss leading to poor cycling stability. Hence more robust material designing is imminent considering the limitations of graphite.[45]

Carbonaceous materials, for example, expanded graphite, graphene, carbon nanotubes, and other amorphous carbon, have been studied as alternatives. The high chemical stability in addition to high electrical conductivity makes carbon-based materials one of the sought after materials to serve as the charge host.[77] Hence, if we are looking into a future where the primary idea is to employ carbonaceous materials as the active material, one of the important strategies is to understand and develop carbon materials with optimized pore structure and high surface area. Exploring precursor materials for designing nanoporous carbons remains one of the scientific endeavors. The intricate microstructure and morphology of carbonaceous materials hold significance as these features intricately regulate lithium-ion diffusion within the anode, and fundamentally influence its electrochemical characteristics.[78]

In this regard, heteroatom doped porous carbon materials (HPCMs) have been recognized to have outstanding electrochemical performance in alkali metal ion batteries. These materials are endowed with the structural advantage of porous structures, which results in fostering a high density and low diffusion resistance towards active sites. Furthermore, the physicochemical properties of the carbons can be modified and tailored by the introduction of the different heteroatoms.[79] However, the modification strategies of carbon-based materials to comprehensively improve their electrochemical application in energy storage devices remains a challenge. Even though introduction of heteroatoms into porous carbon architectures is an effective method, most of the heteroatom doping techniques involve the use of template methods which can be time consuming, by direct

addition of the dopant to the preformed carbon which can be environmentally hazardous or involve expensive techniques like Chemical Vapor Deposition or plasma treatment which are expensive. Hence, the judicious choice of the carbon precursors is crucial for the manufacture of heteroatom doped porous carbon materials to synthesize such materials in a more environmentally more friendly manner.[39,79–82]

Deriving carbon from porous organic polymers (POPs) emerge as a strategic imperative. POPs have demonstrated great promise because of their versatile molecular and nanoscale structures, tunable chemical compositions, and versatile processing techniques of synthesis. Furthermore, such polymers have highly conjugated polymeric main chains as well as a sufficient content of heteroatoms. Homogenously introducing the heteroatoms into the polymer in a sp^2 or sp hybridization state is advantageous as it guarantees improved preservation compared to nonconjugated species during carbonization. Besides, heteroatoms introduced in such manner exhibit greater stability under the typical conditions applied to carbons. Furthermore, POP based materials can offer the advantage of introducing multiple dopants into the carbon framework from a single source. Hence, POP based self-templating ensures the potential preservation of high surface area and a hierarchical micro/mesoporous architecture without post modification and activation,

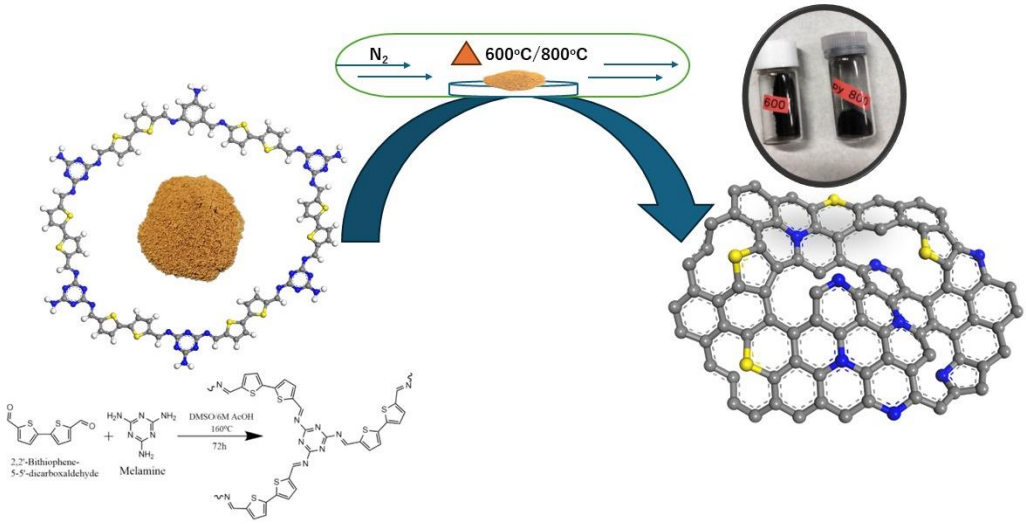

Fig 3.1: Synthetic scheme for the synthesis of PY 102@x

facilitating more active sites for lithium-ion storage besides minimizing the volume expansion. The interconnected pore network also allows for efficient electrolyte penetration and ion diffusion porosity with a uniform distribution of the heteroatoms.[40,79,82]

Metal Organic Polymers as precursors for porous carbons for application in battery has been explored relatively more than covalent organic materials and POPs.[83–88] While most of the porous carbons derived from such sources have been evaluated as electrocatalysts, they hold a lot of potential as active materials in anodes as well. Recently, Zhang et al synthesized porous carbon materials with high surface area from hyper crosslinked porous organic polymer as porous precursor with KOH activation.[89] Even though the resultant carbon delivered high specific discharge capacity of 1221 mAh/g at 100 mA/g, the retention in capacity was a matter of concern. Also, Mitra et al reported carbon derived from The BIAN-Bismarck brown based azo and imine functional porous organic polymer (BBP), specifically PyBBP600 (pyrolyzed at 600°C) and PyBBP800 (pyrolyzed at 800°C), demonstrated outstanding rate capability and long-term cyclability at a high current density of 4 A/g. PyBBP800 exhibited exceptional performance, delivering a specific capacity of 125 mAh/g over 5000 cycles.[90] Also, carbon derived from BIAN-Melamine based POP, PyPBM600 and PyPBM800 based anodic half-cells demonstrated exceptional rate capability and capacity up to 4 A/g for more than 1000 cycles. Besides, a 15-minute charging time with a reversible capacity of 1.2 mAh could be achieved with a 99.8% columbic efficiency for up to 300 cycles.[42] However, the effects of pore volume and size, and the application of POP based precursor to design hierarchical nanoporous structures for active materials in SIBs were not explored in these materials.

Realizing the need to address the existing gaps, herein we report a porous organic polymer POL 102 derived N, S co-doped hierarchical micro/mesoporous carbon with high surface area and pore volume which was studied for its lithium and sodium storage properties. Nitrogen atoms effectively enhance the conductivity of carbon electrodes, while sulfur atoms can increase the interlayer spacing within carbon structures. This dual effect enhances charge mobility and accessibility to reactive species, making such carbon materials well-suited for storing lithium and sodium ions.[91,92] Through this study, the effects of surface area and pore volume of the obtained porous carbon on lithium ion and sodium ion storage was assessed. It also addresses the advantages of designing hierarchical nanoporous carbon architectures without the use of any activation agents like KOH, which combine high specific surface areas with proper channels and provide free volume to allow efficient diffusion of any substance and are advantageous in rapid charging applications in LIBs and SIBs. This research aims towards the development of fundamental science and aims at exploring the possible alternatives to the traditional graphite material. Moreover, it tries to add to the existing pool of knowledge of HPCMs and their prospective applications as anode materials in metal ion batteries.

Experimental

Materials

2,2'-bithiophene-5,5'-dicarboxaldehyde, glacial acetic acid and N-methyl pyrrolidone (NMP), Propylene carbonate (PC) was procured from Tokyo Chemical Industries, Ltd.(TCI), and were used without further purification or modification. Melamine (1,3,5-Triazine-2,4,6-triamine), 1.0 M $LiPF_6$(50/50) ethylene carbonate/diethyl carbonate (EC/DEC) electrolyte and poly (vinylidene difluoride) (PVDF)binder (MW: 540,000) were purchased from Sigma-Aldrich. Battery-grade Carbon black Super P was purchased from Alfa Aesar. Copper foil of a thickness of 20μm was purchased from the Nilaco Corporation. Sodium perchlorate ($NaClO_4$) was purchased from Wako Chemicals.

Synthesis of Heterodoped Porous Carbons (PY 102 @x)

POL 102 was synthesized via a Schiff's base condensation reaction between 2,2'-Bithiophene-5,5'-dicarboxaldehyde and Melamine. Briefly, 6 mmol (1.32 g) of 2,2'-Bithiophene-5,5'-dicarboxaldehyde was taken with 4 mmol (0.504 g) of melamine in 20 mL of DMSO and 0.5 mL of 6M acetic acid was added to the reaction mixture. The contents were heated under reflux at 160^{o}C for 72 hours. An orangish precipitate (POL 102) was obtained (yield = ~60%) which was washed with THF, Acetone and Methanol in succession and dried at 80^{o}C under vacuum. Following this, POL 102 was pyrolyzed at 2 different temperatures, i.e., 600^{o}C, and 800^{o}C. The precursor was first heated up to 200^{o}C at a rate of 5^{o}C followed by pyrolysis for 1 h at 600^{o}C and 800^{o}C in two different cases to obtain PY 102@600 PY 102@800 respectively (yield=~40%). The carbon obtained was washed with 1M HCl to remove any carbonates formed and was then washed with copious amount of distilled water and dried under vacuum at 70^{o}C for 12h to obtain the final product PY POL 102@x (x = 600/800^{o}C) (Fig 3.1).

Synthetic Characterization

Following the synthesis of PY 102@600 and PY 102@800, the physical and chemical nature of the polymer was investigated by characterization techniques. Surface area and pore size distributions were determined using a BELSORP mini accelerated surface area and porosity analyzer. X-ray photoelectron spectroscopy (XPS) measurements were performed using a Fisons Instruments S-Probe TM 2803 instrument. Powder X-ray diffraction (XRD) studies were conducted on a SmartLab X-ray diffractometer from Rigaku, utilizing Cu Kα radiation (λ = 0.154 nm) with a step size of 0.02°.

Electrode fabrication

A slurry composed of PY POL 102@x as the active material, PVDF as the binder and Super P as the conductive additive in the weight ratio 80:10:10 was prepared in N-methylpyrrolidine (NMP).

The slurry in each of the cases was then cast onto a 20µm copper foil using a 0.1mm doctor blade and was dried under vacuum at 80^{o}C for 24 hours. Then it was roll pressed at 0.4 mm thickness at 80^{o}C. Electrodes were punched and weighed. The mass of the electrode was calculated to be between 1.0 mg and 1.1 mg (0.56 mg/cm^2). Following this, CR2025 anodic half cells were fabricated inside the glove box (H_2O and O_2 < 0.5ppm). For lithium-ion anodic half-cell, lithium metal was used as the counter and reference electrode and $LiPF_6$ (1.0M in EC: DEC 50:50 v/v) was used as the electrolyte. Electrochemical studies were performed using lithium-ion anodic half cells (CR 2025) where lithium metal foil was used as the counter and reference electrode.

In the case of sodium ion anodic half-cell, sodium metal was used as the counter and reference electrode. $NaClO_4$ (1.0 M in EC: PC 50:50 v/v) was used as the electrolyte.

Electrochemical Tests

Cyclic voltammetry (CV) studies were conducted using Bio-Logic Science Instruments. For lithium-ion anodic half-cells, scans were performed between 0.01 V and 3.0 V, and for sodium-ion anodic half-cells, between 0.005 V and 3.0 V. Various scan rates of 0.1, 0.3, 0.5, 0.8, and 1.0 mV/s were applied to investigate the charge storage mechanisms for lithium and sodium ions. Electrochemical impedance spectroscopy (EIS) was performed both before and after CV over a frequency range from 1.0 MHz to 0.1 Hz, using an AC amplitude of 10 mV. Dynamic electrochemical impedance spectroscopy (DEIS) measurements were also conducted at different voltage perturbations within the same frequency range and AC amplitude. Galvanostatic cycling measurements were carried out using an Electrofield ABE 1024 instrument. For lithium-ion batteries (LIBs), cycling was performed between 0.01 V and 3.0 V in constant-current mode, while for sodium-ion batteries (SIBs), the range was from 0.005 V to 3.0 V. Activation studies were conducted using Bio-Logic Science Instruments at different temperatures to determine the activation energy of lithium diffusion in LIBs.

Results and discussions

Material characterization

POL 102 was synthesized via a simple polycondensation reaction (Fig 3.1) between 2,2'-Bithiophene-5,5'-dicarboxaldehyde and melamine and the final product was characterized via ATR and BET to understand its chemical nature and the surface area (Fig 3.2).

Considering the potential advantages of using POP based precursors as discussed earlier, POL 102 was pyrolyzed at two different temperatures and the effects of the temperature on the surface and pore morphology of the N, S co-doped carbon derived from POL 102 was studied and subsequently its effect on lithium-ion storage was evaluated.

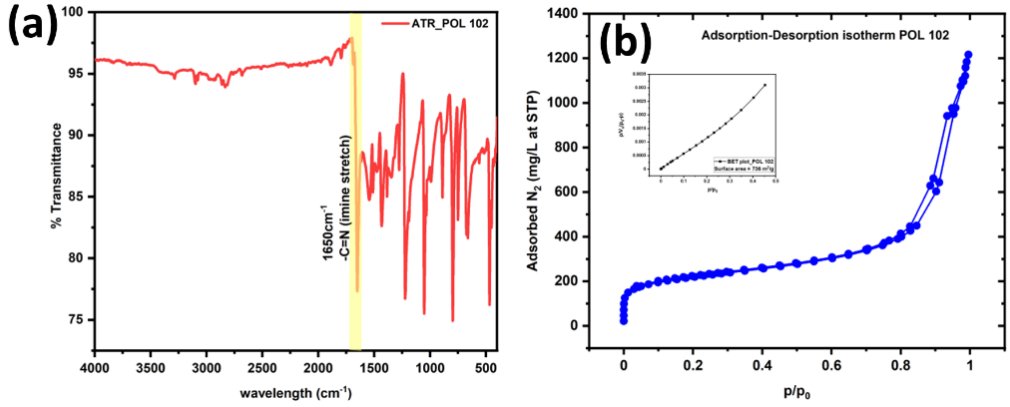

Fig 3.2 (a)ATR characterization of POL 102. The peak at 1650 cm^{-1} shows the formation of the imine linked polymer. (b)Nitrogen adsorption isotherm for POL 102. The BET surface area was determined to be 736 m^2/g confirming the high surface area of this conjugated polymer.

The nitrogen adsorption-desorption isotherm was carried out to evaluate the surface area of the synthesized carbon. A high surface area in the pyrolyzed materials was observed. This shows that porous organic polymers can be used as robust precursor materials as such high surface area carbons can be obtained without any post modification of the obtained carbon such as etching with KOH/acid was seen. PY 102@600 shows a surface area of 411 m^2/g while the surface area of PY 102 @800 is observed to be 579 m^2/g (Fig 3.3a). Furthermore, the pore volume (calculated by BJH method) is observed to be 0.20 cm^3/g, and 0.29 cm^3/g for PY 102@600 and PY 102@800 respectively. For both the carbon samples, at a relative pressure of p/p_0 ranging between 0.4 and 1, the isotherms exhibit a combination of type I and type IV patterns with H4-type hysteresis loops. This observation suggests the presence of both micro- and mesopores in the material.[93–96] The pore size distribution, analyzed using the NL-DFT method as shown in Figure 3.4, shows

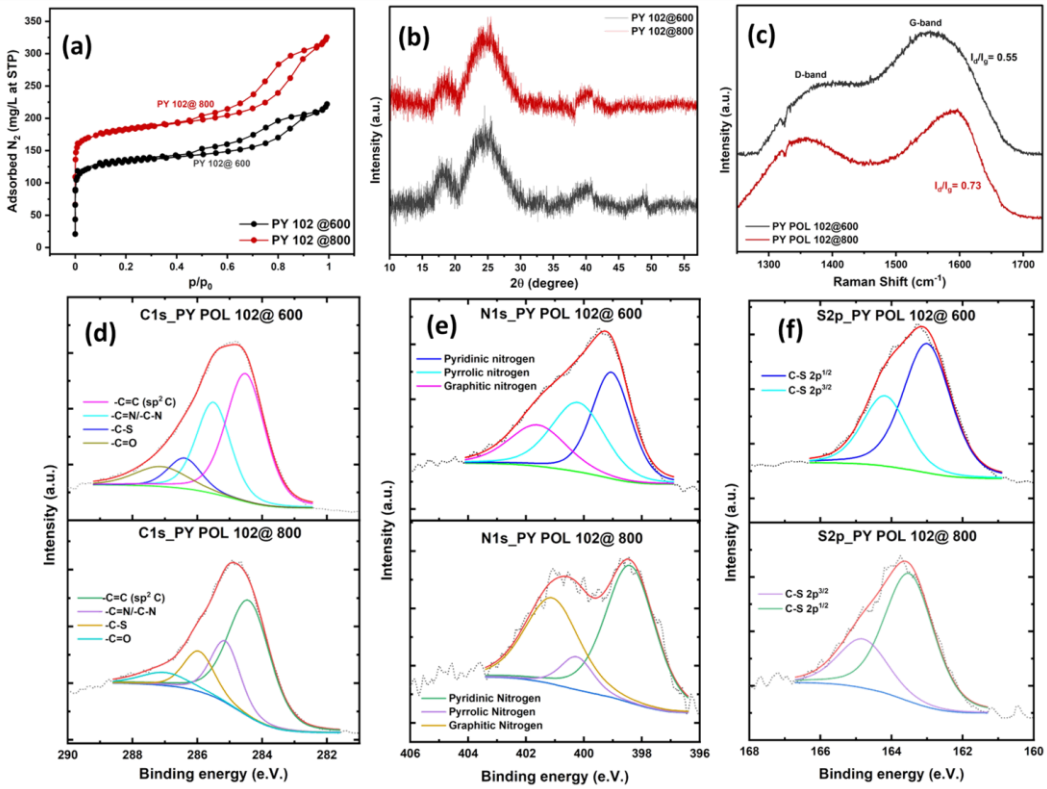

Fig 3.3 (a) BET adsorption isotherm (b) p-XRD spectra (c) Raman Spectra (d)Deconvoluted C1s spectra of PY 102@600 and PY 102@800 (e)Deconvoluted N1s spectra of PY 102@600 and PY 102@800 (f)Deconvoluted S2p spectra of PY 102@600 and PY 102@800

the distribution of both micro and mesopores. The increase in the surface area was complemented with an increment in the amorphous nature which was concluded from the XRD data (Fig 2b). On increasing the carbonization temperature from 600 to 800°C, the material becomes more disordered. This change is evident not only in the XRD (as shown by the full width at half maximum values and XRD Crystallite grain size in Table 1) but also in Raman spectroscopy (Fig 2c), where we observe an increase in the I_d/I_g ratio. As the temperature increases, thermal decomposition and loss of more edge groups and functional groups results in creation of more defects leading to a higher surface area and pore volume.[35] This can be observed in the decline of the atomic weight percentage of N and S with the increase in the carbonization temperature as well. Moreover, due to the shrinkage and the collapse of pore structure with the increase in the carbonization temperature, we see an increase in the pore volume with an increase in the temperature (Table 3.1). The pore volume and surface area become an important factor when we consider the charge storage applications in lithium and sodium ion batteries as discussed

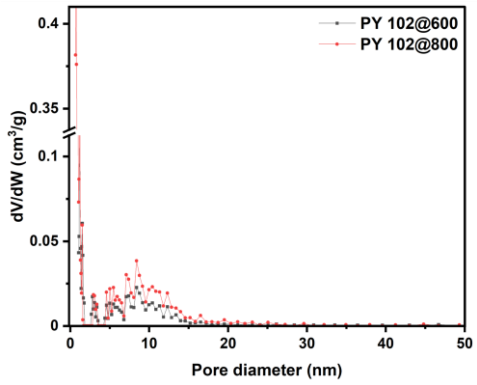

Fig 3.4 The pore size distribution in the range of micro and mesopores is seen in PY 102@600 and PY 102@800

later. We can speculate that the carbonization procedure involves a slow elimination of CO_2, CO, SO_2, H_2S, NH_3 and other gases along with the creation of the sp^2 carbon at 600°C. The BET, Raman, XPS and EDS analysis provides an understanding that at a carbonization temperature of 800°C, a larger scale formation of sp^2 carbon network and pore development occurs (Table 3.1). [97] XPS was conducted to understand the chemical states of the elements present and for the quantitative analysis the elements present. The table showing the atomic concentration of different elements has been presented in Table 3.2. In the deconvoluted C 1s spectrum, in both the pyrolyzed materials (Fig 2d) we can observe the -C=C, -C-S and C-N peaks. The C-O peaks observed may be due to the oxygen functionalities present at the edge of the carbon.[96,98] It is noteworthy that on deconvolution of the N1s spectrum (Fig 2e), the amount of pyrrolic nitrogen is higher in the case of PY POL 102@600 compared to that of the 800. This result is of significance when we try to understand the electrochemical and charge storage properties of the individual materials as discussed later. The deconvoluted XPS spectra of S 2p (Fig 2f) showed the presence of an S $2p^{3/2}$ and $2p^{1/2}$ doublet with an energy separation of 1.2 eV in PY 102@600 and 1.3 eV in PY 102@300, which reconfirms the presence of C–S bonds and it can be concluded that the sulfur is present in the form of thiophene rings.[99] Furthermore, the FE-SEM micrographs for PY 102@600 at 2µm (Fig 3 a) and PY 102@800 (Fig 3.5 c) show the porous nature of the material. Besides, the HR-TEM micrographs at 20nm for the materials (Fig 3.5 b,

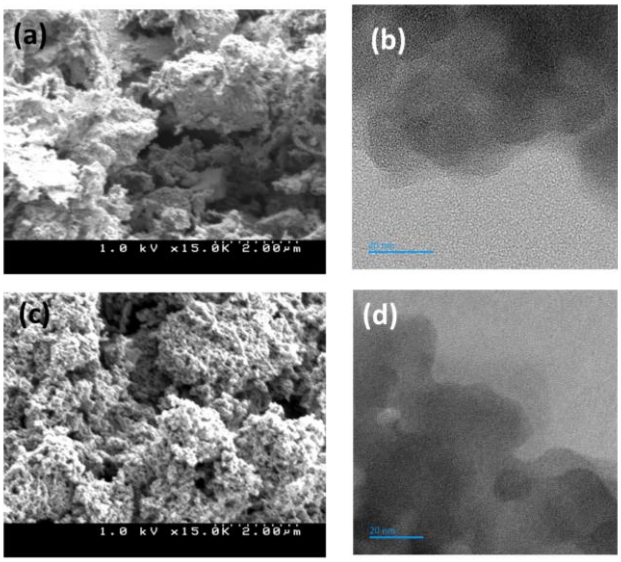

Fig 3.5 FE-SEM images at 2µm (a)PY 102@600 (c)PY 102@800. HR-TEM images at 20nm(b)PY 102@600 (d)PY 102@800

d) shows an amorphous porous stacked nature of the materials. The TEM-EDS plot (Figure 3.6) shows a uniform distribution of the heteroatoms.

Table 3.1 Physical characteristics of PY 102@x

Material	FWHM	Crystal-lite grain size (nm)	d-spac ing (nm)	I_d/I_g ratio	V_{meso} (cm^3/g)	V_{mic} (cm^3/g)	S_{meso} (m^2/g)	S_{mic} (m^2/g)
PY 102@ 600	5.21	1.63	0.34	0.55	0.20	0.32	159.1	653.8
PY 102@ 800	5.95	1.43	0.37	0.73	0.29	0.46	192.5	921.9

Table 3.2 Atomic weight percentage of the elements present in PY 102@x.

Material	C at weight %	N at weight %	S at weight %
PY 102@600	73	21.4	5.6
PY 102@800	83.6	12.9	3.5

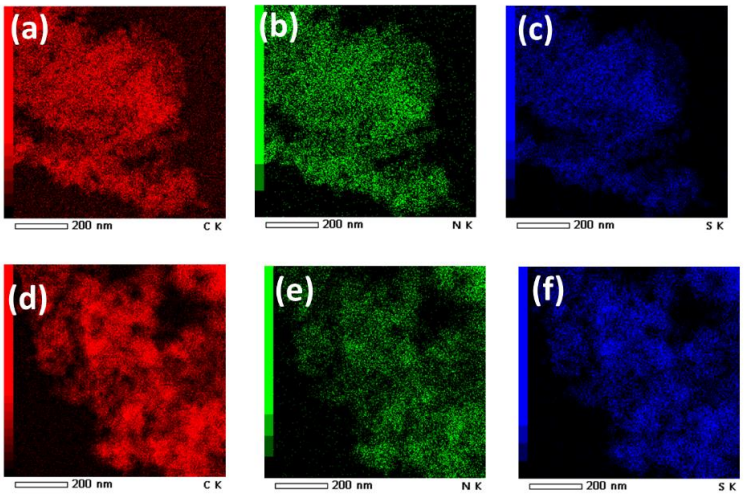

Fig 3.6 TEM-EDS mapping of Carbon, Nitrogen and Sulfur (a, b, c) PY 102@600 (d, e, f) PY 102@800

Electrochemical Studies

Cyclic Voltametric and Impedance Studies

Cyclic voltagrammic (CV) studies were conducted for the CR 2025 Li-ion anodic half cells in the potential window of 0.01V and 3V (vs Li/Li^+). During the initial cycle, an irreversible peak was observed at 0.3-0.5 V during the lithiation half (Fig 3.7 a, b) which can be assigned to the formation of the Solid Electrolyte Interface (SEI) layer due to electrolyte reduction.[100] At a scan rate of 0.1 mV/s, in the subsequent cycles, overlapping voltammograms were observed which shows the electrode stability. Redox peaks at 2.3/1.5 V can be attributed to the redox reaction at sulfur moiety.[70] Potentiostatic Electrochemical Impedance Spectroscopy (PEIS) was conducted on OCV before and after CV studies in both sodium and lithium-ion anodic half cells. Figure 3.8 a, b shows the Nyquist plots for PY 102@x-based Li -ion anodic half-cells. As observed, there was a notable decrease in the internal resistance of the cell following the completion of CV studies. This reduction can be attributed to improved lithium-ion diffusion across the interface facilitated by the conductive solid electrolyte interphase (SEI) layer. A further

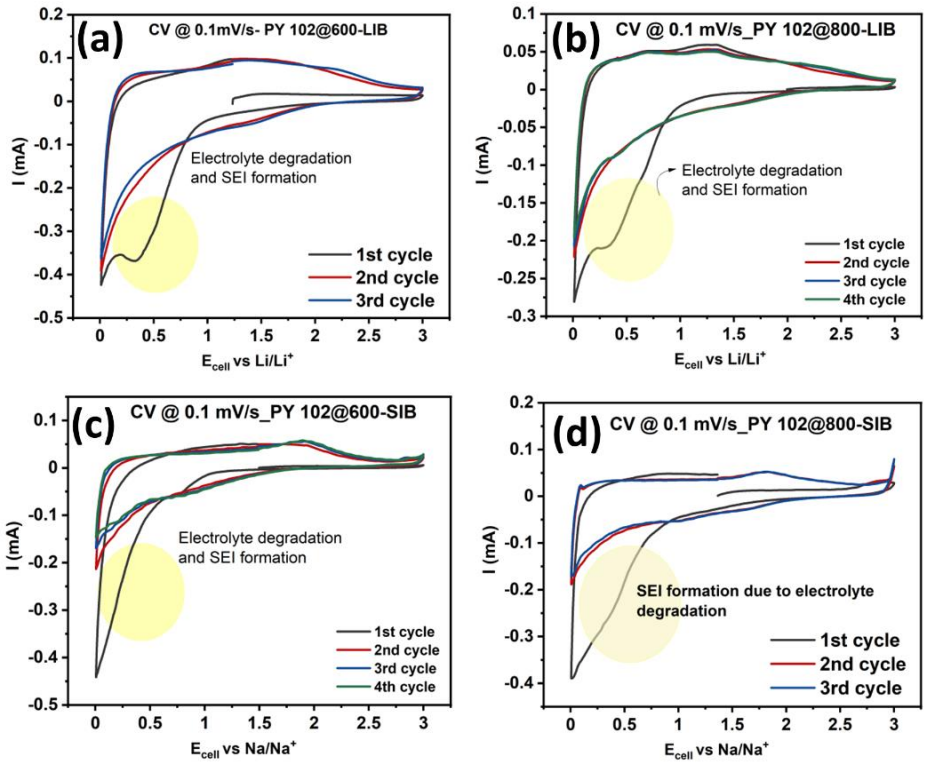

Fig 3.7 Cyclic Voltammograms for Li/Na- anodic half cells at 0.1mV/s (a, c) for PY 102@600 based electrode (b, d) PY 102@800 based electrode.

analysis conducted by fitting the data shows the contribution of individual components. (Figure 3.10 and Table 3.3).

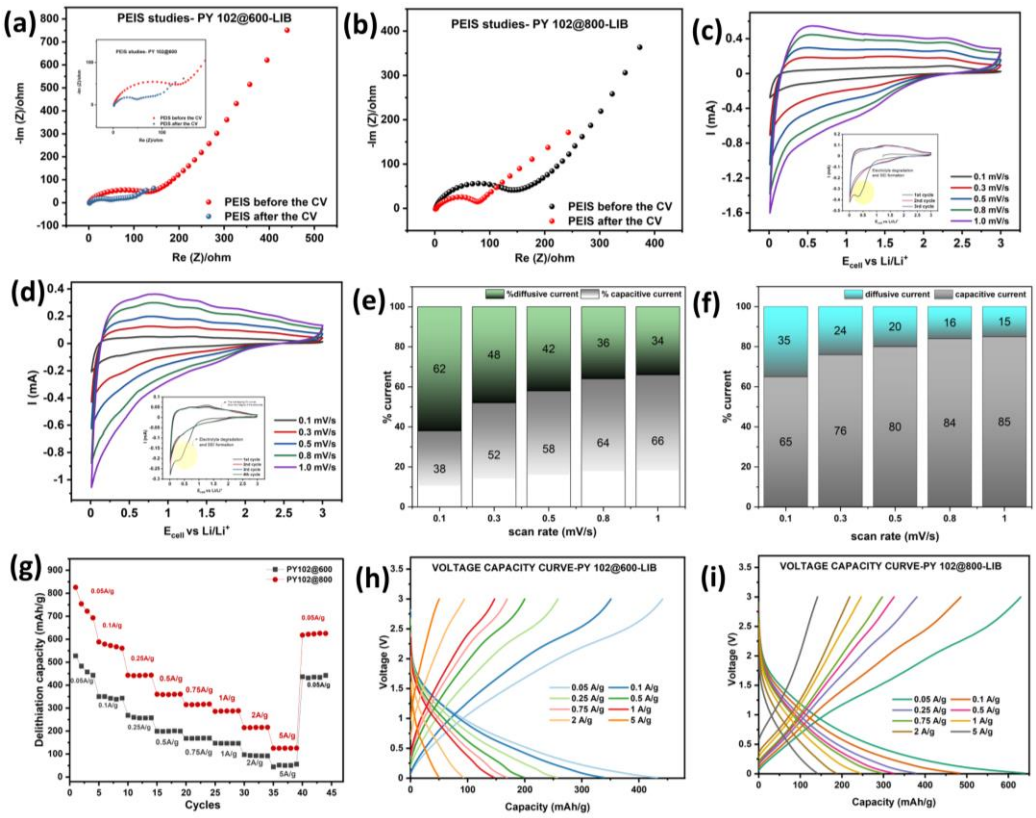

Fig 3.8: PEIS Nyquist plot of anodic half-cell before and after cyclic voltammetry (a)PY 102@600 (b)PY 102@800 based Li-anodic half-cell. CV studies at various scan rates for (c) PY 102@600 (d) PY 102@800 based Li-anodic half-cell. Comparison of the capacitive and diffusive current (e) PY 102@600 (f) PY 102@800 based Li-anodic half-cell (g)Galvanostatic charge discharge studies with PY 102@x-based Li-ion anodic half cells at different current rates (h, i) Voltage-Capacity curve profile with PY 102@x-based Na-ion anodic half cells at different current rates

For Na-ion anodic half cells, CV studies were conducted between 0.005 V and 3 V at various current rate densities to evaluate the specific capacity of the active material when used as an electrode. An irreversible peak between 0.3-0.5V was observed which is due to the SEI formation (Fig 3.9 c, d) PEIS was recorded for PY 102@x based Na-cells before and after the CV (Fig 3.9 a, b) and there was a decrease in the charge resistance after the CV was conducted proving an ease in the Na^+ ions transfer across the interface due to the conductive SEI. The anodic and cathodic peaks in the cyclic voltammograms at 0.9 V and 1.8 V (vs Na/Na^+) can be attributed to the redox reaction occurring at the S

moiety. As we can observe, this peak is consistent with all CV curves which indicates that doped S supplies great Faraday contribution on the reversible capacity.[101,102]

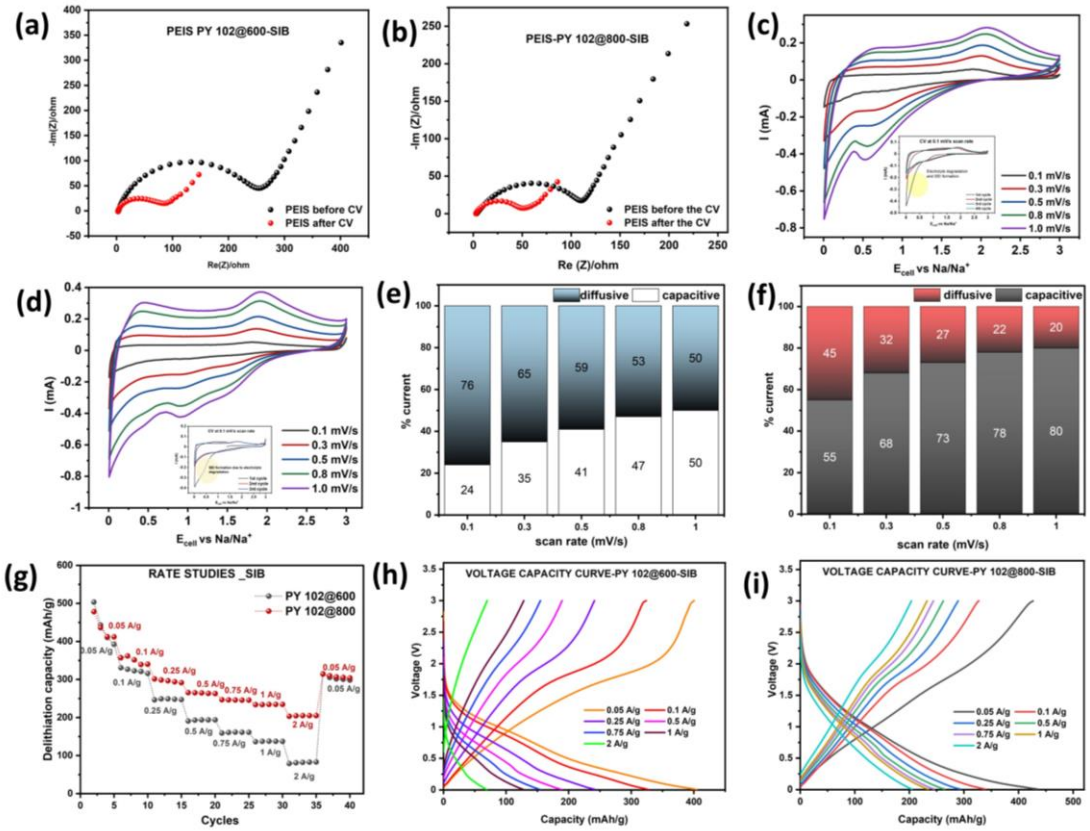

Fig 3.9: PEIS Nyquist plot of Na-anodic half-cell before and after cyclic voltammetry (a)PY 102@600 (b)PY 102@800 based Na-anodic half-cell. CV studies at various scan rates for (c) PY 102@600 (d) PY 102@800 based Na-anodic half-cell. Comparison of the capacitive and diffusive current (e) PY 102@600 (f) PY 102@800 based Na-anodic half-cell (g)Galvanostatic charge discharge studies with PY 102@x-based Na-ion anodic half cells at different rates (h, i) Voltage-Capacity curve profile with PY 102@x-based Na-ion anodic half cells at different current rates

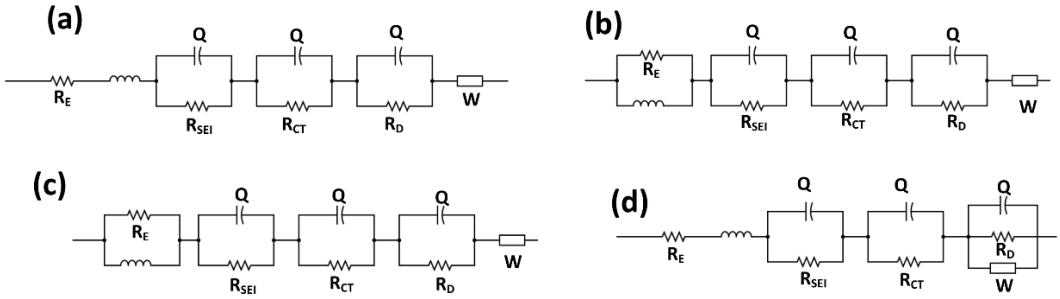

Fig 3.10 Circuit fitting analysis for PEIS data after conducting CV studies (a)PY 102@600 based Li-ion anodic half cell (b)PY 102@800 based electrode (c) PY 102@600 based Na-ion anodic half cell (b)PY 102@800 based Na-ion anodic half-cell.

Table 3.3 Circuit fitting details for PEIS data.

	R_e	R_{ct}	R_s	R_{diff}	χ^2
PY 102@600-LIB	2.369	54.76	21.5	50.54	5.72×10^{-4}
PY 102@800-LIB	2.22	35.59	19.71	20.24	4.98×10^{-4}
PY 102@600-SIB	2.746	42.7	34.69	39.437	1.312×10^{-4}
PY 102@800-SIB	2.57	43.97	41.45	113.5	8.92×10^{-5}

Charge Storage Mechanism Evaluation

To evaluate the charge storage mechanism in the case of Li-ion anodic half cells, CV studies were carried out at various scan rates and power law as mentioned in the equation 3.1 was employed[41,90],

$$i=av^b \text{ (equation 3.1)}$$

In the above equation 3.1, the peak current, while ν is the scan rate, 'b' is the exponent of the scan rate, and 'a' is the proportionality constant. Cyclic voltametric studies at 0.1, 0.3, 0.5, 0.8, and 1.0 mV/s were carried out for PY 102@x-based Li-ion anodic half cells (Fig 3.8 c, d) and Na-ion anodic half cells (Fig 3.9 c, d). Figure 3.11 (a, b, c, d) shows a plot of linear log i vs log ν. In the case of Li anodic half cells, the value of b was evaluated from the slope to be 0.74 for PY 102@600 and 0.87 for PY 102@800 which signifies a mixed charge storage mechanism including both diffusion and a capacitive process which is a surface phenomenon.

Similarly, the value of b was calculated in the case of Na-ion anodic half cells, the value of b was calculated to be 0.70 and 0.86 for PY 102@ 600 and PY 102@800 respectively which verifies the pseudocapacitive storage mechanism that is followed by the materials.

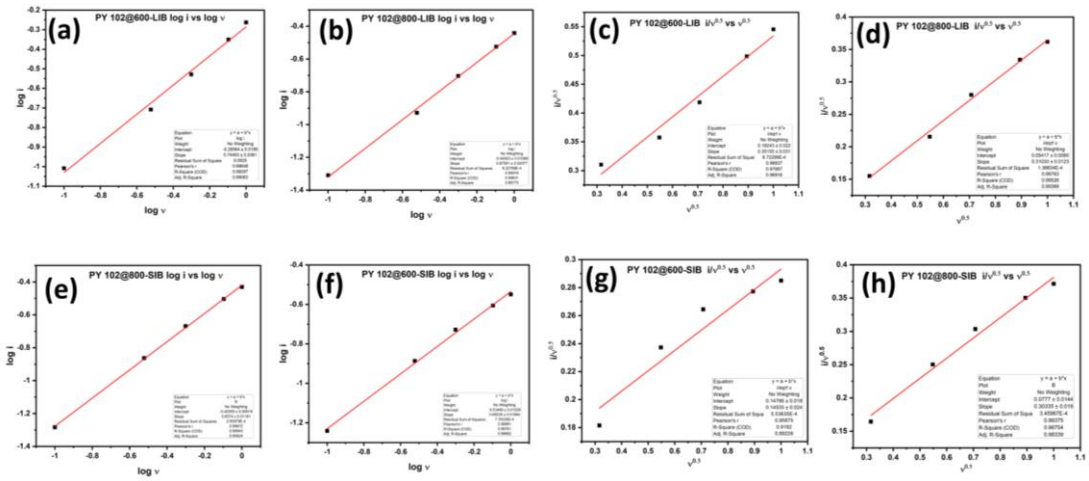

Fig 3.11 log i vs log v plots to calculate the value of b from power law (a)PY 102@600 in Li ion anodic half cell (b) PY 102@800 in Li ion anodic half cell (c) PY 102@600 in Na ion anodic half cell (d) PY 102@800 in Na ion anodic half-cell. $i/v^{0.5}$ vs $v^{0.5}$ plots to calculate the contribution of capacitive and diffusive current (e)PY 102@600 in Li ion anodic half cell (f) PY 102@600 in Li ion anodic half cell (g) PY 102@600 in Na ion anodic half cell (h) PY 102@800 in Na ion anodic half-cell.

Considering the pseudocapacitive nature, the contribution of the diffusion controlled and pseudocapacitive current in the charge storage was evaluated in each of the cases. It was observed that with the increase in the amorphous nature of the material and increase in the surface area, there was an increase reaction on the surface leading to more capacitive than faradaic current. Furthermore, at higher scan rates, the charge storage mechanism was predominantly by a capacitive behavior (Fig 3.8 e, f)[42,90].

$$i = k_c v + k_d v^{0.5} \text{ (equation 3.2)}$$

wherein i is the peak current, k_c and k_d are the proportionality constants for capacitance and diffusion, respectively, and v is the scan rate. The values for k_d and k_c were determined by constructing a plot of $i/v^{0.5}$ vs $v^{0.5}$ (Figure 3.11 e, f, g, h)

A similar behavior was observed in the case of sodium ion anodic half cells, wherein with an increase in the scan rate the charge storage mechanism tended more towards a

capacitive behavior as shown in Fig 3.9 (e, f). PY 102@800 showed predominantly capacitive behavior compared to PY 102@600.

Calculation of activation energy and diffusion coefficient

The activation energy for PY 102@x was calculated from the charge transfer resistance during the lithiation/sodiation. In the case of Li-ion anodic half cells, the cycling was carried out at 2A/g current density and at 0.2V, PEIS was recorded. Similarly for Na-ion anodic half cells, the cycling was carried out at 0.5A/g current density and a PEIS was carried out at 0.2V during the sodiation process. This was done at different temperatures, and a plot of $\ln(1/R_{ct})$ vs $10^3/T$ was plotted (Fig 3.12 g and 3.13 b). The activation energy was calculated from the slope from the formula[20],

$$\ln (1/R_{ct}) = \ln A + E_a/RT \text{ (equation 3.3)}$$

wherein $1/R_{ct}$ corresponds to conductivity, A denotes the pre-exponential factor, R is the gas constant (8.314 J/K mol), and E_a denotes the activation energy and T is the temperature (in Kelvin). Moreover, the diffusion coefficient for both the materials were calculated in both Li/Na-ion half cells.

cells in the Warburg region of the PEIS data using equation 3.4[20,103].

$$D_{Li+/Na+} = R^2T^2/2A^2n^4F^4C^2\sigma^2 \text{ (equation 3.4)}$$

In this given context, R is the gas constant, T is the absolute temperature, A is the area of the electrode, n is the charge number of the electroactive species (n = 1), F is the Faraday constant, C is the concentration of lithium ions, and σ is the Warburg factor. The Warburg factor is determined from the slope of the plots of Z′ vs $1/\omega^{-1/2}$ (wherein ω denotes the angular frequency) in the Warburg region (Fig 3.12 h and Fig 3.13 c).

The results have been tabulated below in table 3.4

Table 3.4 Activation energy and diffusion coefficient values for PY 120@x based electrodes in Li/Na-ion half cells.

Material	**Activation energy (kJ/mol)**		**Diffusion coefficient (cm^2/s)**	
	LIB	*SIB*	*LIB*	*SIB*
PY 120@600	-42.93	-39.90	$3.25*10^{-12}$	$5.59*10^{-13}$

PY 102@800	-41.27	-35.76	$1.39*10^{-11}$	$2.24*10^{-12}$

A higher surface area results in shorter diffusion pathways and higher number of transport channels and hence PY 102@800 shows a higher diffusion coefficient and lower activation energy than PY 102@600.

Rate and Long Cycling Studies for Lithium/Sodium-Ion Batteries

To investigate and evaluate the reversible lithium-ion storage, the PY POL 102@x-based coin cells were cycled at different current densities between the potential range of 0.01 V and 3 V.

In the case of Li-ion anodic half cells, for PY 102@600 based cells, the capacities observed at 50 mA/g current density is 485 mAh/g while at higher current densities of 500, 750 and 1000 mA/g the specific capacity is observed to be 200mAh/g, 168 mAh/g and 148 mAh/g respectively. In the case of PY 102@800, the specific capacity is observed to be 700 mAh/g at 50 mA/g while the specific capacities at 500 and 1000 mA/g current rate density is observed to be 358 mAh/g and 286 mAh/g respectively (Fig 3.8 g).

To understand the long cycling behavior of the materials at very high current rates, galvanostatic charge discharge studies were conducted at 1, 2, 5 and 10 A/g current density. The PY 102@600 based cells show a reversible capacity of 268 mAh/g at 1 A/g, 172 mAh/g at 2 A/g and 133 mAh/g at 5A/g current density for up to 2000 cycles with a capacity retention of more than 80% in each of the cases. The reversible capacity recorded at a very high rate of 10 A/g current density is 51 mAh/g with a retention of around 80% after 8000 cycles (Fig 3.12 a, b, c).

However, the reversible capacity obtained is 330 mAh/g, 204 mAh/g and 155 mAh/g at a current density of 1, 2 and 5 A/g for up to 2000 cycles with a retention of more than 80%. An attractive result of this material was that at a current density of 10 A/g which is equivalent to 26 C in case of graphite, the reversible capacity obtained is 80 mAh/g with a retention of 85% after 8000 cycles (Fig 3.12 d). These results show the excellent electrochemical and charge storage properties of the material and its long cycling high performance ability.

Considering the excellent performance in the LIBs and the d-spacing as calculated earlier, the materials were studied for their Na-ion storage properties in Na-ion anodic half cells. Galvanostatic charge discharge was carried out at different current densities between 0.005 V and 3 V.

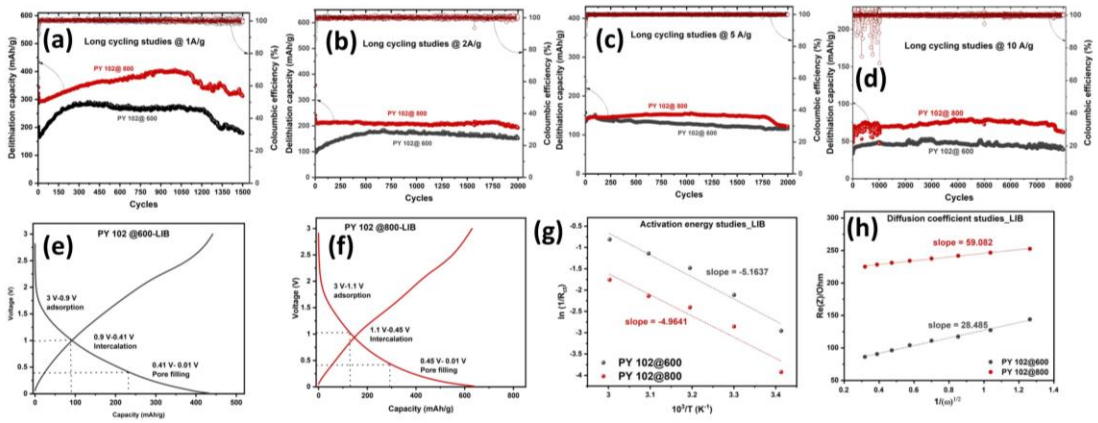

Fig 3.12: Long cycling studies with Li ion anodic half-cell at high current densities (a) 1A/g (b)2 A/g (c)5A/g (d)10 A/g. Stages of charge storage in (e)PY 102@600 (f)PY 102@800 (g) Temperature-dependent Arrhenius plot during lithiation for activation energy calculation (h) Re(Z) vs $1/\omega^{1/2}$ plot for diffusion coefficient calculation from the Warburg impedance

In the study, PY 102@600 and PY 102@800 exhibited varying specific capacities across different current densities. For PY 102@600, the specific capacity was observed to be 400 mAh/g at a current density of 50 mA/g. However, as the current density increased to 500, 750, and 1000 mA/g, the specific capacities decreased to 150 mAh/g, 120 mAh/g, and 100 mAh/g, respectively. Conversely, PY 102@800 demonstrated a specific capacity of 415 mAh/g at 50 mA/g. At higher current densities of 500 and 1000 mA/g, the specific capacities were recorded as 260 mAh/g and 220 mAh/g, respectively (see Figure 3.9g). These findings highlight the performance differences between PY 102@600 and PY 102@800 under varying charge and discharge conditions, providing insights into their suitability for different applications in energy storage technologies.

Furthermore, long cycling studies at current rates of 1 A/g were studied for PY 102@x-based materials in Na-ion anodic half cells. While PY 102@600 shows an initial capacity of 120 mAh/g at 1 A/g respectively, an initial capacity of 250 mAh/g is recorded at 1 A/g current density for PY 102@800 based cells (Fig 3.13 a).

To test the practical applicability of such materials, PY 102@x-based Li-ion full cells were fabricated (anode mass loading = ~2.8 mg/cm^2) and were cycled against NCA cathode (capacity = 175 mAh/g) between the potentials 2.8 V and 4.2 V at a current rate of 0.5 C current rate (with respect to cathode, 1C = 2.64 mAh/cm^2). PY 102@600 based electrode rendered a capacity of 150 mAh/g while PY 102@800 based electrode rendered a capacity of 165 mAh/g (Fig 3.13d).

The relationship between surface area, pore volume, and charge storage is important in understanding the performance of materials with respect to their charge storage

properties. A higher surface area material provides more active sites for reactions to occur.[38,89] Furthermore, since the reaction occurs at the surfaces leading to the capacitive current, these materials can be employed for fast charging applications. The difference in the specific capacity and the stability of PY 102@600 and PY 102@800 based cells can be explained based by drawing relationship between specific surface area and pore size and volume of the obtained carbon and its crystallinity. A lower surface area and pore volume in the case of PY 102@600 leads to poor interaction of the lithium ions with the active sites as this can limit the electrolyte infiltration and reduce the area available for ion adsorption leading to a lower specific capacity. In comparison to micropores, electrode materials with mesopores are reported to enable fast diffusion of electrolyte ions onto the inner surface of the electrode.[104] Hence, even the high number of dopants in PY 102@600, which probably can serve the active sites are failed to be accessed by the Li and Na ions. Furthermore, since the PY 102@600 has a more crystallite grain size, a higher diffusive charge storage behavior is observed which makes it relatively unsuitable compared to PY 102@800 for fast charging applications.[105] This also leads to the understanding that as we saw in the case of Na-ion anodic half cells, the charge storage

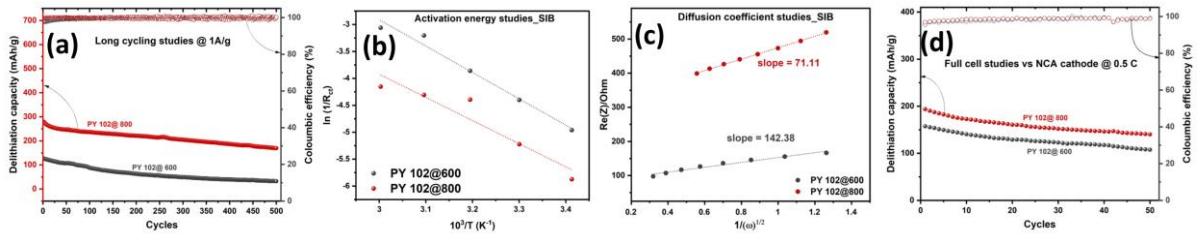

Fig 3.13 (a)Long cycling rate studies with PY 102@x-based electrodes in Na-ion anodic half cells at 1A/g current density (b) Temperature-dependent Arrhenius plot during lithiation for activation energy calculation (c) Re(Z) vs $1/\omega^{1/2}$ plot for diffusion coefficient calculation from the Warburg impedance (d)Li-ion full cell studies with NCA at 0.5C

mechanism is highly diffusion controlled. PY 102@600 type materials may not be best suited for fast charging applications in SIBs. However, in the case of PY POL 102@800, the higher mesopore volume results in an increased access and interaction with the active sites on the electrode surface for the ion storage.[49,82,96]

The adsorption within mesopores can be significant owing to the capillary condensation occurring within them. Hence, optimal usage of the active sites results in higher charge storage and capacity. The high amorphous nature, higher d-spacing and lower crystallite grain size of the material makes it suitable for fast charging applications in LIBs and is better suited than PY 102@600 for fast charging in sodium-based cells. Hence at higher rates, capacity fading also becomes very evident in the case of PY 102@600. The

lithiation of the carbons can be speculated to occur in three sequential steps: adsorption on the carbon layers, intercalation between the layers, and pore filling which was schematically depicted in Fig 3.12 e/f.[106] Furthermore, the amount of pyridinic nitrogen in the case of PY 102@800 is higher compared to PY 102@600. As per Ma et al and Kong et al, pyridinic nitrogen is highly favorable for the Li-ion storage and high storage capacity as it being a p type dopant results in a strong interaction with lithium for lithium adsorption.[107,108] Hence this can be speculated to be another reason for a higher specific capacity obtained in the case of PY 102@800 carbon in comparison to PY 102@600.
Hence nanoporous materials from POP based precursors can be attractive carbon alternatives as the adsorption in nanopores can be significant due to the enhanced volume filling and high surface area of nanoporous walls resulting in rendering of high capacity and fast charging.

Postmortem Studies

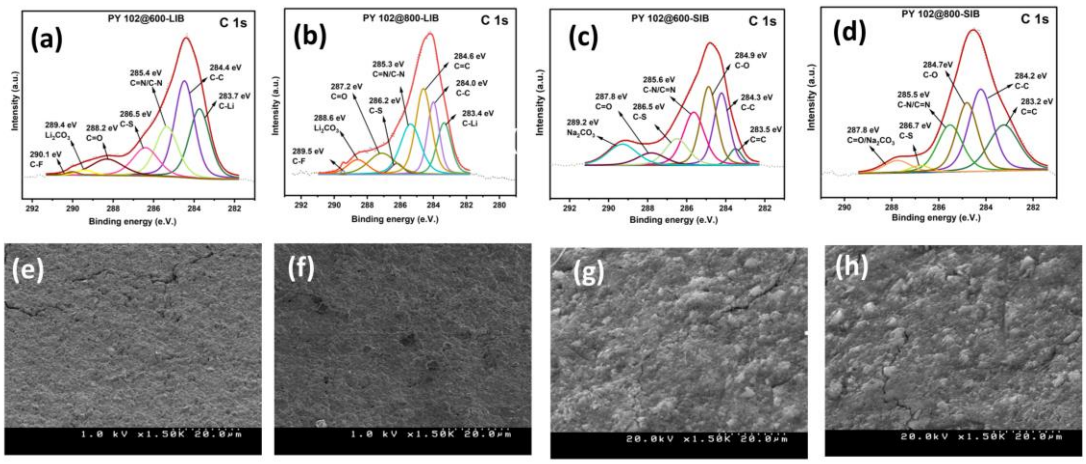

Fig 3.14: Deconvoluted C1s spectrum of cycled electrodes (a)PY 102@600 based anode in LIB (b) PY 102@800 based anode in LIB (c) PY 102@600 based anode in SIB (d) PY 102@800 based anode in SIB. FE-SEM images of cycled electrode in LIBs (e)PY 102@600 based electrode (f)PY102@800 based electrode. FE-SEM images of cycled electrode in SIBs (g)PY 102@600 based electrode (h)PY 102@800 based electrode.

XPS analysis was carried out on the disassembled cycled Li/Na-electrode (cycled at 2 A/g current density for LIB and 0.1 A/g for SIB) in a lithiated state to study the chemical composition after the charge−discharge studies and understand the nature of SEI and the interfacial properties and composition. The deconvoluted C 1s spectra of the disassembled cycled electrode showed a peak at 283.7 eV in case of PY 102@600 (Fig 8a) and 283.4 eV in PY 102@800 (Fig 3.14 b) based electrode, which corresponds to the C-Li group. Also, peaks around 285.4eV and 286.2 eV in PY 102@600 based electrode

are resultant from the heteroatoms.[35] Peaks at 286.2, 288.6, 289.7 and 290.5 eV in the deconvoluted spectra correspond to C=O, C−O−C, Li_2CO_3, and C−F groups respectively, and these are the components of SEI resulting from the electrolyte degradation.

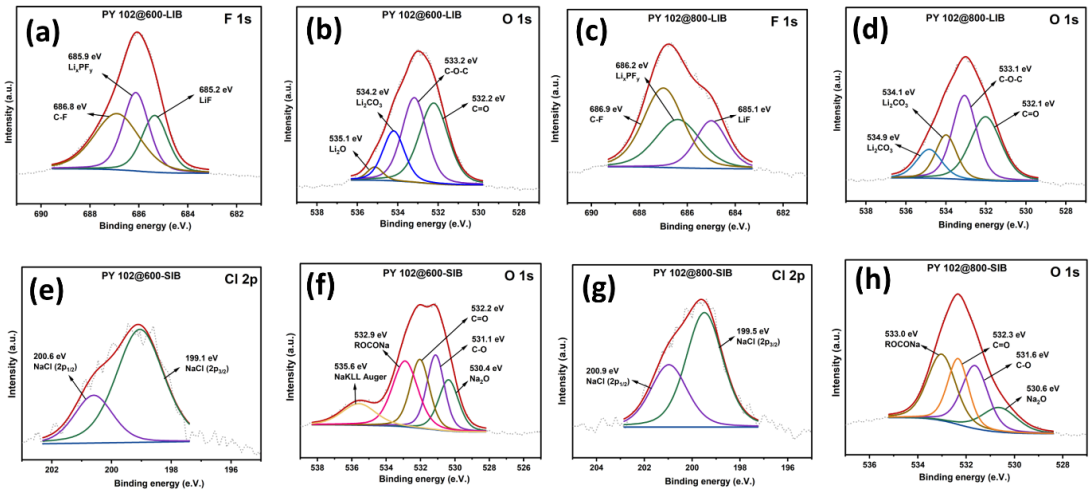

Fig 3.15 (a, b) Deconvoluted F1s and O1s spectra of cycled PY 102@600 based electrodes (LIB) (c, d) Deconvoluted F1s and O1s spectra of cycled PY 102@800 based electrodes (LIB) (e, f) Deconvoluted Cl2p and O1s spectra of cycled PY 102@600 based electrodes (SIB) (g, h) Deconvoluted Cl2p and O1s spectra of cycled PY 102@800 based electrodes (SIB)

In the case of the disassembled cycled electrode from Na-ion anodic half-cell, the deconvoluted spectra showed peaks at 289.5 eV in PY 102@600 and 289.2 eV in PY 102@800 which corresponds to the carbonate species formed due to the electrolyte degradation during the initial cycles. The other deconvoluted spectrum from the components of SEI, i.e. F 1s in lithium batteries and Cl 2p in the case of sodium batteries, and O1s for each of the batteries considered under this study has been presented in the Fig 3.15.The presence of rich inorganic species in the inner of the double layer of SEI helps in the easy and fast diffusion of lithium and sodium ions helping in better kinetics and prevention of continuous reduction of electrolyte. Besides, FE-SEM was carried out on the cycled electrodes in each of the cases to understand the change in the morphology of the active material and SEI after cycling (Fig 3.14 e, f, g, h).

Conclusion

In conclusion, a Porous organic Polymer, POL 102 was synthesized via Schiff's base reaction to obtain a highly conjugated porous polymeric material which was pyrolyzed at two different temperatures, 600 and 800°C to obtain PY 102@600 and PY 102@800 respectively. The high surface area of the precursor material was preserved as the carbon

obtained was found out to have high surface area and pore volume without the use of any activating agents. Considering these advantages, it was considered as an exploratory active material in the case of lithium and sodium-ion batteries. POL 102 based Li/Na-anodic half cells showed excellent electrochemical properties. Notably, PY 102@800 owing to its greater surface area and higher mesopore volume renders a reversible capacity of 850 mAh/g at 100 mA/g current density. At higher current densities of 1000, 2000 and 5000 mA/g, the reversible capacity observed was 510, 270 and 205 mAh/g respectively. The most striking feature of the carbon derived was that at 10 A/g current density, a reversible capacity of 80 mAh/g is observed. Furthermore, in the case of Na-ion anodic half cells, with PY 102@800 based electrodes, a reversible capacity of 270 mAh/g is recorded. Moreover, the rich inorganic species in the inner of the double layer of SEI which was characterized by FE-SEM and XPS in all the electrodes facilitates the easy diffusion of the Li/Na-ions. While the applications of carbons obtained from such self-template-based POP precursors in metal ion batteries is limited, this work adds to the scientific knowledge and development and provides an avenue for such materials.

CHAPTER 4 CONCLUSION

General Conclusion

In conclusion, this thesis has explored the enhancement of storage and rate performance in lithium and sodium-ion batteries through the application of donor-acceptor based conjugated polymers and N, S-co doped carbon materials derived from porous organic polymers. The research demonstrated that these types of materials offer significant improvements in electrochemical properties, attributed to their unique structural features and functional properties. Polymers designed with donor-acceptor motifs, exhibited abundant active sites, and a low redox potential facilitating efficient ion transport and robust electrochemical stability. These properties were critical in achieving high-capacity retention and superior rate capabilities in lithium-ion batteries.

Furthermore, porous organic polymer derived hierarchical porous carbon materials were explored and these had the advantages of enhanced electrical conductivity and optimal textual and pore properties resulting in an augmented electrochemical performance in lithium and sodium ion batteries.

Experimental results confirmed that the synthesized materials not only surpassed conventional electrode materials in terms of capacity and cycling stability but also provided insights into the mechanisms driving these improvements. In summary, this work underscores the potential of donor-acceptor based conjugated porous polymers and their carbon derivatives as attractive avenues for active materials. By addressing the key challenges in battery technology, such as capacity degradation and rate performance, the findings of this research contribute to the advancement of more efficient, durable, and high-performing lithium and sodium-ion batteries. Future research may build upon these insights to further refine material properties and explore new applications in energy storage.

Learnings from the work:

With graphite's limitations as a suitable anode material for fast-charging applications and as an active material in sodium-ion batteries, the scientific community has recently shown interest in developing sustainable polymers. One key strategy to enhance materials with fast-charging abilities is to reduce path length and increase specific capacity by incorporating more active sites. Due to their tunable structure and low carbon footprint, conjugated organic polymers have garnered significant attention.

In Chapter 2, a donor-acceptor-based conjugated polymer with enhanced pseudocapacitive nature was investigated. The presence of donor-acceptor motifs—nitrogen and sulfur—results in increased power density. The alternating electron-donating

and electron-accepting groups create pathways for efficient charge transport along the polymer chain, while porosity aids in reducing diffusion path length, facilitating fast-charging processes. In POL 202, a low redox potential enables efficient electron transfer between donor and acceptor units within the polymer, enhancing charge carrier mobility crucial for fast electron movement in batteries and capacitors.

Tuning precursor materials can yield different pore complexities, impacting charge and mass transport within the material, making organic polymers attractive as anode materials. Furthermore, inherent porosity in such materials can be exploited to derive nanoporous carbon materials without additional modification steps. By altering precursor materials from benzene tetraamine to melamine, introducing more nitrogen moieties into resulting polymers enhances carbon derived from pyrolysis, expectedly increasing nitrogen content. The high surface area of such materials can effectively yield nanoporous carbon with superior surface area utilization. This feature of high surface area and nanopores can aid in the reduction of the diffusion length and hence can help in the fast-charging applications.

Overall, Chapter 2 and Chapter 3 outline the advantages of designing tunable conjugated polymers and their multiple advantage in terms of their evaluation of their applications in energy storage devices.

Chapter 1 Summary

In the modern era, with energy pivotal for economic advancement, the reliance on fossil fuels like oil, natural gas, and coal has led to environmental concerns and highlighted the need for sustainable energy sources. Electrochemical Energy Storage (EES) solutions, including supercapacitors and fuel cells, have emerged as promising technologies to address these challenges.

Supercapacitors, or electric double-layer capacitors (EDLCs), store energy electrostatically, offering rapid energy delivery and storage, making them ideal for applications requiring quick energy transfer such as regenerative braking in cars and energy harvesting systems. With high power density, exceptional cycle life, and temperature performance, they surpass traditional batteries. Research focuses on enhancing their energy density through materials science and nanotechnology for broader applications.

Fuel cells, renowned for their high efficiency and environmental friendliness, convert chemical energy directly into electrical energy while generating heat and water as

byproducts. They find applications in stationery and portable power generation, with various types like proton exchange membrane fuel cells (PEMFC) and solid oxide fuel cells (SOFC) offering diverse advantages. Ongoing research aims to improve fuel cell performance and broaden their applications.

Batteries, crucial for storing and providing electrical energy, consist of electrochemical cells enabling electron flow from anode to cathode through an external circuit. Lithium-ion batteries (LIBs) have become preferred for their low reduction potential, rapid diffusion, and high volumetric power density. They operate on "intercalation" chemistry, wherein lithium ions migrate between electrodes during charge and discharge cycles. Advanced electrolytes and innovative polymeric binders are integral for enhancing LIB performance, ensuring high ionic conductivity, stability, and temperature resilience.

Innovative electrolytes contribute to higher energy density, power density, and extended cycle life, supporting the evolution of secondary batteries as sustainable energy storage solutions. Polymeric binders, crucial components in LIBs, link active materials, conductive additives, and current collectors. Traditional binders like poly(vinylidene fluoride) (PVDF) pose issues with high-loading electrodes, prompting research into alternative polymers like sodium alginate, poly(acrylic acid) (PAA), and polyionic liquids (PILs). PILs show promise for improving wettability, solid electrolyte interphase (SEI) formation, and lithium-ion diffusion coefficient, enhancing LIB performance and longevity.

Cathodes, essential for facilitating lithium-ion insertion and extraction, include various materials like lithium cobalt oxide ($LiCoO_2$), lithium nickel manganese cobalt oxide (NMC), and lithium iron phosphate ($LiFePO_4$), each with unique advantages for diverse applications. Research explores novel cathode chemistries like solid-state cathodes and sulfur-based cathodes to enhance energy density and sustainability alongside conventional materials.

The different types of anodes are intercalation-type, conversion-type, and alloy-type and are based primarily in the way they store charge. Carbonaceous materials and transition metal oxides (TMOs) represent intercalation-type anodes, offering minimal structural distortion and volume changes during ion insertion. Conversion-type anodes, exemplified by TMOs like Fe_2O_3 and MnO, boast high specific capacity but face challenges with low ionic conductivity. Alloy-type anodes, blending Si, Ge, Sn, and other metals, promise

large capacities but encounter issues with material pulverization and SEI instability.

Furthermore, heteroatom doping with elements like N, S, P, and B in carbon materials stands as a prominent method to enhance anode properties crucial for LIBs. Boron doping introduces p-type characteristics, enhancing electron conductivity, while N-doping improves conductivity and introduces redox active sites. P and S doping contribute to conductivity and facilitate faster Li-ion diffusion. Microstructure regulation, introducing pores and disorderliness, enhances Li-ion kinetics, although challenges with hard carbons remain.

Sodium-ion batteries (SIBs) emerge as promising alternatives to LIBs, with research focusing on electrode materials, electrolytes, and cell design optimization. The thesis aims to explore the applications of conjugated organic polymers in energy devices, particularly LIBs and SIBs, contributing to scientific understanding and potential industrial products.

Chapter 2 Summary

Current research in lithium-ion batteries (LIBs) focuses on high-capacity materials and improved kinetics. Organic conjugated polymers have drawn interest for their tunable structure and robustness. An effective strategy to enhance the electrochemical performance is by the introduction of a donor-acceptor pairs as it improves the electronic interaction due to reduction in the band gap and results in increasing the power density. The study introduced POL 202, a donor-acceptor-based porous polymer, synthesized via simple polycondensation. Cyclic voltammetry revealed a pseudocapacitive charge storage mechanism crucial for fast charging. POL 202 exhibited impressive capacity retention, with 850 mAh/g at 100 mA/g and 8-minute charging time, alongside reversible capacities at various current densities. This research highlighted the potential of designing donor acceptor based polymeric active materials with improved electrochemical properties.

Chapter 3 Summary

The microstructure of carbonaceous materials crucially influences ion diffusion in anodes, but synthesizing optimal carbon structures is challenging. Porous Organic Polymers (POPs) show promise due to their rigid, π-π stacking, enabling high surface area and heteroatom incorporation from one source. This chapter focused upon a hierarchical N, S co-doped micro/mesoporous carbon, derived from a POP, POL 102 at 600°C and 800°C. Carbon at 800°C exhibited superior electrochemical performance in

Li/Na-ion cells, owing to its ideal pore volume and surface area, rendering high reversible capacities in both Li and Na-ion anodic half cells. This research highlighted the potential of heterodoped nanoporous materials from conjugated polymers for enhanced electrochemical applications.

PROSPECTS

Organic polymers offer a sustainable, versatile, and safer alternative to conventional battery materials. With abundant renewable sources, they promise affordable energy storage solutions. Their tunable properties enable tailored performance, including high charge capacities and fast charging rates. Despite challenges like limited conductivity and scalability issues, ongoing research aims to optimize their performance. As we address these hurdles, organic polymer-based batteries could drive innovation in energy storage, fostering a greener and more sustainable future. Furthermore, research can be dedicated towards finding more inexpensive starting reactants for the development of porous organic polymers. Using porous organic polymers or porous carbon materials holds promise due to their tunable pore structures, high surface areas, and chemical versatility without the use of any hazardous chemicals and activating agents. These also employ renewable resources and reduce environmental impact, aligning with sustainability goals. Also, a certain amount of research can be dedicated towards finding renewable precursors like biomass-derived monomers or sustainable synthetic routes.

Hence, POPs may contribute towards mitigating environmental impact and advancing sustainability objectives in materials science and engineering.

PUBLICATIONS AND CONFERENCES

Publications

1. "Donor Acceptor Based Conjugated Polymeric Active Material with Enhanced Pseudocapacitive Contribution for Ultra-Fast Charging Lithium-Ion Batteries."
Revisions submitted to the Editorial Office.
Saibrata Punyasloka, Koichi Higashimine and Noriyoshi Matsumi
ACS Appl. Energy Materials
Selected for cover page artwork.

2. "Enabling Ultrafast Charging in Graphite Anodes Using BIAN-Based/Lithium polyacrylate as a Binder."
Sameer Nirupam Mishra, Saibrata Punyasloka, Bharat Srimitra Mantripragada, Anusha Pradhan and Noriyoshi Matsumi
ACS Appl. Energy Materials

3. Improving the Storage and Rate Performance of Lithium/Sodium-Ion Batteries with Porous Polymer Derived N, S Co-doped Hierarchical Micro/Mesoporous Carbon
Saibrata Punyasloka, Kottisa Sumala Patnaik, Koichi Higashimine and Noriyoshi Matsumi
Manuscript under preparation.

Conferences

Poster Presentations

1. Charge-Discharge Study of Lithium-Ion Secondary Batteries Using Bithiophene Containing Imine-Based Conjugated Polymer as Anodic Active Material

第 72 回高分子学会年次大会

会期：2023 年 5 月 24 日（水）～26 日（金）

会場：Gメッセ群馬

2. Bithiophene Based Donor Acceptor Type Network Polymeric Host with Pseudocapacitive Charge Storage For Fast Charging Lithium-Ion Batteries.

第 72 回高分子討論会

会期：2023 年 9 月 26 日（火）～28 日（木）

会場：香川大学 幸町キャンパス

Oral presentation-

3. Study of storage and rate capability of Lithium-Ion Secondary Batteries Using Bithiophene Containing Imine-Based Conjugated Polymer as Anodic Active Material (Online presentation)
6th International Conference on Clean Energy and Technology (CEAT 2023), 7th - 8th June 2023
Penang, Malaysia
4. Donor Acceptor Type Polymeric Active Material with Pseudocapacitive Storage for Fast Charging Lithium-Ion Batteries
The 64th Battery Symposium in Japan, November 28th to 30th, 2023
Osaka International Convention Center, Osaka, Japan

REFERENCES

(1) Energy-Storage-Systems-Market-Size-to-Surpass-Us.

(2) Ahmad, T.; Zhang, D. A Critical Review of Comparative Global Historical Energy Consumption and Future Demand: The Story Told so Far. *Energy Reports*. Elsevier Ltd November 1, 2020, pp 1973–1991. https://doi.org/10.1016/j.egyr.2020.07.020.

(3) Drummond, R.; Huang, C.; Grant, P. S.; Duncan, S. R. Overcoming Diffusion Limitations in Supercapacitors Using Layered Electrodes. *J Power Sources* **2019**, *433*. https://doi.org/10.1016/j.jpowsour.2019.04.107.

(4) Lakshmi, K. C. S.; Vedhanarayanan, B. High-Performance Supercapacitors: A Comprehensive Review on Paradigm Shift of Conventional Energy Storage Devices. *Batteries*. MDPI April 1, 2023. https://doi.org/10.3390/batteries9040202.

(5) Chaudhary, M.; Nayak, A. K.; Muhammad, R.; Pradhan, D.; Mohanty, P. Nitrogen-Enriched Nanoporous Polytriazine for High-Performance Supercapacitor Application. *ACS Sustain Chem Eng* **2018**, *6* (5), 5895–5902. https://doi.org/10.1021/acssuschemeng.7b04254.

(6) Chen, T.; Dai, L. Carbon Nanomaterials for High-Performance Supercapacitors. *Materials Today*. July 2013, pp 272–280. https://doi.org/10.1016/j.mattod.2013.07.002.

(7) Kim, S. I.; Lee, J. S.; Ahn, H. J.; Song, H. K.; Jang, J. H. Facile Route to an Efficient Nio Supercapacitor with a Three-Dimensional Nanonetwork Morphology. *ACS Appl Mater Interfaces* **2013**, *5* (5), 1596–1603. https://doi.org/10.1021/am3021894.

(8) Yan, S. Xue; Wang, Q.; Luo, S. Hua; Zhang, Y. hui; Liu, X.; Liu, Y. Guo; Wang, Z. Yuan; Hao, A. Min; Yi, T. Feng. Coal-Based S Hybrid Self-Doped Porous Carbon for High-Performance Supercapacitors and Potassium-Ion Batteries. *J Power Sources* **2020**, *461*. https://doi.org/10.1016/j.jpowsour.2020.228151.

(9) Sharaf, O. Z.; Orhan, M. F. An Overview of Fuel Cell Technology: Fundamentals and Applications. *Renewable and Sustainable Energy Reviews*. April 2014, pp 810–853. https://doi.org/10.1016/j.rser.2014.01.012.

(10) Fan, L.; Tu, Z.; Chan, S. H. Recent Development of Hydrogen and Fuel Cell Technologies: A Review. *Energy Reports*. Elsevier Ltd November 1, 2021, pp 8421–8446. https://doi.org/10.1016/j.egyr.2021.08.003.

(11) Bryner, M. *Lithium-Ion Batteries*; 2013; Vol. 109. https://doi.org/10.5104/jiep.2.45.

(12) Xu, W.; Welty, C.; Peterson, M. R.; Read, J. A.; Stadie, N. P. Exploring the Limits of the Rapid-Charging Performance of Graphite as the Anode in Lithium-Ion Batteries. *J Electrochem Soc* **2022**, *169* (1), 010531. https://doi.org/10.1149/1945-

7111/ac4b87.

(13) Asenbauer, J.; Eisenmann, T.; Kuenzel, M.; Kazzazi, A.; Chen, Z.; Bresser, D. The Success Story of Graphite as a Lithium-Ion Anode Material-Fundamentals, Remaining Challenges, and Recent Developments Including Silicon (Oxide) Composites. *Sustainable Energy and Fuels*. Royal Society of Chemistry November 1, 2020, pp 5387–5416. https://doi.org/10.1039/d0se00175a.

(14) Manthiram, A. A Reflection on Lithium-Ion Battery Cathode Chemistry. *Nature Communications*. Nature Research December 1, 2020. https://doi.org/10.1038/s41467-020-15355-0.

(15) Kim, T.; Song, W.; Son, D. Y.; Ono, L. K.; Qi, Y. Lithium-Ion Batteries: Outlook on Present, Future, and Hybridized Technologies. *Journal of Materials Chemistry A*. Royal Society of Chemistry 2019, pp 2942–2964. https://doi.org/10.1039/C8TA10513H.

(16) Mishra, A. K.; Monika; Patial, B. S. A Review on Recent Advances in Anode Materials in Lithium Ion Batteries. *Materials Today Electronics* **2024**, *7*. https://doi.org/10.1016/j.mtelec.2024.100089.

(17) Nitta, N.; Wu, F.; Lee, J. T.; Yushin, G. Li-Ion Battery Materials: Present and Future. *Materials Today*. Elsevier B.V. June 1, 2015, pp 252–264. https://doi.org/10.1016/j.mattod.2014.10.040.

(18) Gupta, A.; Badam, R.; Nag, A.; Kaneko, T.; Matsumi, N. Bis-Imino-Acenaphthenequinone-Paraphenylene-Type Condensation Copolymer Binder for Ultralong Cyclable Lithium-Ion Rechargeable Batteries. *ACS Appl Energy Mater* **2021**, *4* (3), 2231–2240. https://doi.org/10.1021/acsaem.0c02742.

(19) Gupta, A.; Badam, R.; Matsumi, N. Heavy-Duty Performance from Silicon Anodes Using Poly(BIAN)/Poly(Acrylic Acid)-Based Self-Healing Composite Binder in Lithium-Ion Secondary Batteries. *ACS Appl Energy Mater* **2022**, *5* (7), 7977–7987. https://doi.org/10.1021/acsaem.2c00278.

(20) Mishra, S. N.; Punyasloka, S.; Mantripragada, B. S.; Pradhan, A.; Matsumi, N. Enabling Ultrafast Charging in Graphite Anodes Using BIAN-Based Conjugated Polymer/Lithium Polyacrylate as a Binder. *ACS Appl Energy Mater* **2023**. https://doi.org/10.1021/acsaem.3c02129.

(21) Liu, C.; Neale, Z. G.; Cao, G. Understanding Electrochemical Potentials of Cathode Materials in Rechargeable Batteries. *Materials Today*. Elsevier B.V. March 1, 2016, pp 109–123. https://doi.org/10.1016/j.mattod.2015.10.009.

(22) Gupta, A.; Badam, R.; Takamori, N.; Minakawa, H.; Masuo, S.; Takaya, N.; Matsumi, N. Microbial Pyrazine Diamine Is a Novel Electrolyte Additive That

Shields High-Voltage LiNi1/3Co1/3Mn1/3O2 Cathodes. *Sci Rep* **2022**, *12* (1). https://doi.org/10.1038/s41598-022-22018-1.

(23) Zhang, H.; Yang, Y.; Ren, D.; Wang, L.; He, X. Graphite as Anode Materials: Fundamental Mechanism, Recent Progress and Advances. *Energy Storage Materials*. Elsevier B.V. April 1, 2021, pp 147–170. https://doi.org/10.1016/j.ensm.2020.12.027.

(24) Persson, K.; Sethuraman, V. A.; Hardwick, L. J.; Hinuma, Y.; Meng, Y. S.; Van Der Ven, A.; Srinivasan, V.; Kostecki, R.; Ceder, G. Lithium Diffusion in Graphitic Carbon. *Journal of Physical Chemistry Letters* **2010**, *1* (8), 1176–1180. https://doi.org/10.1021/jz100188d.

(25) Zhang, H.; Yang, Y.; Xu, H.; Wang, L.; Lu, X.; He, X. Li4Ti5O12 Spinel Anode: Fundamentals and Advances in Rechargeable Batteries. *InfoMat*. John Wiley and Sons Inc April 1, 2022. https://doi.org/10.1002/inf2.12228.

(26) Lu, Y.; Yu, L.; Lou, X. W. (David). Nanostructured Conversion-Type Anode Materials for Advanced Lithium-Ion Batteries. *Chem*. Elsevier Inc. May 10, 2018, pp 972–996. https://doi.org/10.1016/j.chempr.2018.01.003.

(27) Xu, H.; Li, H.; Wang, X. The Anode Materials for Lithium-Ion and Sodium-Ion Batteries Based on Conversion Reactions: A Review. *ChemElectroChem*. John Wiley and Sons Inc May 2, 2023. https://doi.org/10.1002/celc.202201151.

(28) Tao, W.; Wang, P.; You, Y.; Park, K.; Wang, C. Y.; Li, Y. K.; Cao, F. F.; Xin, S. Strategies for Improving the Storage Performance of Silicon-Based Anodes in Lithium-Ion Batteries. *Nano Res* **2019**, *12* (8), 1739–1749. https://doi.org/10.1007/s12274-019-2361-4.

(29) Chen, X.; Zheng, J.; Li, L.; Chu, W. Strategy for Enhanced Performance of Silicon Nanoparticle Anodes for Lithium-Ion Batteries. *RSC Adv* **2022**, *12* (28), 17889–17897. https://doi.org/10.1039/d2ra02007f.

(30) Yang, M.; Long, X.; Li, H.; Chen, H.; Liu, P. Porous Organic-Polymer-Derived Nitrogen-Doped Porous Carbon Nanoparticles for Efficient Oxygen Reduction Electrocatalysis and Supercapacitors. *ACS Sustain Chem Eng* **2019**, *7* (2), 2236–2244. https://doi.org/10.1021/acssuschemeng.8b04919.

(31) Tan, K. T.; Ghosh, S.; Wang, Z.; Wen, F.; Rodríguez-San-Miguel, D.; Feng, J.; Huang, N.; Wang, W.; Zamora, F.; Feng, X.; Thomas, A.; Jiang, D. Covalent Organic Frameworks. *Nature Reviews Methods Primers* **2023**, *3* (1). https://doi.org/10.1038/s43586-022-00181-z.

(32) Xu, D.; Liang, M.; Qi, S.; Sun, W.; Lv, L. P.; Du, F. H.; Wang, B.; Chen, S.; Wang, Y.; Yu, Y. The Progress and Prospect of Tunable Organic Molecules for Organic

Lithium-Ion Batteries. *ACS Nano* **2021**, *15* (1), 47–80. https://doi.org/10.1021/acsnano.0c05896.

(33) Optical, E. T. N. Donor − Acceptor Covalent Organic. **2023**. https://doi.org/10.1021/acsmaterialslett.2c01196.

(34) Zhu, D.; Xu, G.; Barnes, M.; Li, Y.; Tseng, C. P.; Zhang, Z.; Zhang, J. J.; Zhu, Y.; Khalil, S.; Rahman, M. M.; Verduzco, R.; Ajayan, P. M. Covalent Organic Frameworks for Batteries. *Advanced Functional Materials*. John Wiley and Sons Inc August 1, 2021. https://doi.org/10.1002/adfm.202100505.

(35) Mantripragada, B. S.; Badam, R.; Matsumi, N. BIAN-Based Porous Organic Polymer as a High-Performance Anode for Lithium-Ion Batteries. *ACS Appl Energy Mater* **2022**, *5* (6), 6903–6912. https://doi.org/10.1021/acsaem.2c00530.

(36) Varma, A.; Badam, R.; James, A. L.; Higashimine, K.; Jasuja, K.; Matsumi, N. Titanium Diboride-Based Hierarchical Nanosheets as Anode Material for Li-Ion Batteries. *ACS Appl Nano Mater* **2022**, *5* (11), 16154–16163. https://doi.org/10.1021/acsanm.2c03054.

(37) Yu, X.; Li, C.; Ma, Y.; Li, D.; Li, H.; Guan, X.; Yan, Y.; Valtchev, V.; Qiu, S.; Fang, Q. Crystalline, Porous, Covalent Polyoxometalate-Organic Frameworks for Lithium-Ion Batteries. *Microporous and Mesoporous Materials* **2020**, *299*. https://doi.org/10.1016/j.micromeso.2020.110105.

(38) Liu, X.; Liu, C. F.; Xu, S.; Cheng, T.; Wang, S.; Lai, W. Y.; Huang, W. Porous Organic Polymers for High-Performance Supercapacitors. *Chemical Society Reviews*. Royal Society of Chemistry 2022. https://doi.org/10.1039/d2cs00065b.

(39) Yuan, Y.; Chen, Z.; Yu, H.; Zhang, X.; Liu, T.; Xia, M.; Zheng, R.; Shui, M.; Shu, J. Heteroatom-Doped Carbon-Based Materials for Lithium and Sodium Ion Batteries. *Energy Storage Materials*. Elsevier B.V. November 1, 2020, pp 65–90. https://doi.org/10.1016/j.ensm.2020.07.027.

(40) Xu, F.; Wu, D.; Fu, R.; Wei, B. Design and Preparation of Porous Carbons from Conjugated Polymer Precursors. *Materials Today*. Elsevier B.V. December 1, 2017, pp 629–656. https://doi.org/10.1016/j.mattod.2017.04.026.

(41) Patnaik, K. S.; Badam, R.; Peng, Y.; Higashimine, K.; Kaneko, T.; Matsumi, N. Extremely Fast Charging Lithium-Ion Battery Using Bio-Based Polymer-Derived Heavily Nitrogen Doped Carbon. *Chemical Communications* **2021**, *57* (100), 13704–13707. https://doi.org/10.1039/d1cc04931c.

(42) Mantripragada, B. S.; Patnaik, M. K. S.; Higashimine, K.; Badam, R.; Matsumi, N. Energy Efficient and Fast Charging Nitrogen Doped Carbon Anodes Derived from BIAN-Melamine Based Porous Organic Polymer for Lithium-Ion Batteries. *Batter*

Supercaps **2024**. https://doi.org/10.1002/batt.202300515.

(43) Wu, Y. P.; Rahm, E.; Holze, R. *Carbon Anode Materials for Lithium Ion Batteries*.

(44) Hwang, J. Y.; Myung, S. T.; Sun, Y. K. Sodium-Ion Batteries: Present and Future. *Chemical Society Reviews*. Royal Society of Chemistry June 21, 2017, pp 3529–3614. https://doi.org/10.1039/c6cs00776g.

(45) Shao, W.; Shi, H.; Jian, X.; Wu, Z. S.; Hu, F. Hard-Carbon Anodes for Sodium-Ion Batteries: Recent Status and Challenging Perspectives. *Advanced Energy and Sustainability Research*. John Wiley and Sons Inc July 1, 2022. https://doi.org/10.1002/aesr.202200009.

(46) Fang, G.; Wu, Z.; Zhou, J.; Zhu, C.; Cao, X.; Lin, T.; Chen, Y.; Wang, C.; Pan, A.; Liang, S. Observation of Pseudocapacitive Effect and Fast Ion Diffusion in Bimetallic Sulfides as an Advanced Sodium-Ion Battery Anode. *Adv Energy Mater* **2018**, *8* (19). https://doi.org/10.1002/aenm.201703155.

(47) Aslfattahi, N.; Samylingam, L.; Kiai, M. S.; Kadirgama, K.; Kulish, V.; Schmirler, M.; Said, Z. State-of-the-Art Review on Electrolytes for Sodium-Ion Batteries: Potential Recent Progress and Technical Challenges. *Journal of Energy Storage*. Elsevier Ltd November 30, 2023. https://doi.org/10.1016/j.est.2023.108781.

(48) Deng, D. Li-Ion Batteries: Basics, Progress, and Challenges. *Energy Science and Engineering*. John Wiley and Sons Ltd September 1, 2015, pp 385–418. https://doi.org/10.1002/ese3.95.

(49) Li, A.; Tong, Y.; Cao, B.; Song, H.; Li, Z.; Chen, X.; Zhou, J.; Chen, G.; Luo, H. MOF-Derived Multifractal Porous Carbon with Ultrahigh Lithium-Ion Storage Performance. *Sci Rep* **2017**, *7*. https://doi.org/10.1038/srep40574.

(50) Usseglio-Viretta, F. L. E.; Mai, W.; Colclasure, A. M.; Doeff, M.; Yi, E.; Smith, K. Enabling Fast Charging of Lithium-Ion Batteries through Secondary- /Dual- Pore Network: Part I - Analytical Diffusion Model. *Electrochim Acta* **2020**, *342*. https://doi.org/10.1016/j.electacta.2020.136034.

(51) Liu, Y.; Jiang, S. P.; Shao, Z. Intercalation Pseudocapacitance in Electrochemical Energy Storage: Recent Advances in Fundamental Understanding and Materials Development. *Materials Today Advances*. Elsevier Ltd September 1, 2020. https://doi.org/10.1016/j.mtadv.2020.100072.

(52) Sun, T.; Xie, J.; Guo, W.; Li, D. S.; Zhang, Q. Covalent–Organic Frameworks: Advanced Organic Electrode Materials for Rechargeable Batteries. *Advanced Energy Materials*. Wiley-VCH Verlag May 1, 2020. https://doi.org/10.1002/aenm.201904199.

(53) Shea, J. J.; Luo, C. Organic Electrode Materials for Metal Ion Batteries. *ACS Appl*

Mater Interfaces **2020**, *12* (5), 5361–5380. https://doi.org/10.1021/acsami.9b20384.

(54) Wang, Z.; Hu, J.; Lu, Z. Covalent Organic Frameworks as Emerging Battery Materials. *Batter Supercaps* **2023**. https://doi.org/10.1002/batt.202200545.

(55) Lu, Y.; Chen, J. Prospects of Organic Electrode Materials for Practical Lithium Batteries. *Nat Rev Chem* **2020**, *4* (3), 127–142. https://doi.org/10.1038/s41570-020-0160-9.

(56) Yuan, Q.; Li, C.; Guo, X.; Zhao, J.; Zhang, Y.; Wang, B.; Dong, Y.; Liu, L. Electrochemical Performance and Storage Mechanism Study of Conjugate Donor–Acceptor Organic Polymers as Anode Materials of Lithium-Ion Battery. *Energy Reports* **2020**, *6*, 2094–2105. https://doi.org/10.1016/j.egyr.2020.08.001.

(57) Yadav, S.; Ingle, D. S.; Venkata Rao, K.; Kurra, N. Organic Materials as Charge Hosts for Pseudocapacitive Energy Storage. *Sustain Energy Fuels* **2023**, *7* (12), 2802–2818. https://doi.org/10.1039/D3SE00406F.

(58) Lee, S.; Hong, J.; Jung, S. K.; Ku, K.; Kwon, G.; Seong, W. M.; Kim, H.; Yoon, G.; Kang, I.; Hong, K.; Jang, H. W.; Kang, K. Charge-Transfer Complexes for High-Power Organic Rechargeable Batteries. *Energy Storage Mater* **2019**, *20*, 462–469. https://doi.org/10.1016/j.ensm.2019.05.001.

(59) Chen, H.; Zhang, Y.; Xu, C.; Cao, M.; Dou, H.; Zhang, X. Two π-Conjugated Covalent Organic Frameworks with Long-Term Cyclability at High Current Density for Lithium Ion Battery. *Chemistry - A European Journal* **2019**, *25* (68), 15472–15476. https://doi.org/10.1002/chem.201903733.

(60) Haldar, S.; Roy, K.; Nandi, S.; Chakraborty, D.; Puthusseri, D.; Gawli, Y.; Ogale, S.; Vaidhyanathan, R. High and Reversible Lithium Ion Storage in Self-Exfoliated Triazole-Triformyl Phloroglucinol-Based Covalent Organic Nanosheets. *Adv Energy Mater* **2018**, *8* (8). https://doi.org/10.1002/aenm.201702170.

(61) Wang, J.; Chen, C. S.; Zhang, Y. Hexaazatrinaphthylene-Based Porous Organic Polymers as Organic Cathode Materials for Lithium-Ion Batteries. *ACS Sustain Chem Eng* **2018**, *6* (2), 1772–1779. https://doi.org/10.1021/acssuschemeng.7b03165.

(62) Meng, Y.; Li, J.; Gu, S.; Fu, Y.; Wang, Z.; Liu, J.; Gong, X. Li-Ion Complex Enhances Interfacial Lowest Unoccupied Molecular Orbital for Stable Solid Electrolyte Interface of Natural Graphite Anode. *Electrochim Acta* **2023**, *449*. https://doi.org/10.1016/j.electacta.2023.142262.

(63) Xue, X.; Luo, J.; Kong, L.; Zhao, J.; Zhang, Y.; Du, H.; Chen, S.; Xie, Y. The Synthesis of Triazine-Thiophene-Thiophene Conjugated Porous Polymers and

Their Composites with Carbon as Anode Materials in Lithium-Ion Batteries. *RSC Adv* **2021**, *11* (18), 10688–10698. https://doi.org/10.1039/d0ra10862f.

(64) Rajalakshmi, K.; Muthusamy, S.; Xie, M.; Nam, Y. S.; Lee, B. hyeon; Lee, K. B.; Xu, Y.; Xie, J. Fabrication of Thiophene Decorated Side Chain Entanglement Free COFs for Highly Regenerable Mercury Extraction. *Chemical Engineering Journal* **2022**, *430*. https://doi.org/10.1016/j.cej.2021.133149.

(65) Pachfule, P.; Acharjya, A.; Roeser, J.; Sivasankaran, R. P.; Ye, M. Y.; Brückner, A.; Schmidt, J.; Thomas, A. Donor-Acceptor Covalent Organic Frameworks for Visible Light Induced Free Radical Polymerization. *Chem Sci* **2019**, *10* (36), 8316–8322. https://doi.org/10.1039/c9sc02601k.

(66) Fang, Q.; Wang, J.; Gu, S.; Kaspar, R. B.; Zhuang, Z.; Zheng, J.; Guo, H.; Qiu, S.; Yan, Y. 3D Porous Crystalline Polyimide Covalent Organic Frameworks for Drug Delivery. *J Am Chem Soc* **2015**, *137* (26), 8352–8355. https://doi.org/10.1021/jacs.5b04147.

(67) Zhang, Y. B.; Su, J.; Furukawa, H.; Yun, Y.; Gándara, F.; Duong, A.; Zou, X.; Yaghi, O. M. Single-Crystal Structure of a Covalent Organic Framework. *J Am Chem Soc* **2013**, *135* (44), 16336–16339. https://doi.org/10.1021/ja409033p.

(68) Xin, Y.; Wang, C.; Wang, Y.; Sun, J.; Gao, Y. Encapsulation of an Ionic Liquid into the Nanopores of a 3D Covalent Organic Framework. *RSC Adv* **2017**, *7* (3), 1697–1700. https://doi.org/10.1039/c6ra27213d.

(69) Zhou, B.; Yan, F.; Li, X.; Zhou, J.; Zhang, W. An Interpenetrating Porous Organic Polymer as a Precursor for FeP/Fe 2 P-Embedded Porous Carbon toward a PH-Universal ORR Catalyst. *ChemSusChem* **2019**, *12* (4), 915–923. https://doi.org/10.1002/cssc.201802369.

(70) Yang, T.; Zhang, C.; Ma, W.; Gao, X.; Yan, C.; Wang, F.; Jiang, J. X. Thiophene-Rich Conjugated Microporous Polymers as Anode Materials for High Performance Lithium- and Sodium-Ion Batteries. *Solid State Ion* **2020**, *347*. https://doi.org/10.1016/j.ssi.2020.115247.

(71) Zhang, C.; He, Y.; Mu, P.; Wang, X.; He, Q.; Chen, Y.; Zeng, J.; Wang, F.; Xu, Y.; Jiang, J. X. Toward High Performance Thiophene-Containing Conjugated Microporous Polymer Anodes for Lithium-Ion Batteries through Structure Design. *Adv Funct Mater* **2018**, *28* (4). https://doi.org/10.1002/adfm.201705432.

(72) Patnaik, S. G.; Vedarajan, R.; Matsumi, N. Rational Design of a BIAN-Based Multi-Functional Additive for Higher Durability and Performance of LiMn1/3Ni1/3Co1/3O2 Cathodes. *Mol Syst Des Eng* **2019**, *4* (4), 939–950. https://doi.org/10.1039/c9me00046a.

(73) Haldar, S.; Schneemann, A.; Kaskel, S. Covalent Organic Frameworks as Model Materials for Fundamental and Mechanistic Understanding of Organic Battery Design Principles. *J Am Chem Soc* **2023**, *145* (25), 13494–13513. https://doi.org/10.1021/jacs.3c01131.

(74) Cao, Y.; Wang, M.; Wang, H.; Han, C.; Pan, F.; Sun, J. Covalent Organic Framework for Rechargeable Batteries: Mechanisms and Properties of Ionic Conduction. *Advanced Energy Materials*. John Wiley and Sons Inc May 1, 2022. https://doi.org/10.1002/aenm.202200057.

(75) Hou, C. C.; Ma, C.; Zhang, S. N.; Wang, L. Y.; Wang, K. X.; Chen, J. S. Polymeric Schiff Base with Thiophene Rings for Sodium-Ion Batteries. *ACS Appl Energy Mater* **2022**. https://doi.org/10.1021/acsaem.2c02436.

(76) Nandan, R.; Takamori, N.; Higashimine, K.; Badam, R.; Matsumi, N. Zinc Blende Inspired Rational Design of a B-SiC Based Resilient Anode Material for Lithium-Ion Batteries. *J Mater Chem A Mater* **2022**, *10* (10), 5230–5243. https://doi.org/10.1039/d1ta08516f.

(77) Mou, X.; Xin, X.; Dong, Y.; Zhao, B.; Gao, R.; Liu, T.; Li, N.; Liu, H.; Xiao, Z. Molecular Design of Porous Organic Polymer-Derived Carbonaceous Electrocatalysts for Pinpointing Active Sites in Oxygen Reduction Reaction. *Molecules*. MDPI May 1, 2023. https://doi.org/10.3390/molecules28104160.

(78) Salunkhe, R. R.; Kaneti, Y. V.; Kim, J.; Kim, J. H.; Yamauchi, Y. Nanoarchitectures for Metal-Organic Framework-Derived Nanoporous Carbons toward Supercapacitor Applications. *Acc Chem Res* **2016**, *49* (12), 2796–2806. https://doi.org/10.1021/acs.accounts.6b00460.

(79) Wang, H.; Shao, Y.; Mei, S.; Lu, Y.; Zhang, M.; Sun, J. K.; Matyjaszewski, K.; Antonietti, M.; Yuan, J. Polymer-Derived Heteroatom-Doped Porous Carbon Materials. *Chemical Reviews*. American Chemical Society September 9, 2020, pp 9363–9419. https://doi.org/10.1021/acs.chemrev.0c00080.

(80) Rangraz, Y.; Heravi, M. M. Recent Advances in Metal-Free Heteroatom-Doped Carbon Heterogonous Catalysts. *RSC Advances*. Royal Society of Chemistry July 5, 2021, pp 23725–23778. https://doi.org/10.1039/d1ra03446d.

(81) Zhang, J.; Dai, L. Heteroatom-Doped Graphitic Carbon Catalysts for Efficient Electrocatalysis of Oxygen Reduction Reaction. *ACS Catalysis*. American Chemical Society October 23, 2015, pp 7244–7253. https://doi.org/10.1021/acscatal.5b01563.

(82) Dutta, S.; Bhaumik, A.; Wu, K. C. W. Hierarchically Porous Carbon Derived from Polymers and Biomass: Effect of Interconnected Pores on Energy Applications.

Energy and Environmental Science. Royal Society of Chemistry November 1, 2014, pp 3574–3592. https://doi.org/10.1039/c4ee01075b.

(83) Xu, Z.; Huang, Y.; Chen, C.; Ding, L.; Zhu, Y.; Zhang, Z.; Guang, Z. MOF-Derived Hollow Co(Ni)Se_2/N-Doped Carbon Composite Material for Preparation of Sodium Ion Battery Anode. *Ceram Int* **2020**, *46* (4), 4532–4542. https://doi.org/10.1016/j.ceramint.2019.10.181.

(84) Cheng, Q.; Pan, Y.; Chen, Y.; Zeb, A.; Lin, X.; Yuan, Z.; Liu, J. Nanostructured Iron Fluoride Derived from Fe-Based Metal-Organic Framework for Lithium Ion Battery Cathodes. *Inorg Chem* **2020**, *59* (17), 12700–12710. https://doi.org/10.1021/acs.inorgchem.0c01783.

(85) Li, X.; Zheng, S.; Jin, L.; Li, Y.; Geng, P.; Xue, H.; Pang, H.; Xu, Q. Metal-Organic Framework-Derived Carbons for Battery Applications. *Advanced Energy Materials*. Wiley-VCH Verlag August 16, 2018. https://doi.org/10.1002/aenm.201800716.

(86) Jin, W. Wu; Li, H. Jun; Zou, J. Zhao; Inguva, S.; Zhang, Q.; Zeng, S. Zhong; Xu, G. Zhong; Zeng, X. Rong. Metal Organic Framework-Derived Carbon Nanosheets with Fish-Scale Surface Morphology as Cathode Materials for Lithium–Selenium Batteries. *J Alloys Compd* **2020**, *820*. https://doi.org/10.1016/j.jallcom.2019.153084.

(87) Lu, G.; Wang, H.; Zheng, Y.; Zhang, H.; Yang, Y.; Shi, J.; Huang, M.; Liu, W. Metal-Organic Framework Derived N-Doped CNT@ Porous Carbon for High-Performance Sodium- and Potassium-Ion Storage. *Electrochim Acta* **2019**, *319*, 541–551. https://doi.org/10.1016/j.electacta.2019.07.026.

(88) Luo, Y. M.; Sun, L. X.; Xu, F.; Wang, Z. Q. Porous Carbon Derived from Metal-Organic Framework as an Anode for Lithium-Ion Batteries with Improved Performance. In *Key Engineering Materials*; Trans Tech Publications Ltd, 2017; Vol. 727, pp 705–711. https://doi.org/10.4028/www.scientific.net/KEM.727.705.

(89) Zhang, C.; Kong, R.; Wang, X.; Xu, Y.; Wang, F.; Ren, W.; Wang, Y.; Su, F.; Jiang, J. X. Porous Carbons Derived from Hypercrosslinked Porous Polymers for Gas Adsorption and Energy Storage. *Carbon N Y* **2017**, *114*, 608–618. https://doi.org/10.1016/j.carbon.2016.12.064.

(90) Srimitra Mantripragada, B.; Sumala Patnaik, K.; Higashimine, K.; Badam, R.; Matsumi, N. POP Based Nitrogen Containing Anodic Materials for High Capacity and Fast Charge-Discharge Applications in LIB. *Electrochem commun* **2023**, *157*. https://doi.org/10.1016/j.elecom.2023.107616.

(91) Wang, X.; Li, G.; Hassan, F. M.; Li, J.; Fan, X.; Batmaz, R.; Xiao, X.; Chen, Z.

Sulfur Covalently Bonded Graphene with Large Capacity and High Rate for High-Performance Sodium-Ion Batteries Anodes. *Nano Energy* **2015**, *15*, 746–754. https://doi.org/10.1016/j.nanoen.2015.05.038.

(92) Ye, J.; Zang, J.; Tian, Z.; Zheng, M.; Dong, Q. Sulfur and Nitrogen Co-Doped Hollow Carbon Spheres for Sodium-Ion Batteries with Superior Cyclic and Rate Performance. *J Mater Chem A Mater* **2016**, *4* (34), 13223–13227. https://doi.org/10.1039/c6ta04592h.

(93) Hu, X.; Sun, X.; Song, Q.; Zhu, Y.; Long, Y.; Dong, Z. N,S Co-Doped Hierarchically Porous Carbon Materials for Efficient Metal-Free Catalysis. *Green Chemistry* **2020**, *22* (3), 742–752. https://doi.org/10.1039/c9gc03863a.

(94) Zhao, X.; Liang, R. R.; Jiang, S. Y.; Ru-Han, A. Two-Dimensional Covalent Organic Frameworks with Hierarchical Porosity. *Chemical Society Reviews*. Royal Society of Chemistry June 21, 2020, pp 3920–3951. https://doi.org/10.1039/d0cs00049c.

(95) Chen, M.; Le, T. H.; Zhou, Y.; Kang, F.; Yang, Y. Thiourea-Induced N/S Dual-Doped Hierarchical Porous Carbon Nanofibers for High-Performance Lithium-Ion Capacitors. *ACS Appl Energy Mater* **2020**, *3* (2), 1653–1664. https://doi.org/10.1021/acsaem.9b02157.

(96) Leng, Q.; Tian, F.; Yuan, Y.; Li, W. N/S Codoped Three-Dimensional Porous Carbons for High-Performance Supercapacitors with Remarkable Rate Performance. *Energy and Fuels* **2023**, *37* (7), 5499–5507. https://doi.org/10.1021/acs.energyfuels.2c04111.

(97) Ramar, A.; Sakthivel, M.; Wang, F. M.; Ho, K. C. Super Microporous Sulfur-Doped Hard Carbon Synthesized from a π-Stacked Polybenzo[c]Thiophene Boosting Reversible Lithium-Ion Insertion at Room Temperature. *Carbon N Y* **2023**, *213*. https://doi.org/10.1016/j.carbon.2023.118223.

(98) Rehman, A.; Park, S. J. Facile Synthesis of Nitrogen-Enriched Microporous Carbons Derived from Imine and Benzimidazole-Linked Polymeric Framework for Efficient CO2 Adsorption. *Journal of CO2 Utilization* **2017**, *21*, 503–512. https://doi.org/10.1016/j.jcou.2017.08.016.

(99) Hu, A.; Jin, S.; Du, Z.; Jin, H.; Ji, H. NS Codoped Carbon Nanorods as Anode Materials for High-Performance Lithium and Sodium Ion Batteries. *Journal of Energy Chemistry* **2018**, *27* (1), 203–208. https://doi.org/10.1016/j.jechem.2017.11.022.

(100) Ren, S. Bin; Ma, W.; Zhang, C.; Chen, L.; Wang, K.; Li, R. R.; Shen, M.; Han, D. M.; Chen, Y.; Jiang, J. X. Exploiting Polythiophenyl-Triazine-Based Conjugated

Microporous Polymer with Superior Lithium-Storage Performance. *ChemSusChem* **2020**, *13* (9), 2295–2302. https://doi.org/10.1002/cssc.202000200.

(101) Yan, S. Xue; Wang, Q.; Luo, S. Hua; Zhang, Y. Hui; Liu, X.; Liu, Y. Guo; Wang, Z. Yuan; Hao, A. Min; Yi, T. Feng. Coal-Based S Hybrid Self-Doped Porous Carbon for High-Performance Supercapacitors and Potassium-Ion Batteries. *J Power Sources* **2020**, *461*. https://doi.org/10.1016/j.jpowsour.2020.228151.

(102) Shen, G.; Li, B.; Xu, Y.; Chen, X.; Katiyar, S.; Zhu, L.; Xie, L.; Han, Q.; Qiu, X.; Wu, X.; Cao, X. Waste Biomass Garlic Stem-Derived Porous Carbon Materials as High-Capacity and Long-Cycling Anode for Lithium/Sodium-Ion Batteries. *J Colloid Interface Sci* **2024**, *653*, 1588–1599. https://doi.org/10.1016/j.jcis.2023.09.150.

(103) Patra, A.; Matsumi, N. Water-Soluble Densely Functionalized Poly(hydroxycarbonylmethylene) Binder for Higher-Performance Hard Carbon Anode-Based Sodium-Ion Batteries. *J Mater Chem A Mater* **2024**. https://doi.org/10.1039/D4TA00285G.

(104) Fang, Y.; Zhang, Q.; Cui, L. Recent Progress of Mesoporous Materials for High Performance Supercapacitors. *Microporous and Mesoporous Materials*. Elsevier B.V. February 1, 2021. https://doi.org/10.1016/j.micromeso.2020.110870.

(105) Weiss, M.; Ruess, R.; Kasnatscheew, J.; Levartovsky, Y.; Levy, N. R.; Minnmann, P.; Stolz, L.; Waldmann, T.; Wohlfahrt-Mehrens, M.; Aurbach, D.; Winter, M.; Ein-Eli, Y.; Janek, J. Fast Charging of Lithium-Ion Batteries: A Review of Materials Aspects. *Advanced Energy Materials*. John Wiley and Sons Inc September 1, 2021. https://doi.org/10.1002/aenm.202101126.

(106) Ramar, A.; Sakthivel, M.; Wang, F. M.; Ho, K. C. Super Microporous Sulfur-Doped Hard Carbon Synthesized from a π-Stacked Polybenzo[c]Thiophene Boosting Reversible Lithium-Ion Insertion at Room Temperature. *Carbon N Y* **2023**, *213*. https://doi.org/10.1016/j.carbon.2023.118223.

(107) Ma, C.; Shao, X.; Cao, D. Nitrogen-Doped Graphene Nanosheets as Anode Materials for Lithium Ion Batteries: A First-Principles Study. *J Mater Chem* **2012**, *22* (18), 8911–8915. https://doi.org/10.1039/c2jm00166g.

(108) Kong, X. K.; Chen, Q. W. Improved Performance of Graphene Doped with Pyridinic N for Li-Ion Battery: A Density Functional Theory Model. *Physical Chemistry Chemical Physics* **2013**, *15* (31), 12982–12987. https://doi.org/10.1039/c3cp51987b.